Graphene and Graphane Functionalization using Hydrogen and Nitrogen: Electronic, Optical and Vibrational Signatures

By: Phillip McNelles

April 28, 2011

Supervisor: Dr. Franco Gaspari

Co-Supervisor: Dr. Anatoli Chkrebtii

Table of Contents

List of Tables

List Of Figures

List of Acronyms

BO:	Born-Oppenheimer
BOMD:	Born-Oppenheimer Molecular Dynamics
BZ:	Brillouin Zone
C:	Carbon
CPA:	Central Potential Approximation
DFT:	Density Functional Theory
DoS:	Density of States
E:	Energy
E_k:	Kinetic Energy
E_{cut}:	Cut-off Energy
eV:	Electron Volt
H:	Hydrogen
HK or H-K:	Hohenberg and Kohn
IBZ:	Irreducible Brillouin Zone
JDOS:	Joint Density of States
KS or K-S:	Kohn and Sham
LDA:	Local Density Approximation
MD:	Molecular Dynamics
N:	Nitrogen
PP or PS:	Pseudopotential
PSPW:	Pseudopotential Plane-Wave
PW:	Plane-Wave
Ry:	Rydberg

List of Presentations:

The following is a list of presentations and publications that have or will incorporate information used in this research:

A. I. Shkrebtii, J. L. Cabellos, N. Arzate, B. S. Mendoza, and P. McNelles, *"Controlled hydrogenation of graphene, graphene-like silicon and germanium by optical injection current, linear and nonlinear optics"*, International School of Solid State Physics Epioptics-11, Erice, Sicily, 19-25 July 2010.

A. I. Shkrebtii, J. L. Cabellos, N. Arzate, B. S. Mendoza, and P. McNelles, *"Nonlinear optical characterization of hydrogenated two-dimensional honeycomb carbon (graphene), silicon (silicene) and germanium layer"*, 7th International Symposium on Ultrafast Surface Dynamics (USD7) Croatia Brijuni Island, 22-26 Aug. 2010.

A.I. Shkrebtti, P. McNelles, J.L. Cabellos, B.S. Mendoza, F. Gaspari. *"Partially hydrogenated graphene: semiconductor material with a tuneable gap and its non-destructive optical characterization."* Materials Research Society Conference, San Francisco, California, April 25-29, 2011.

A.I. Shkrebtii, P. McNelles, J.L. Cabellos, B.S. Mendoza and F. Gaspari. "Graphene and graphane functionalization with hydrogen and nitrogen: Electronic, Optical and Vibrational Signatures" ICFSI 13 Conference.

List of Publications:

A.I. Shkrebtti, P. McNelles, J.L. Cabellos, B.S. Mendoza, F. Gaspari. *"Partially hydrogenated graphene: semiconductor material with a tuneable gap and its non-destructive optical characterization."* Materials Will be published in proceedings of Materials Research Society (MRS) Spring 2011 Meeting

(MRS Publication)

A.I. Shkrebtii, P. McNelles, J.L. Cabellos, B.S. Mendoza and F. Gaspari. "Graphene and graphane functionalization with hydrogen and nitrogen: Electronic, Optical and Vibrationa". Physica status solidi.

Acknowledgements

I would like to thank Dr. Franco Gaspari and Dr. Anatoli Chkrebtii for taking me on and agreeing to be my supervisor and co-supervisor, respectively.

I would also like to thank Tim Teatro for the use of his programs to compute vibrational spectra, and Fredric Zimmer-De-Iuliis for his help during the research.

I would also like to thank Dr. Fedor Naumkin for his continuous support.

Outline

The first chapter of this thesis will serve as an introduction to the work. It will provide descriptions of graphene, graphane and partially hydrogenated graphene (sometimes referred to as graphone), as well as a brief overview of the properties and applications of graphene. The main goal of this research (create a library of computational data) will also be stated.

The second chapter will focus on the theoretical background for the research, especially Density Functional Theory (DFT) within the Local Density Approximation (LDA). Also being discussed will be the theory of plane-waves and Pseudopotentials and how they pertain to DFT in solids. Lastly, Molecular Dynamics (MD), specifically Born-Oppenheimer Molecular Dynamics (BOMD) will be looked into.

In chapter three, the optimized structure (also known as relaxed ground state structure) calculations will be discussed. This includes optimization for C_8, C_{16} and C_{32} supercells with varying amounts of hydrogen attached (ranging from 2 to 8 H atoms). This will include discussions of the most favourable arrangements, as well as pictures of the supercells. It will also include Band Structures and DoS graphs and analysis of the most energetically favourable systems.

The fourth chapter will be devoted to the discussion of the optical response of the systems. This involves analysis of ε (epsilon), the complex dielectric constant in the solid in 3 directions. Also looked at is the Reflectance Anisotropy Spectra (RAS), which is the difference in the optical response between the x and y directions in the plane of the graphene and is derivatives. Lastly, the Joint Density of State (JDOS) calculations will be discussed.

The fifth chapter will discuss the results of the BOMD calculations, as well as the vibrational frequencies that are calculated using these results. This will determine the stability of these systems, as well as their properties at higher temperatures and provide another way to characterize them experimentally. Also discussed briefly was the doping of the graphene with nitrogen atoms.

In chapter six, the conclusions that are drawn from this thesis will be stated, along with an explanation of them. Furthermore, ways to expand on this work in the future will be discussed.

Chapter 1: Introduction to Graphene and Graphenated Systems

The material known as graphene was discovered in 2004, and is a flat, one atom thick structure of Carbon atoms. These carbon atoms are packed in densely into a honeycomb shaped lattice, with a bond distance of about 1.42 angstroms (A). Graphene also provides the basis for other allotropes of carbon, such as fullerenes (buckyballs), carbon nanotubes, or can be stacked into layers to make graphite. [1-3]. It is also the thinnest type of material possible, as it is just one atom thick, and it is chemically very stable. Graphene can exist as a stand-alone material in macroscopic films (largest size currently at about 1m) [4], as well as being grown on top of metallic or semiconductor substrates [5-8]. The discovery of graphene garnered the 2010 Nobel Prize in Physics. In principle, a graphene sheet would look like:

Figure 1.1: Flat Graphene Sheet

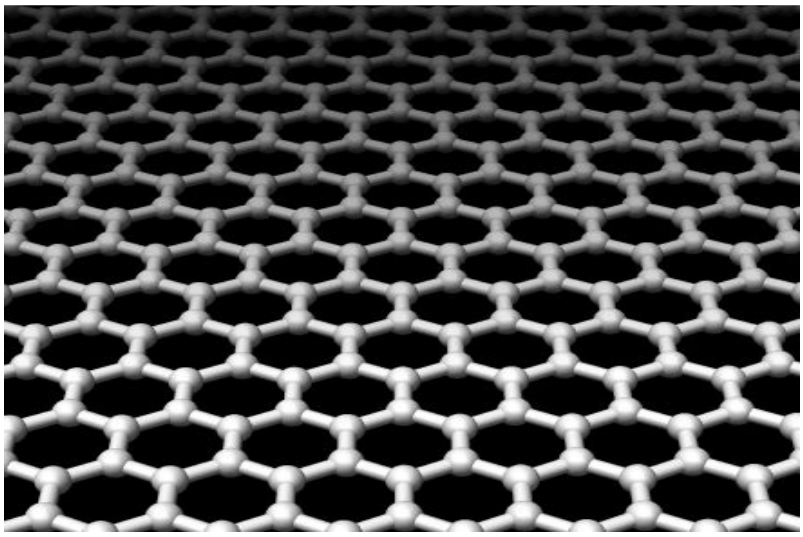

For a long time (since the 1930's) it was believed that 2D crystal structures (such as graphene) would be thermodynamically unstable, and should not exist. According to the Mermin-Wagner theorem, the long-wavelength fluctuations would break the long range order of these crystal structures, and that any 2D single atom thick substance must be crumpled, and therefore not exist in a standalone film [9]. (For the original papers on this theory, please see references 43 and 44). It was shown later that these long-wavelength fluctuations can be overcome by the anharmonic coupling between the stretching and the bending modes, and allowing the substances like graphene to exist. However, this means that these 2D membranes will not be flat, and it has been shown that when not on a substrate, graphene is no longer flat [9], as shown below:

Figure 1.2: Corrugations (ripples) in an Isolated Graphene Sheet

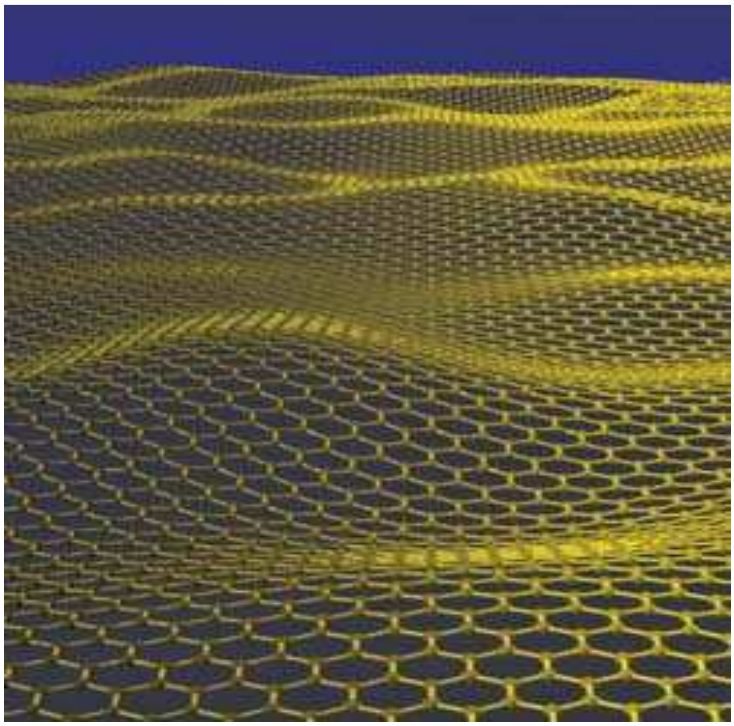

The discovery of graphene has also led to research into an entire new class of materials, such as a one atom thick honeycomb silicon (silicene) that was produced experimentally [10]. Furthermore, a germanium version has been predicted experimentally [11]. Although graphene and its Si and Ge variants have many interesting properties, the fact that graphene is metallic (zero-band gap), does put a limit on its uses in certain microelectronic applications which require a band gap for a p-n junction.

In 2007, a graphene based structure, now called graphane was predicted theoretically, and then verified experimentally in 2009. Graphane is fully hydrogenated graphene, meaning that each carbon atom is bonded to a hydrogen atom. This extra bond causes sp^3 hybridization, so graphane is not a flat shape. However, unlike graphene, graphane is a semi-conductor with a high band gap (close to 5 eV) [3, 12, 13]. It was produced by exposing graphene to atomic hydrogen. This was accomplished by passing hydrogen gas (H_2) through an electrical discharge, which broke apart the H_2 gas, producing H atoms. These hydrogen atoms then drift towards a sample of graphene and bond with the carbon, resulting in graphane [3, 12, 13]. A picture of what graphane looks like is shown below:

Figure 2: Graphane Sheet. The blue (large) spheres are carbon, the red (small) are hydrogen

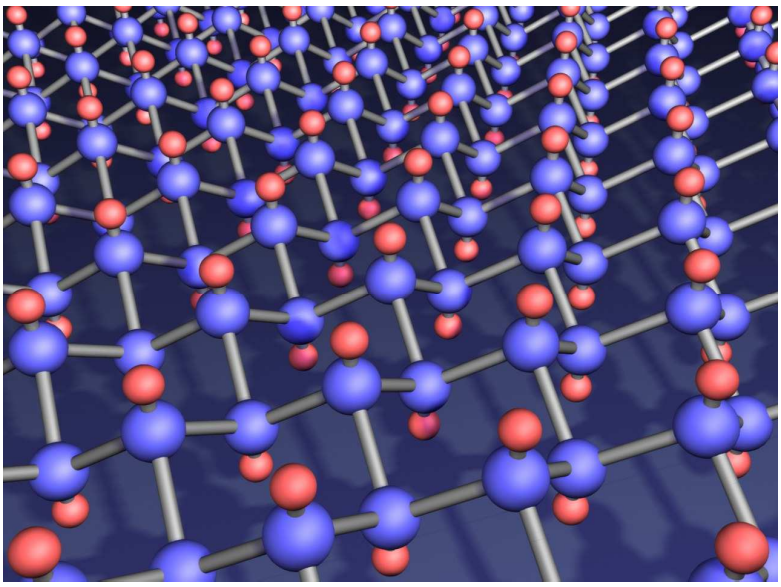

The difference in the shape of the flat graphene and the buckled graphane is due to the hybrid orbitals. Graphene is sp^2 hybridized (planar), while graphane is sp^3 hybridized (tetrahedral, similar to diamond). A picture illustrating this is shown below:

Figure 3: Schematic view of sp^2 hybrid orbital (top) and sp^3 hybrid orbital (bottom)

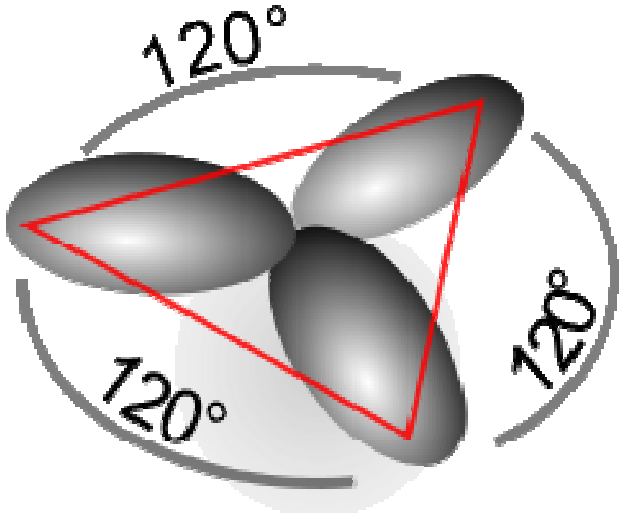

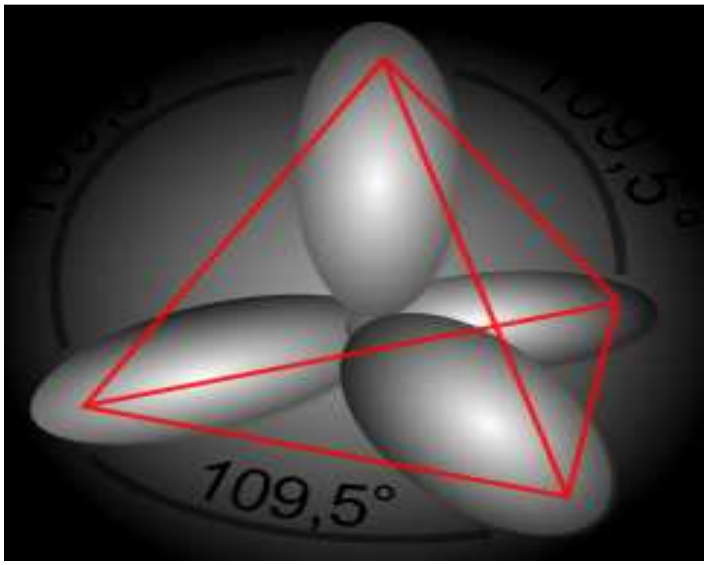

While there are many theorised applications for graphene, such as gas detectors, biodevices, ultracapcitors and even hydrogen storage, the interest here is in microelectronics. As discussed earlier, both graphene and graphane have potential use as a semiconductor in semiconductor applications, like transistors and integrated circuits. There is an issue with the current material use in semiconductors (silicon), because it produces a lot of heat. A problem in modern times is to try and make these microchips smaller and more powerful, without creating extra heat. It is believed that graphene based transistors could run at much faster speeds and produce less heat than silicon transistors. Due to the extremely high conductivity of graphene, it is believed to be a good choice in material for this.

The goal of this research project is to theoretically investigate the possibility of tuning the band gap of partially hydrogenated graphene for use in microelectronics applications as well as theorize an efficient way of controlling the gap. A band gap of 1-2 eV would be ideal. Since graphene has a band gap of 0, and graphane has a high gap, it is believed that partially hydrogenating graphene will lead to a good semiconductor for use in p-n junctions [50, 51]. An important part of this research is to also be able to characterize the systems, so if and when experimental results are available, they can then be matched up with the computational results, to see if a certain structure (or certain type of structure) was created. This will be done by running computational simulations of the linear and non-linear optical response, as it has been shown to be a good method for this kind of characterization [14, 15]. Other characterisations will be included, such as the Joint Density of States (JODS), and molecular dynamics calculations used to find the vibrational spectra of the larger C_{32} unit cells. This research can be thought of as making a sort of library of computational information on hydrogenated graphene that could be referred to by those who are trying to make these systems experimentally.

Chapter 2: Theoretical Background

2.1: Introduction

In this chapter, the theoretical background behind the methods used in the research will be discussed and explained in more detail. The main method used for this thesis is a widely known method known as DFT, or density functional theory, as well as LDA (Local Density Approximation) and SCF (self consistent field). Much of this research (and computational research done by many others) is based on those techniques, and they will be discussed in detail. Another facet of DFT when working in solids is Planewave (PW) and Pseudopotential (PP, or PS) methods, which contribute to making the calculations accurate and more efficient. For the molecular dynamics calculations (chapter 5), they were produced using BOMD (Born-Oppenheimer molecular dynamics), which will also be discussed. At the end of the chapter, the main computational program used, Quantum Espresso, and a minor program known as Molekel molecular viewer will be briefly looked into.

2.2: Self-Consistent Field and Hartree-Fock Methods

The SCF method for (approximately) calculating the ground state energies and wavefunctions for a many-body, quantum system was formulated by D.A. Hartree in 1927. It is sometimes also referred to as the Hartree method. It should be noted that typically the Hartree-Fock (HF) method is known as SCF, and Hartree's original method is known simply as the Hartree Method. It was based on what is known as the independent electron approximation, which neglects electron correlation. Here, nonlinear equations for the one-electron wavefunctions and energies would be solved by iteration. The Hartree-Fock method began to form in 1930 when V.A. Fock and Slater (the same Slater of Slater determinant fame) independently showed that the Hartree method violated the antisymmetry of the wave function, and took the current form in 1935 when Hartree reworked the theory to perform better with calculations. The main difference is what is known as the exchange energy or exchange interaction, which occurs when the wave functions of identical particles (such as electrons) overlap [16-19]. This extra term came about to keep with the Pauli exclusion principle, and maintain antisymmetric wavefunctions (which the original Hartree method failed to do). One can also think of the Hartree method as an approximation of the HF method that ignores the exchange energy. The HF method did not come into much popularity however, until the computer was invented since it was difficult to compute. A weakness of the model however was in the approximation that

neglected electron correlation, which can be strong in certain atoms. It did work well for atoms and simple molecules, but larger systems were too numerically complicated when taking into account all the wave functions. There are different variations of the HF method depending on the type of system. The above information dealt with the Restricted HF method (for closed shell systems). Open shell systems require The ROHF (Restricted open-shell Hartree-Fock) or the UHF (Unrestricted Hartree-Fock) methods, but the latter 2 methods are not dealt with here.

2.3: Thomas-Fermi Method

The Thomas-Fermi model (TF), was formulated independently by L. Thomas and E. Fermi in 1927, and was used as a way to approximate the distribution of electrons in an atom. The basis for this was that electrons were uniformly distributed in phase space, where there were 2 electrons in every h^3 (cube) of volume. This allowed them to calculate the energy of an atom using the kinetic energy functional along with the already known equations for the electron-electron and electron-nuclear interactions, both of which can be expressed in terms of electron density. It did suffer from some large drawbacks, as the kinetic energy functional is an approximation, and does not include the exchange energy. An exchange energy correction was added by Dirac in 1928, but the error in kinetic energy, exchange energy and the neglect of electron-electron interactions severely limited its accuracy. However, it was an important first step in using electron density for its calculations, and can be considered a precursor to the current DFT method. It also helped lead to the local density approximation, as discussed later in the chapter [45-46].

2.4: Density Functional Theory

2.4.1: Introduction

Much of the work done in the previous sections lead up to the main method used in this research, Density Functional Theory, or DFT. DFT has become a very widely-used method in computational physics and computational chemistry research into the electronic structure of many-body systems, such as atoms and molecules, particularly in the condensed state. It works on the principle of using functionals (functions of a function), which in DFT is the space-dependant electron density. The formulation of DFT dates back to the 1960's; with work done by Walter Kohn, L.J. Sham, and Pierre Hohenberg, which will be discussed later on. The DFT

method has been used in solid state research since the 1970's, but in the field of quantum chemistry it was not accurate enough until better approximations of the correlation and exchange interactions were developed during the 1990's. In most cases the DFT calculations match up very well with experimental information, and with lower computational costs than HF methods. It does however have some drawbacks, notably in the case of this research with strongly correlated materials (where electron correlation cannot be neglected), and in the case of band structure calculations, both which will be discussed in chapter 3. DFT can be applied to both atomic/molecular systems as well as solids. The next part of the chapter will discuss the history and formulation of DFT, and following that will be the discussion of it being applied to solid state systems.

2.4.2: Hohenberg-Kohn Theorems

In 1964, Hohenberg and Kohn did work together and published a well-known paper entitled simply *Inhomogeneous Electron Gas.* It dealt with the problem of the inhomogeneous electron gas (treating the electrons of a system as a gas), and formulated a way to describe this system. In the paper, they showed that there does exist a way to describe a (stationary) electron system by using the electron density of the ground state. There were two theorems presented [20-26]:

Theorem 1: *.If two systems of electrons, one trapped in a potential* $v_1(\vec{r})$ *and the other in* $v_2(\vec{r})$ *have the same ground-state density*$n(\vec{r})$ *then necessarily* $v_1(\vec{r}) - v_2(\vec{r})$ *= constant.*

Theorem 2: *For any positive integer N and potential* $v(\vec{r})$ *the density functional* $E_{(v,N)}[n] = F[n] + \int v(\vec{r})n(\vec{r})d^3r$ *obtains its minimal value at the ground-state density of N electrons in the potential* $v(\vec{r})$ *. The minimal value of* $E_{(v,N)}[n]$ *is then the ground state energy of this system.*

The first theorem shows that in a many-electron system, the ground state properties are uniquely given by an electron density depending on just 3 coordinates in space. This helped with simplifying the many-electron problem, where having N electrons with 3N (spatial) coordinates would reduce to only 3 coordinates, by using functionals of the electron density.

The second theorem introduced the variational principle to density functionals. It also describes an energy functional for the system and most importantly proved that the energy functional will be at a minimum at the proper ground state electron density.

The main issue with these theorems is that although they prove these calculations can be done, they do not show any way of actually carrying them out. This work, however brings us closer to the modern version of DFT, but further modifications were made using the H-K theorems (particularly theorem 2) by Kohn and Sham in the following year. This work would be the basis

for DFT, and Kohn received the 1998 Nobel Prize in Chemistry. The following section deals with the Kohn-Sham (KS) equations.

2.4.3: Kohn-Sham Equations and Electron Density

As mentioned previously, Kohn and Sham then built upon the previous work done by Kohn and Hohenberg the year before. This would lead to the modern incarnation of DFT, and is sometimes referred to as KS DFT. It is worth noting that the term "DFT" refers to KS DFT, even though there are other versions (such as OFDFT, which is more closely based on the TF model, and therefore faster and less accurate), but will not discussed here. The KS equations allowed for the calculations of the electronic properties of the system using the electron density of the ground state (which was shown to be possible by the H-K theorems).

In DFT the Kohn-Sham equation is used as the Schrodinger equation of the so-called Kohn-Sham system, which is a fictitious (or effective) system of non-interacting particles (in this case electrons), that will have the same electron density as a given system of particles. This is described by an effective potential that the (non-interacting) particles will move through. It is referred to as the Kohn-Sham potential, and is usually given as $v_{s.}(\mathbf{r})$ or as $v_{eff}(\mathbf{r})$. Due to the assumption (approximation) that the electrons are not interacting with each other, the KS wavefunction will reduce to a single Slater determinant whose orbitals are the lowest energy (ground state) solutions to the KS equation [21]:

$$\left(-\frac{\hbar^2}{2m}\nabla^2 + v_{\text{eff}}(\mathbf{r})\right)\phi_i(\mathbf{r}) = \varepsilon_i\phi_i(\mathbf{r})$$

where ε_i is the orbital energy for the KS orbital (denoted by φ_i). The electron density for a system with N electrons is denoted ρ, and given as a function of r (distance) by:

$$\rho(\mathbf{r}) = \sum_{i}^{N} |\phi_i(\mathbf{r})|^2.$$

2.4.4: Total Energy Functional and Kohn-Sham Potential

Using the aforementioned KS equations, one can now get the total energy (as a function of density). The total energy is now given by[21, 47]:

$$E[\rho] = T_s[\rho] + \int d\mathbf{r}\; v_{\text{ext}}(\mathbf{r})\rho(\mathbf{r}) + V_H[\rho] + E_{\text{xc}}[\rho],$$

where T_s is defined as the KS kinetic energy. Looking back, this is where the old TF model had the largest failing (could not calculate an accurate kinetic energy). Although the KS kinetic energy is not the true kinetic energy, but when the orbitals are optimised it is a good approximation (much better than in the TF model). It is given by the KS orbitals, and expressed as:

$$T_s[\rho] = \sum_{i=1}^{N} \int d\mathbf{r}\ \phi_i^*(\mathbf{r}) \left(-\frac{\hbar^2}{2m} \nabla^2 \right) \phi_i(\mathbf{r}),$$

The term v_{ext} is an external potential acting on the system (such as electron-nuclei interactions). While the term V_H is the Coulomb energy (sometimes referred to as the Hartree energy) and is expressed as:

$$V_H = \frac{e^2}{2} \int d\mathbf{r} \int d\mathbf{r}'\ \frac{\rho(\mathbf{r})\rho(\mathbf{r}')}{|\mathbf{r} - \mathbf{r}'|}.$$

The E_{xc} term is the exchange-correlation energy (as discussed earlier in the section on LDA). The double integral in the above equation will result in something strange, of a particle interacting with its own field, which is due to the them term ρ(**r**) already containing the term **r**. However, under basic EM laws, the particle should not interact with itself, so this can lead to some error, if it does not get cancelled out by the exchange correlation energy (as it should in theory). This is sometimes referred to as the self interaction energy. In the HF method, it will be cancelled by the Slater exchange term. In DFT however, whether it will be cancelled or not depends on the XC approximation used, as discussed briefly in the next section. The KS equations would then be found by altering the total energy equation for a given set of orbitals, which will give the KS potential:

$$v_{\text{eff}}(\mathbf{r}) = v_{\text{ext}}(\mathbf{r}) + e^2 \int \frac{\rho(\mathbf{r}')}{|\mathbf{r} - \mathbf{r}'|} d\mathbf{r}' + \frac{\delta E_{\text{xc}}[\rho]}{\delta \rho(\mathbf{r})}.$$

The last term in the above equation is the exchange correlation potential:

$$v_{\text{xc}}(\mathbf{r}) \equiv \frac{\delta E_{\text{xc}}[\rho]}{\delta \rho(\mathbf{r})}.$$

It should be noted that the above term (and the energy it gives) are the only unknowns. When an approximation for this potential is found, the equations mentioned previously can all be solved. Since these equations rely on an exchange-correlation potential, the approximation used can make or break the accuracy of the calculation, so finding good approximations (that

are not too computationally expensive) is a source of continuous research. It will be discussed in more detail later on in the chapter.

2.4.5: The XC Potential and the Local Density Approximation

The approximation for the XC (exchange correlation potential) is key to good DFT results, since the exact functional for the correlation and exchange are not known, with the exception being the case of the free electron gas. There is constant research into finding better approximations, as some will work better in certain cases than others. However, there are a number of widely used potentials, such as the local density approximation (LDA), local spin density approximation (LSDA), and the generalized gradient approximation (GGA) as well as many others. For this research, LDA was used exclusively, so only it is discussed below.

LDA was originally developed by Kohn and Sham, and is one of the most widely used methods. The local density approximations are a group of approximations that are based on the density of electrons, not the wavefunctions. Specifically, the functional only depends on the electron density at the spatial coordinates at which it was evaluated at. This would get around the problem of dealing with complicated wavefunctions that the HF method suffered from when applying it to large systems. They are used to approximate the XC (exchange-correlation) energy in DFT calculations at a point in space. The best LDAs are derived from the HEG model (homogeneous electron gas). For a system with no spin polarization, the LDA for the exchange correlation energy is [27-28, 48]:

$$E_{xc}^{LDA}[p] = \int p(r)\epsilon_{xc}(p)dr,$$

where p is the electron density, and ϵ_{xc} is the exchange-correlation energy density, and it is a function of only the electron density. The E_{xc} (exchange-correlation) term is the linear combination of the correlation and exchange terms, E_c and E_x. The ϵ_{xc} term can also be thought of as the exchange-correlation energy of an infinite homogeneous electron gas that is moving through a steady, positively charged background that will neutralize the charge. This can be related to the exchange correlation potential through [52]:

$$v_{xc}^{\mathrm{LDA}}(\mathbf{r}) = \frac{\delta E^{\mathrm{LDA}}}{\delta \rho(\mathbf{r})} = \epsilon_{xc}(\rho(\mathbf{r})) + \rho(\mathbf{r})\frac{\partial \epsilon_{xc}(\rho(\mathbf{r}))}{\partial \rho(\mathbf{r})} \ .$$

The LDA has had good success, even with systems that are very inhomogeneous, and especially in systems where the electron density is slow to change. It does have its issues however, as the self interaction energy (discussed earlier) is not fully cancelled out. Although it is usually eliminated down to a few percent, it will increase the Coulomb repulsion and that will delocalize the electron density field. In general, LDA is known to over-estimate the bond length, and in solids underestimate the band gap. That is of importance to us here, and is discussed later[27-32].

2.4.6: DFT Process

The process involved with solving the KS equations is considered a self-consistent and iterative process. It will begin with an estimation of the electron density ($\rho(\mathbf{r})$), since the potential depends on this density. The process will start with creating both the potential and the exchange correlation terms (using the equations in the previous section). The following estimation of $\rho(\mathbf{r})$ comes from solving the KS equations and then made from the KS wave functions. This new density is found using the KS wavefunctions and then sent back to the start of the process (it is a cyclical process), and then the potential and the XC terms will be calculated again. As the DFT procedure approaches the ground state, there functions (and corresponding energies) should show less variance with each step. This means that the DFT process should converge at the ground state, and the convergence is watched to see whether the value of $\rho(\mathbf{r})$ is a good enough approximation for the actual density at the ground state. It should be noted that while one can always find a value for the energy of the system (one can input starting coordinates and calculate the energy based on that configuration), if one is running a structure optimization calculation, convergence may not occur. If the system breaks apart during structure optimization, there will likely not be convergence as every step in the calculation can move the atoms farther away from each other. Therefore, it is important to visualize the system if it is taken much longer to converge than expected, as the structure may be breaking apart (for more on the optimization process, see Section 2.9). A diagram what this process looks like is given below:

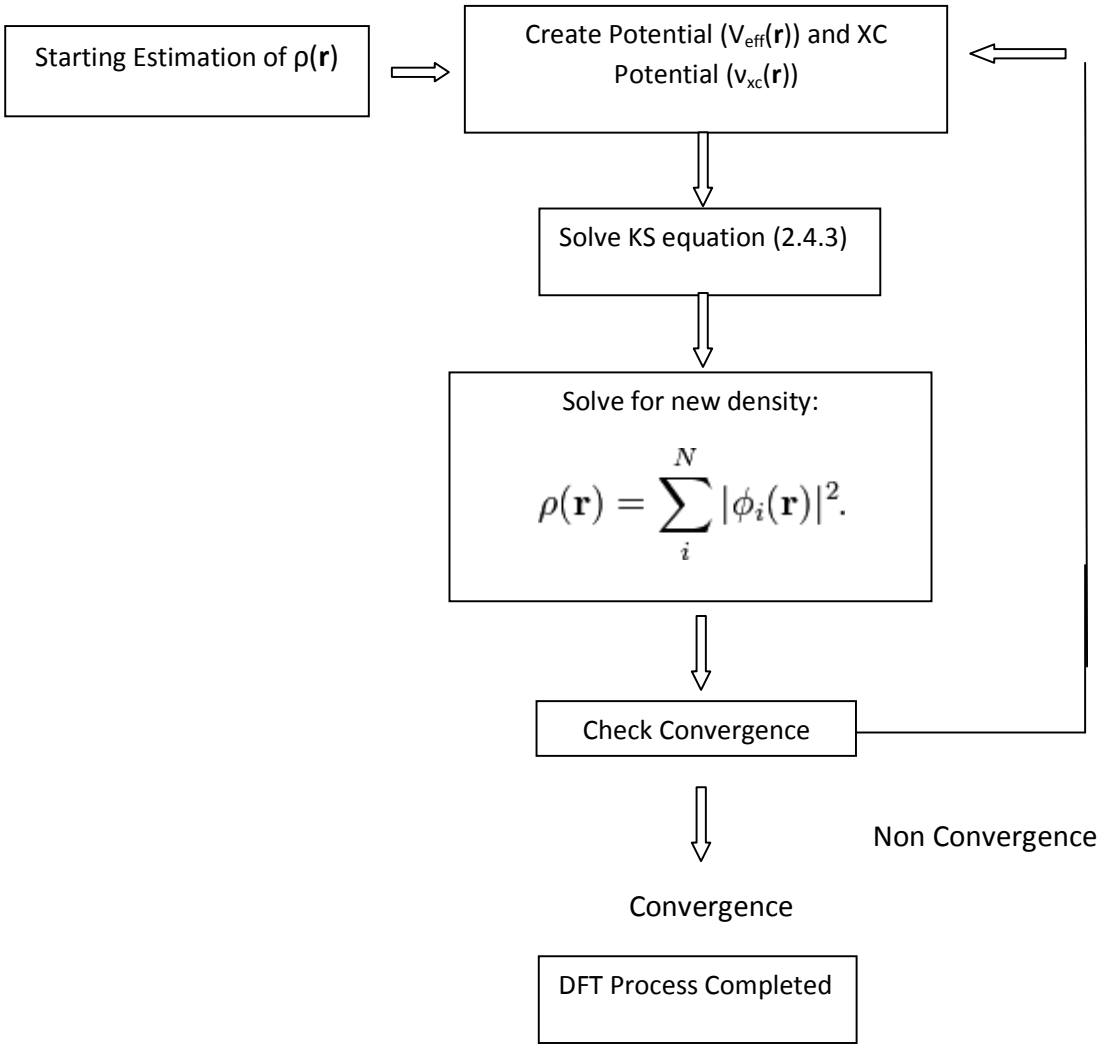

In most cases, the total KS energy will be use as the measure of whether or not convergence has been reached, as the energy will approach the global minimum as ρ(**r**) approaches the ground state electron density. Alternatively, convergence is sometimes defined as the input electron density and output electron density being equal. In some cases, it would be possible for the DFT process to get stuck at a meta-stable region (local minimum), but that is not usually an issue with current DFT programs.

This concludes the information the DFT in general, the next section will deal with DFT and how it is applied to solid state physics, such as in the case of a crystal lattice structure.

2.5 Crystal Lattice Structure and Bloch Theorem

In the case of solids, the situation is more complicated than that of a atom or simple molecule, since the properties of the solid can depend upon very large numbers of electrons, as there are a huge number of atoms in distributed throughout a macroscopic volume. For standard computational methods, that would be an enormous time cost, even for powerful computers if we were to try and compute the electronic structure of the whole system. In the case of crystal structures (those with a crystal lattice), this process is simplified hugely because the lattice is periodic. Since the same lattice structure, or supercell is usually small, and just repeated a huge number of times over, which allows one to consider just that cell for the purpose of calculations (something that cannot be done in a non-crystalline structure). This is done in the calculation by using periodic boundary conditions (PBC), which just repeat the cell over and over in the simulation, just like in a real solid.

Using these conditions as well as the geometry of the lattice itself, one can construct the reciprocal lattice. The Reciprocal lattice is defined as *all points with positions* $\vec{K}$ *such that* $e^{i\vec{K}\cdot\vec{R}} = 1$. *It is in reciprocal space (also known as k-space).* The primitive lattice vectors are typically defined as [a_1, a_2, a_3], and the reciprocal lattice vectors are given as [b_1, b_2, b_3] so that $\vec{K}$ = m_1b_1+m_2b_2+m_3b_3. The reciprocal space is useful for calculations, due to its connection to the crystal momentum as well as Fourier space (the Fourier transform of a spatial function is represented here). The reciprocal lattice has long been used with X-ray diffraction to find the atomic structure, and is again of use to us. The Brillouin Zone (BZ) is the primitive cell (specifically the Wigner-Seitz primitive cell) of the reciprocal lattice. This zone is where all the computational calculations will take place, using a sampling of k-points (also called momentum points) in this zone, with the density of k-points being proportional to the volume of the unit cell. Obviously, the more k-points used, the more accurate (and longer) the calculation will become.

Another useful theorem for these solid-state calculations is called Bloch's Theorem. A Bloch wave is defined as the wavefunction of a particle (in terms of the interest here an electron) inside of a periodic potential. The definition of this theorem is given below.

Bloch's Theorem: The eigenfunction for such a system may be written as the product of a plane wave envelope function and a periodic function (*periodic Bloch function*) $u_{n\mathbf{k}}(r)$ that has the same periodicity as the potential:

$$\psi_{nk}(r) = e^{ik\cdot r}u_{nk}(r)\,.$$

The importance of this is that the plane wave envelope part can be expanded as a series of plane waves, allowing all of the wavefunctions of the electrons to be expressed by plane-waves. This will become important and is discussed more in the next sections [33-34].

2.6: Plane-Waves

One of the most common expansions for DFT when working in solids is known as the pseudopotential plane-wave (sometimes referred to as PSPW, or alternatively plane-wave pseudopotential) method. It basically works off of a set of approximations and symmetries which work well within PBCs of a crystal lattice. It relies on the aforementioned PBC's as well as Bloch's theorem to create a plane-wave basis set. Referring back to the previous section, as it showed the electronic wavefunctions can be expressed as plane-waves, which is the key to how this works. A further approximation, known as the pseudopotential is also incorporated to simplify the plane-wave basis set and is discussed in the next chapter.

In theory, the basis could go onto infinity, as larger **k** values will result in electrons with higher kinetic energy. Due to the fact that the DFT calculations are for the ground state, one can reasonably assume that the wave-functions of the electrons can be given with a curtailed basis set which will only contain the plane waves below the cut-off energy (denoted E_{cut}). Basically, after a certain value of **k** (denoted as $\mathbf{k}_{cut}$), the coefficients for the plane-waves will become very small, and can be neglected, as they are higher than the energy of the electrons. However, one has to be careful to pick the right cut-off energy, as a value too low can lead to significant inaccuracy (although it can be fixed by increasing the cut-off energy). In this research, the cut-off energy varied, but is always in the range of 40-65 Ry. It is worth noting that a Rydberg (Ry) is a unit of energy that corresponds to about 13.61 eV.

2.7: Pseudopotentials

An important aspect of the PSPW method is of course, the pseudopotentials (or PP for short). In the standard Coulomb potential, effects of the motion of the core electrons, as well as the interactions with the nucleus would lead to a very complicated plane-wave basis set (as seen in the depth and steepness of the Coulomb potential, leading to sharp wave-function peaks). This in turn would take a huge amount of computational time, especially when dealing with large unit cells ore atoms with many electrons. In the pseudopotential (sometimes referred to as the effective core potential), it seeks to replace the aforementioned effects with a single effective potential This means that the Schrodinger equation will now contain the PP instead of the

standard Coulomb potential. It was brought about first by Hans Hellman in the 1930's, and the valence wave-function will still be orthogonal to the core states as is required. A visualization of this is shown below:

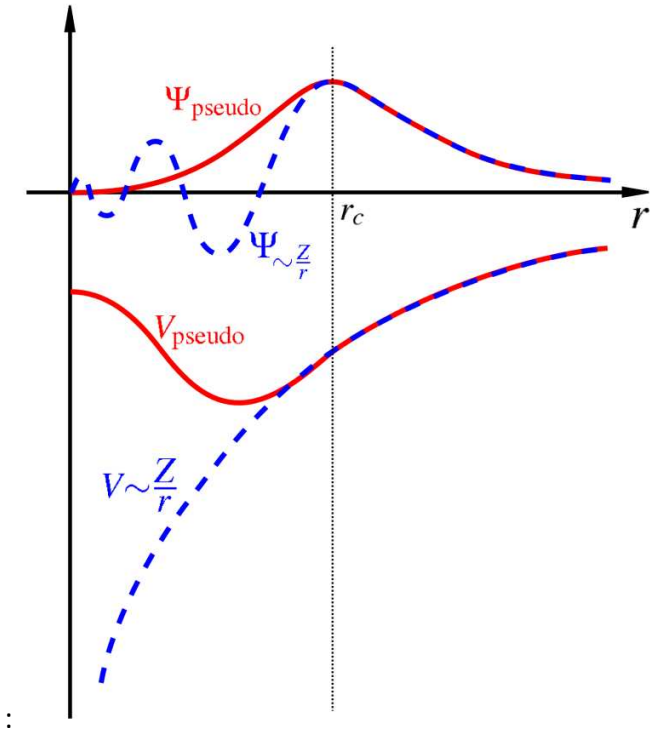

Figure 4: PP approximation: The above figure illustrated the difference between the Coulomb and PP, as well as the real and pseudo wave functions (the real values are blue, pseudo ones are red). As expected, the Coulomb potential is much steeper and deeper than the PP. As part of the requirements of a proper PP, the real and pseudo wavefunctions and potentials must match up after a certain radius (the cut-off radius, r_c).

When using the PPs, it is based on only the valence electrons will contribute to bonding, and only those electrons are explicitly dealt with, while the nucleus are core electrons are considered as an effective potential (which is a very good approximation, as the core electrons are bound very deep). Only having to deal with the valence electrons while maintaining good accuracy is a huge boon to solid state (and many other) calculations, and reduce computing time by a large degree. If the PP has a large r_c, then it is considered to be "soft", and will converge quickly, but be less accurate (again, the issue of accuracy vs. time creeps up again). Calculating the PPs is a whole other task, with many different PPs (and ways to calculate them) being available for the same atom, with some being more suitable in certain situations.

2.8: Born-Oppenheimer Molecular Dynamics (BOMD)

When using the Quantum Espresso program, a form of Ab-initio molecular dynamics known as Born-Oppenheimer molecular dynamics, or BOMD was used. In Ab-initio methods, the electronic behaviour and atomic motion is found through the use of first principles calculations, which in this case is DFT. Ab-initio methods differ from fully classical methods, due to the fact that in classical MD, the force field is represented by a single potential energy surface. Although the ab-initio method is more accurate due to the inclusion of quantum effects, it does take longer to perform the calculations, especially on larger systems. It should be noted that in the case here, the electronic structure is calculated using DFT, but the ions will move according to classical (Newtonian mechanics) [36].

BOMD gets its name from the Born-Oppenheimer approximation. It came out back in 1927, and has been used frequently to simplify quantum chemical/physical calculations. The basis for this is that it makes the approximation that the dynamics of the electrons are extremely fast, far faster than the (comparatively) slow motion of nuclei, that the electrons are treated as reacting instantly to the motion of said nuclei. This means that the two can be separated, and the wave-function can be separated into the electronic and nuclear (or as some would use, vibrational and rotational, respectively) components, giving:

$$\Psi_{\mathrm{total}} = \psi_{\mathrm{electronic}} \times \psi_{\mathrm{nuclear}}.$$

Step one of the BO approximation is solving the electronic Schrodinger equation, giving $\varphi_{\mathrm{electronic}}$. The nuclei are fixed in the equilibrium configuration (typically), and then used as the potential for the nuclei part of the Schrodinger equation, resulting in the latter part of the above equation. Since the nuclei are far heavier relative to the electron, the accuracy of the BO approximation is quite high.

In BOMD calculations, the time dependant ground state electron problem will be solved at each time step in the potential that is created by the nuclei, which are fixed. The steady-state electronic structure is then used to find the force on each ion at the corresponding time step. The ionic equations of motion can be integrated over a very large time scale. The equation of motion for BOMD is given by:

$$M_I \ddot{\mathbf{R}}_I = -\nabla_I \left[\min_{\{\phi_i\}} E^{\mathrm{KS}}[\{\phi_i\}; \mathbf{R}^N] \right],$$

where the total energy of the ground state is found using the KS equations and DFT, as discussed earlier [37].

The importance of BOMD in this research is for finding the vibrational frequencies of the graphene, graphane and the partially hydrogenated systems. Using pre-existing programs (as discussed in Chapter 5), the vibrational frequencies are calculated and then plotted to aid with experimental characterization.

2.9 Quantum Espresso and Molekel Software

The main computational program used for this research is called Quantum Espresso (QE). It is an open source computational software package, designed for use in material science calculations. The website's own description of the program is:

"Quantum ESPRESSO is an integrated suite of computer codes for electronic-structure calculations and materials modeling at the nanoscale. It is based on density-functional theory, plane waves, and pseudopotentials (both norm-conserving and ultrasoft)."

The theoretical background for DFT, plane-waves and pseudopotentials has been explained throughout this chapter. The pseudopotentials that were used were entitled "H.vbc.UPF" (hydrogen) and "C.pz-vbc.UPF" (carbon).

For the actual optimization procedure, the previously discussed DFT method (including LDA) is applied to a system from a set of input coordinates. The unit cell parameters (cell dimensions) were taken from previous work, and will not change during the calculations. Depending on the commands given in the input file, one can calculate the total energy at the current geometry, or if one wants to relax the structure (find the geometry of lowest energy), QE will move the atoms around, changing the bond lengths, bond angles, and in some cases the actual configuration (i.e. breaking certain bonds and creating new bonds elsewhere) of the structure. Depending on how far away from the minimum the input geometry is, there could potential be a large degree of structure morphing until the optimized geometry is reached.

The website for QE is "http://www.pwscf.org/", which the pseudopotentials can be found at "http://www.pwscf.org/pseudo.php". The most current version as of writing this thesis was v.4.2.1, released July 13, 2010 [35, 38, 39].

As for where the programs were run, all runs were done on SHARCnet (shared hierarchical academic research computing network) computers. The computers used were designated as "Bull", "Narwhal" and "Requin". It should be noted that as of February 2011, that "Bull" no longer exists and has been moved into a larger machine, "Kraken".

All of the pictures of the unit cells that were generated in this research were made using a program called Molekel, which describes itself as:

"Molekel is an open-source multi-platform molecular visualization program."

It can be found at "http://molekel.cscs.ch/wiki/pmwiki.php", and at the time of writing this thesis was on version 5.4 [39].

This concludes all the theoretical background on the methods and the programs used during the course of this thesis research. Starting in the next chapter, the findings of this work will be presented.

Chapter 3: Structure Optimization and Electronic Structure

3.1: Introduction

Quantum Espresso uses the methods described in the previous chapter (DFT, Plane-waves and Pseudopotentials) to optimize the geometry of the unit cells by finding the lowest energy configuration. It is sometimes referred to as energy minimization or structure relaxation.

It is worth noting that in the structures shown for many of the unit cells (especially the C_8 cells), there are not actually gaps/disconnects in the structure. Although in some of the unit cells it appears that there are atoms off in space, when the periodic boundary conditions are applied (as these are periodic systems) the atoms from the neighbouring cells with fill in any gaps/disconnects creating continuous solid.

3.2: Graphene and Graphane:

The first structures optimized were that of basic graphene and graphane, using C_8 and C_8H_8 unit cells, respectively. This was done so there would be a good starting point to work with (as many of the structures tried were base on the C_8 unit cells). The unit cells for graphene and graphane, respectively looked like:

Figure 5.1: The C_8 (graphene) unit cell

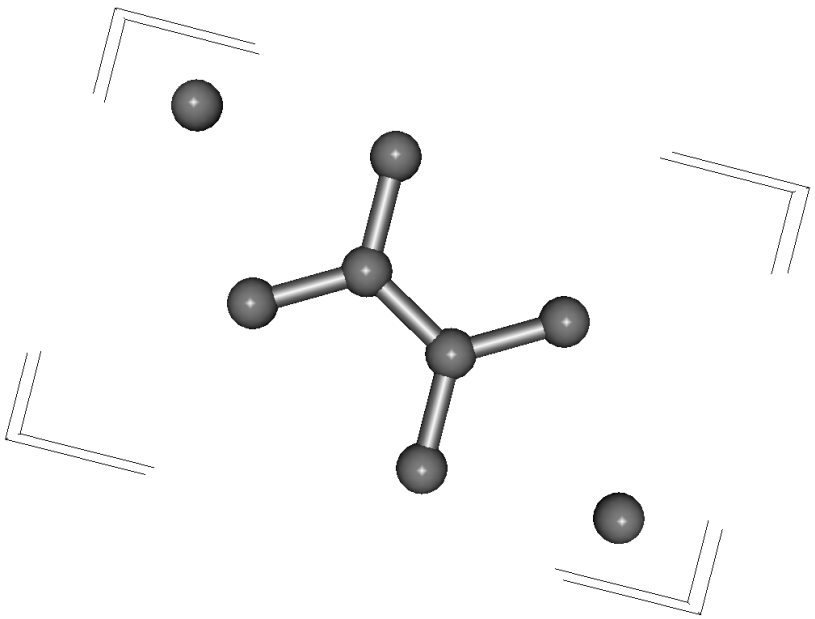

Figure 5.2: The C_8H_8 (graphane) unit cell

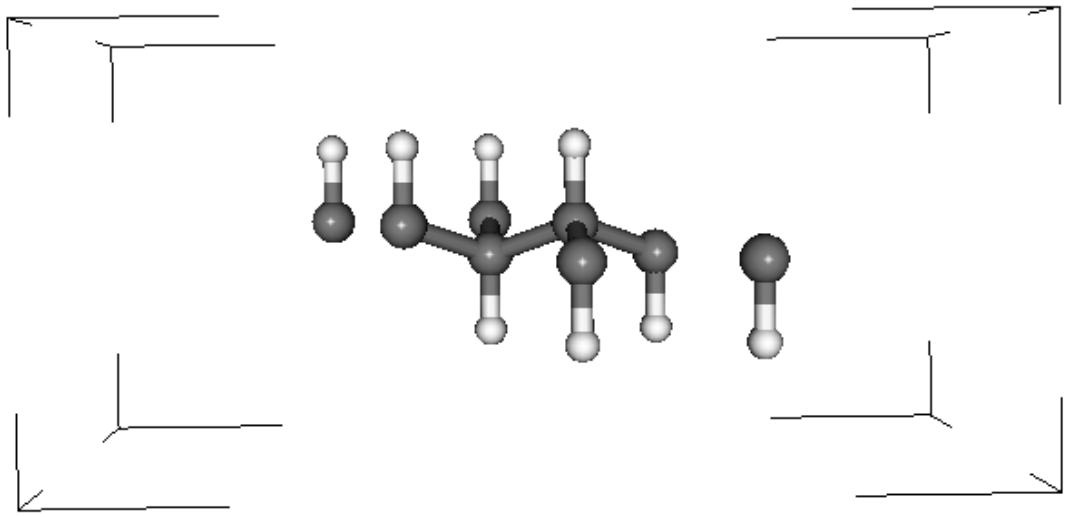

As mentioned previously, the band gap for graphene is 0, while the band gap of graphane is very high, as seen in the literature (**citation)**. It was hoped that taking the intermediate stages between graphene and graphane (partially hydrogenated graphene), would lead to more suitable band gaps. Thus, all of the structures tried using a C_8 backbone were done with 25%, 50% or 75% hydrogenation (meaning that that percentage of carbon atoms were bonded to a hydrogen atom). The next section of the chapter will deal with the C_8H_n structures.

3.3: C_8H_n Systems

This section incorporates the C_8H_2, C_8H_4 and C_8H_6, including geometries, energies and trends of the systems. The first systems to be looked at are the C_8H_2 unit cells.

3.3.1: C_8H_2 Systems

There were four separate types of C_8H_2 systems, which were denoted “Row” and “2H Up”. The term “Row” denotes that there were equal number of hydrogen atoms located above and below the carbon plane (in this case, one H is above the plane, and one H is below the plane). The “2H Up” denotes that both the hydrogen atoms are either above or below the carbon plane. The unit cells for the C_8H_2 Row and C_8H_2 2H Up, respectively are:

Figure 6.1: The Unit Cell for the C_8H_2 Row Structure

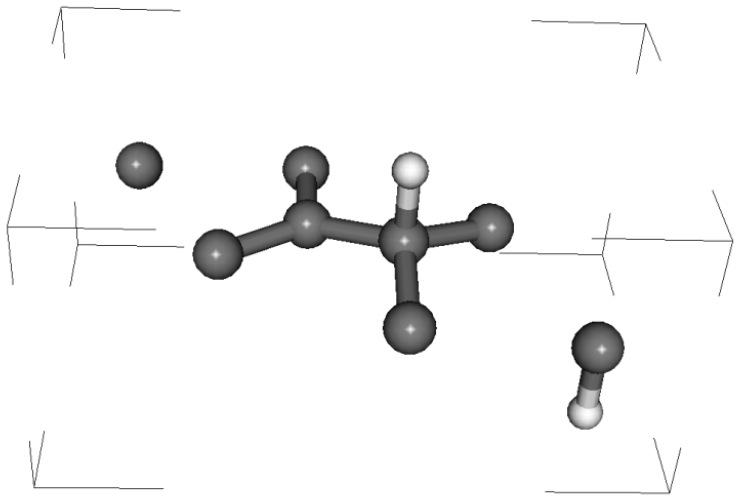

Figure 6.2: The Unit Cell for the C_8H_2 2H Up Structure

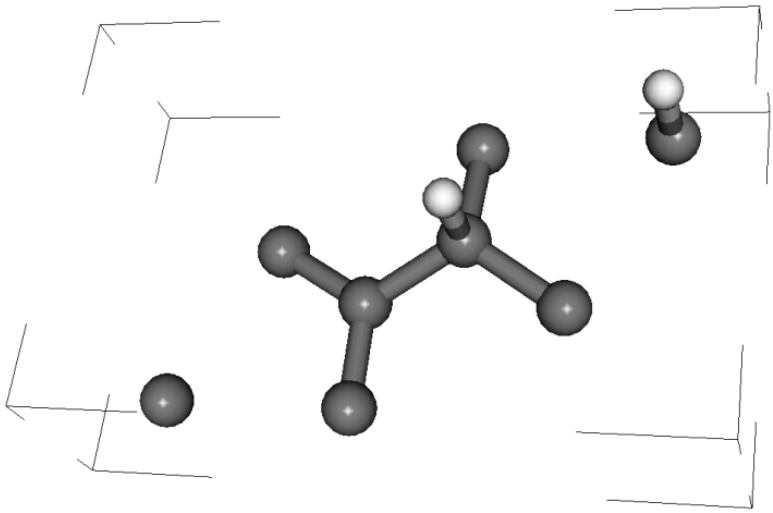

Figure 6.3: The Unit Cell for the C_8H_2 Row Middle Structure

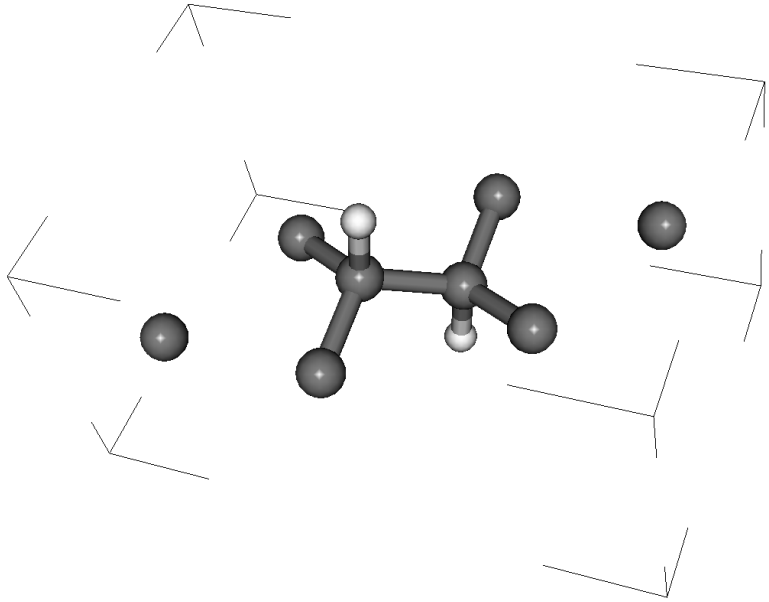

Figure 6.4: The Unit Cell for the C_8H_2 2H Up Middle Structure

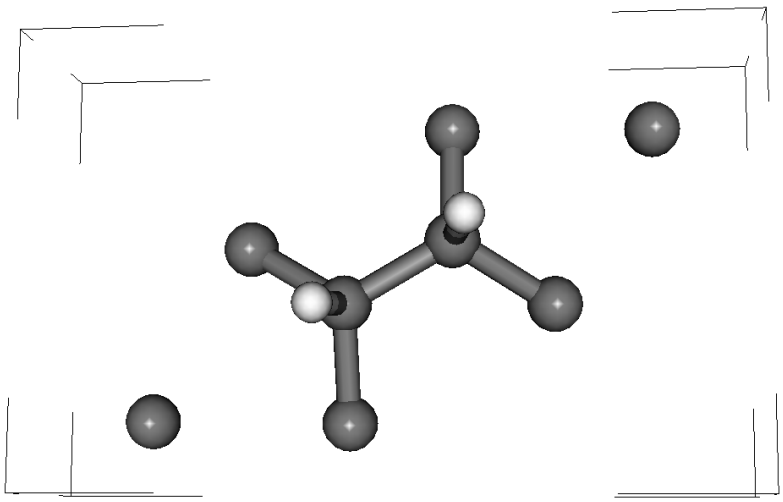

When comparing the energies of the 4 systems, the Row Middle structure had an optimized energy of -93.33000607 Ry, making it the lowest energy, while the 2H Up Middle structure had a final energy of -93.2782589717 Ry, making it the highest energy. It is seen in this case that the Row Middle structure is of lower energy, therefore the more favourable of the two structures. It is also worth noting that in the 2H Up case, if the H atoms are not put on adjacent carbon atoms (i.e. there is a C atom between the 2 C-H bonds), then the hydrogen will move to be on carbon adjacent to each other. A table of these values is shown below;

Table 1: Energies and Relevant Data for C_8H_2 Systems

% Hydrogen	Structure Name	Average Buckling (A)	Band Gap (eV)	Energy (Ry)
25	C_8H_2 Row	0.276	2.805	-93.317
25	C_8H_2 2H Up	0.256	4.124	-93.325
25	C_8H_2 Row Middle	0.662	0.831	-93.330
25	C_8H_2 2H Up Middle	0.590	0.639	-93.278

The term Average Buckling refers to how far, on average, the carbon atoms are from a flat shape. A higher average buckling value means that the carbon atoms are farther away from the flat plane. It was originally believed that the average buckling would have an effect on the band gap, which will be dealt with in the next chapter. In this case, the Row Middle shape had this higher average buckling, while the 2H Up middle had the lowest bad gap.

3.3.2: C_8H_4 Structures

There were a larger number of C_8H_4 structures tried than any other type, 6 in total. The six C_8H_4 structures were denoted: “Row”, “3H Up 1H Down”, “4H Up Straight”, “Row Other”, “Row Pair” and “3H Up 1H Down Straight.” The pictures of the unit cells and description of the different structures are presented below:

Figure 7.1: The "Row" Structure, has equal number of H above and below the C backbone. It also implies that the H are in an alternating pattern, with the first one being above the C, the second one below the C, and repeating that pattern.

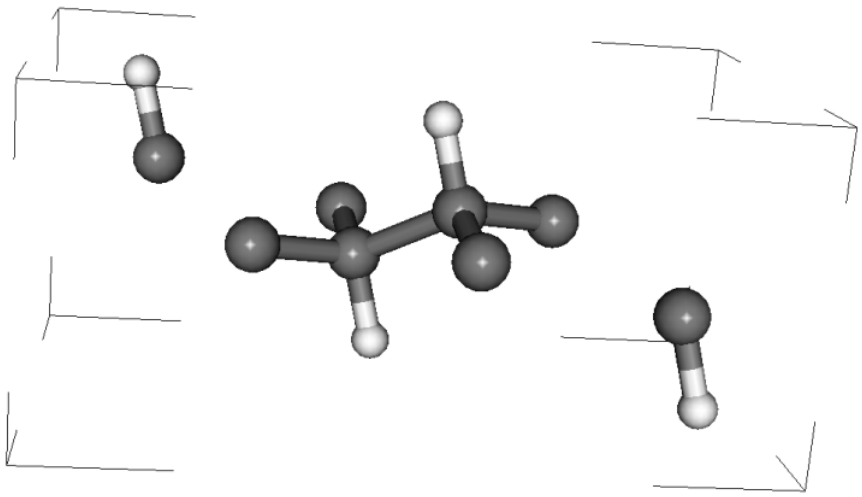

Figure 7.2: The "3H Up 1H Down" Structure, has 3 H atoms above the C backbone, and 1 H atom below the C backbone. This case is analogous to having 3 H atoms below the C, and one H above the C.

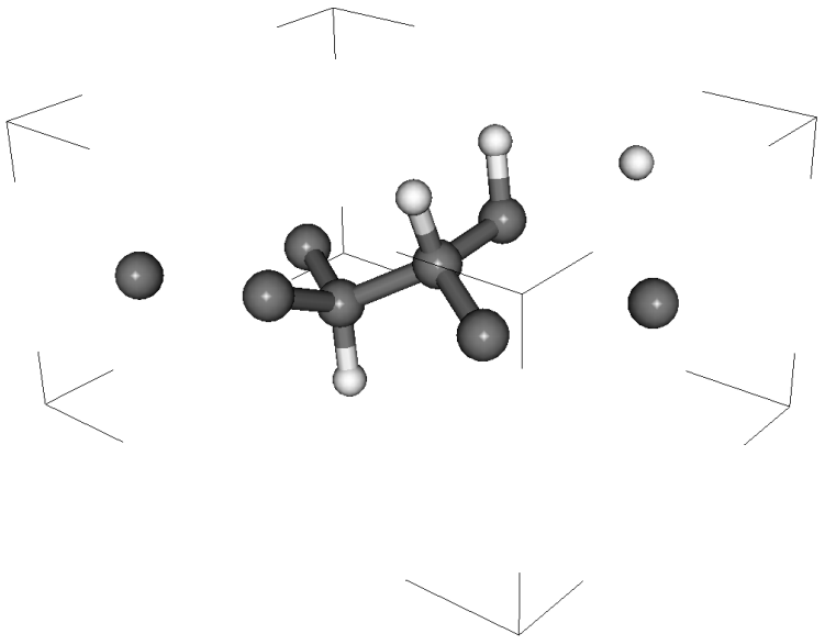

Figure 7.3: The "4H Up Straight" Structure, has all 4 H atoms above the C backbone. The H is also placed in a straight line across the 4 C atoms in the middle of the cell. This case is analogous to having all 4 H atoms below the C.

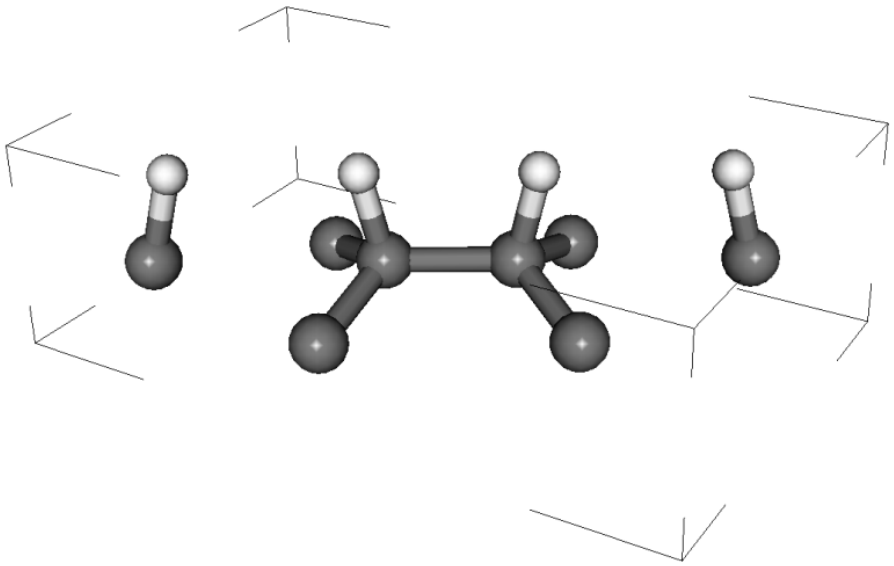

Figure 7.4: The "Row Other" Structure, is a variant on the standard "Row" structure. It has equal number of H above and below the C backbone, however in this case there is not the alternating up/down pattern, as some of the H will be beside H of the same orientation (both up or both down).

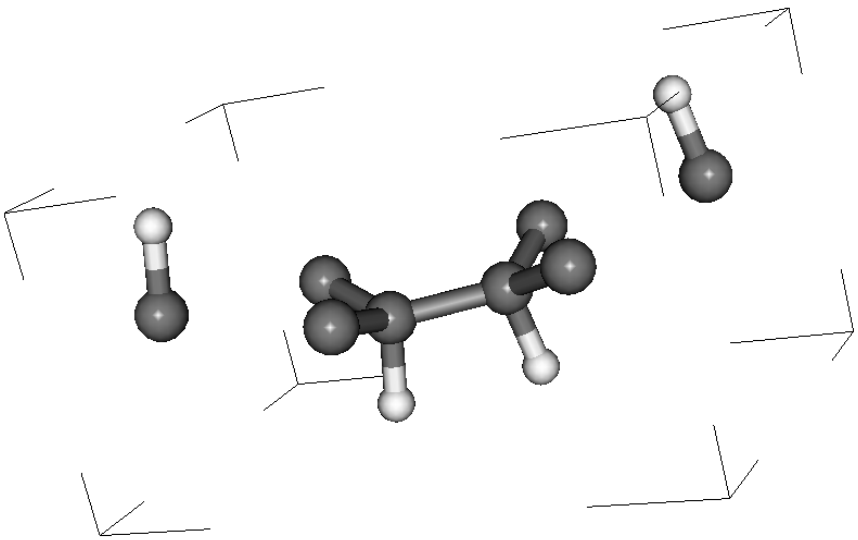

Figure 7.5: The "Row Pair" Structure, is a variant on the standard "Row" structure. It has equal number of H above and below the C backbone, however in this case there is not the alternating up/down pattern, as some of the H will be beside H of the same orientation (both up or both down). It is similar to the above structure, however the carbon backbone is farther from flat in this system.

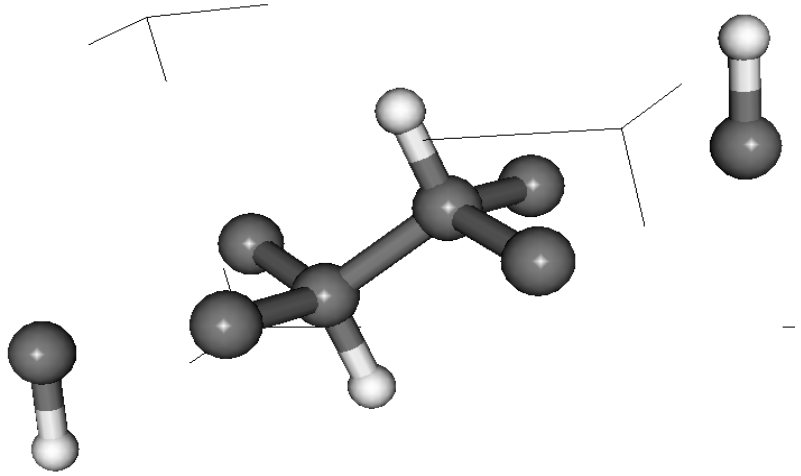

Figure 7.6: The "3H Up 1H Down Straight" Structure, has 3 H atoms above the C backbone, and 1 H atom below the C backbone. The difference in this case is that the H atoms are put in a straight line, meaning they are attached to the 4 carbon atoms in the middle of the cell.

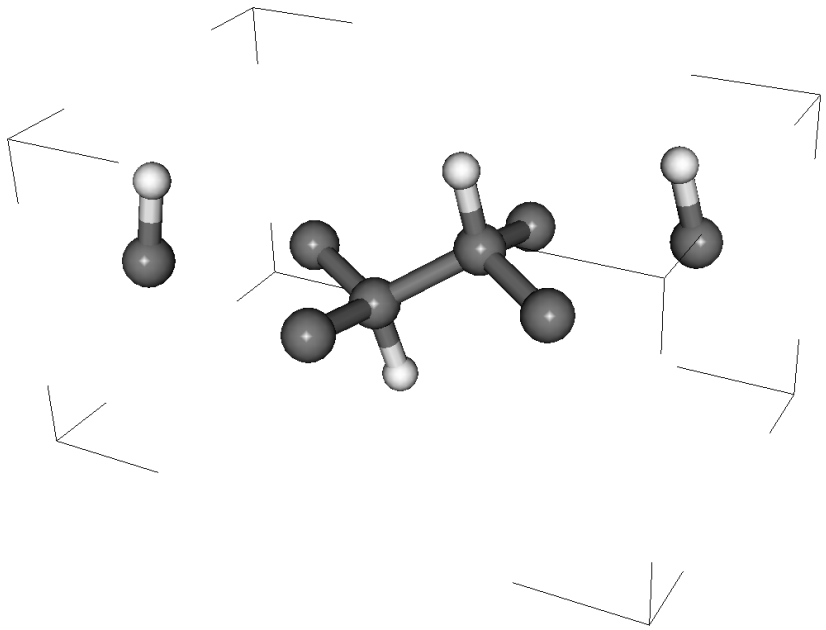

Table 2: Energies and Relevant Data for C_8H_4 Systems

% Hydrogen	Structure Name	Average Buckling (A)	Band Gap (eV)	Energy (Ry)
50	C_8H_4 Row	0.664	3.538	-95.652
50	C_8H_4 3H Up 1H Down	0.571	0.243	-95.599
50	C_8H_4 4H Up Straight	0.409	2.297	-95.515
50	C_8H_4 Row Other	0.574	1.22	-95.425
50	C_8H_4 Row Pair	0.496	3.995	-95.649
50	C_8H_4 3H Up 1H Down Straight	0.552	2.9	-95.557

In the case of the C_8H_4 structures, the "Row" structure was the lowest energy, while the "Row Other" structure had the highest energy, making the standard "Row" shape the most favourable. In terms of buckling, the "Row" shape also had the highest average buckling, while the "4H Up Straight" structure had the least buckling. The "3H Up 1H Down" system had the lowest band gap, while the "Row Pair" shape had the highest energy gap. In fact, the "Row" and "Row Pair" shapes both had a band gap calculated to be higher than that of graphane itself (about 3.1 eV). The band gaps/band structures will be discussed more in depth in the next chapter.

3.3.3: C_8H_6 Structures

The next logical step was to move to 75% hydrogenation while still using the C_8 backbone. In this case, there were 3 structures tried; "Row", "4H Up 2H Down" and "4H Up 2H Down Pair". The pictures of unit cells and descriptions are as follows:

Figure 8.1: The C_8H_6 Row Structure has an equal number of hydrogen atoms above and below the carbon backbone (in this case 3H). Also, along the 4 carbon in the centre, the H has an alternating up/down pattern.

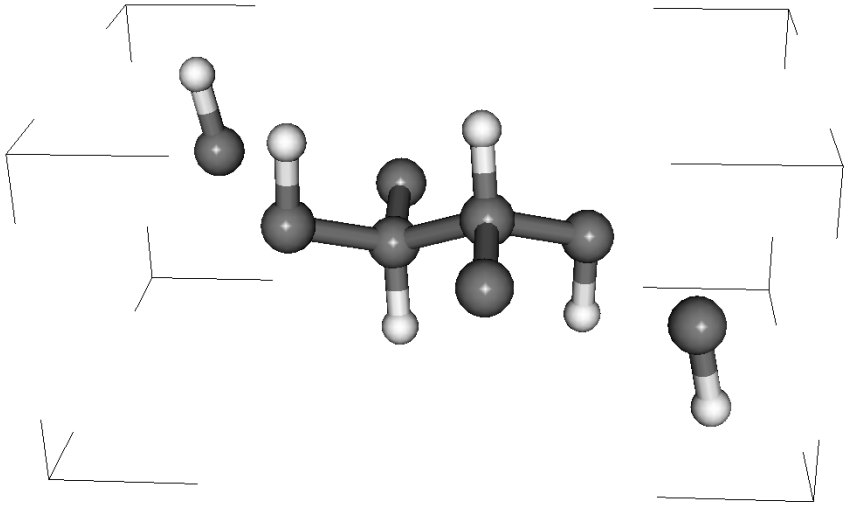

Figure 8.2: The C_8H_6 4H Up 2H Down Structure has 4 Hydrogen above the Carbon backbone, and 2 H below the Carbon backbone. It is analogous to the case of having 2H up and 4H down.

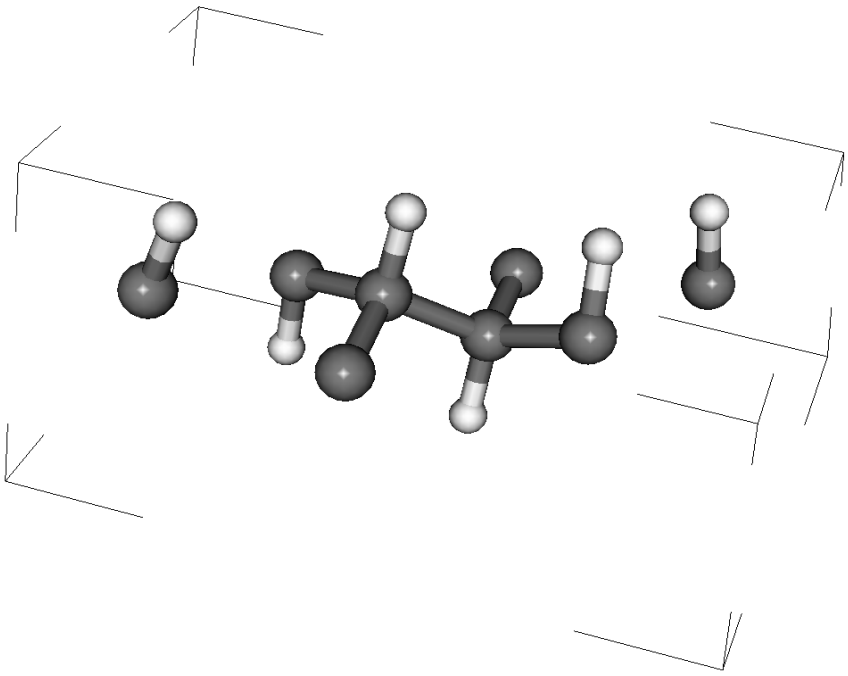

Figure 8.3: The C_8H_6 4H Up 2H Down Pair Structure has 4 Hydrogen above the Carbon backbone, and 2 H below the Carbon backbone. It is said to be "Pair" because there are groups of 2 H atoms with the same configuration (2H Up, 2H Down, 2H Up).

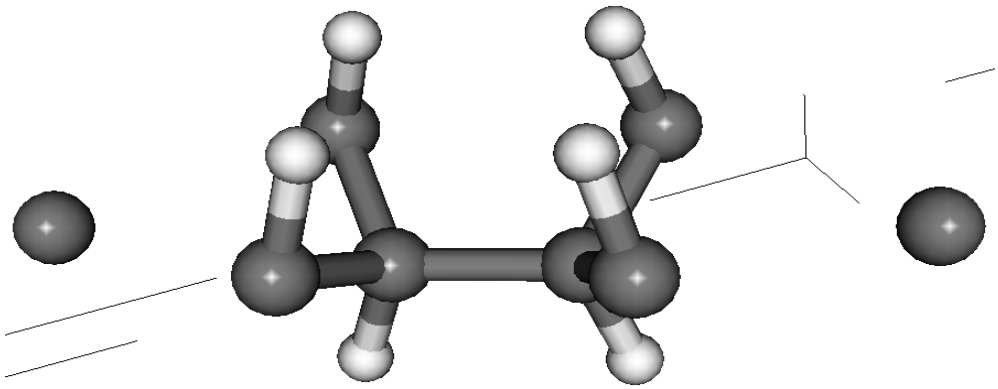

Table 3: Energies and Relevant Data for C_8H_4 Systems

%H	Structure Name	Average Buckling (A)	Band Gap (eV)	Energy (Ry)
75	C_8H_6 Row	0.567	3.302	-98.045
75	C_8H_6 4Hup 2HDown	0.615	2.985	-97.954
75	C_8H_6 4Hup 2H Down Pair	0.617	3.1	-97.975

In the case of the C_8H_6 systems, it is seen that the "Row" structure is the lowest energy state as well as having the lowest buckling. The "4H Up 2H Down" system is the highest energy and the highest buckling. The band gaps for these systems do not show the large variation that the C_8H_4 structures do, however the "Row" shape has the highest band gap, while the "4H Up 2H Down" has the lowest gap.

This concludes the structure optimization calculations for the C_8 unit cells. The next section of this chapter will look into the larger C_{16} unit cells.

3.4: $C_{16}H_2$ Structures

After completing the C_8 structures, it was noticed that the band gaps were very large in many of the cases, usually much larger than the 1-2 eV that would be ideal. It was believed that there was too much hydrogen in this system, and even 2H bonded to the C_8 cell was putting too much

stress on this system. It was reasoned that this hydrogen was buckling the system too much, and therefore was opening a gap that was too large. This will be discussed in more detail in the next chapter, but it was decided to move to the $C_{16}H_2$ unit cell, where it was believed that having only 12.5% hydrogenation would produce a smaller gap.

There were 4 systems tried with this composition; "$C_{16}H_2$ Row Close," "$C_{16}H_2$ Row Far," $C_{16}H_2$ 2H Up Close" and "$C_{16}H_2$ 2H Up Far." The "Row" and "2H Up" identifier denotes the same geometry as discussed earlier in the chapter, which the "Close" and "Far" denotes that the Hydrogen were placed either close together or far apart, respectively on the C_{16} backbone. In this case "close" means that the hydrogen atoms were separated by no more than one carbon atom. The unit cells and descriptions for these structures are below:

Figure 9.1: The $C_{16}H_2$ Row Close Structure has 1 H above the Carbon plane, and 1 H below the carbon plane. In this case, the 2 H atoms are bonded to carbon atoms that are adjacent to each other. It should be noted that the input file had a carbon atom with no H bonded to it between the carbon atoms that are bonded to the hydrogen (there was a separation of one carbon atom). After the optimization, the H atoms shifted to be adjacent carbons.

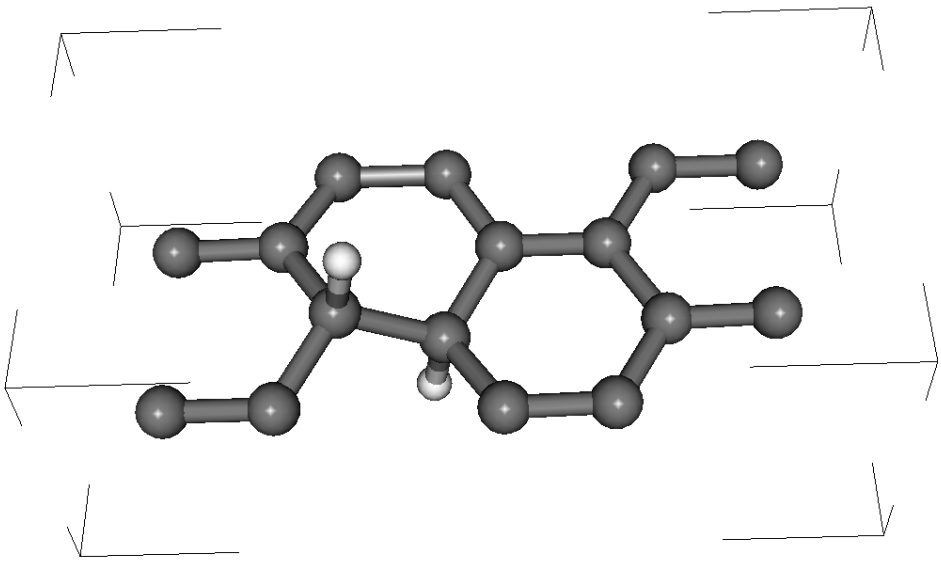

Figure 9.2: The $C_{16}H_2$ Row Far Structure has 1 H above the Carbon plane, and 1 H below the carbon plane. In this case, the 2 H atoms are separated by a multiple carbon atoms, which classifies it as the "Far" structure.

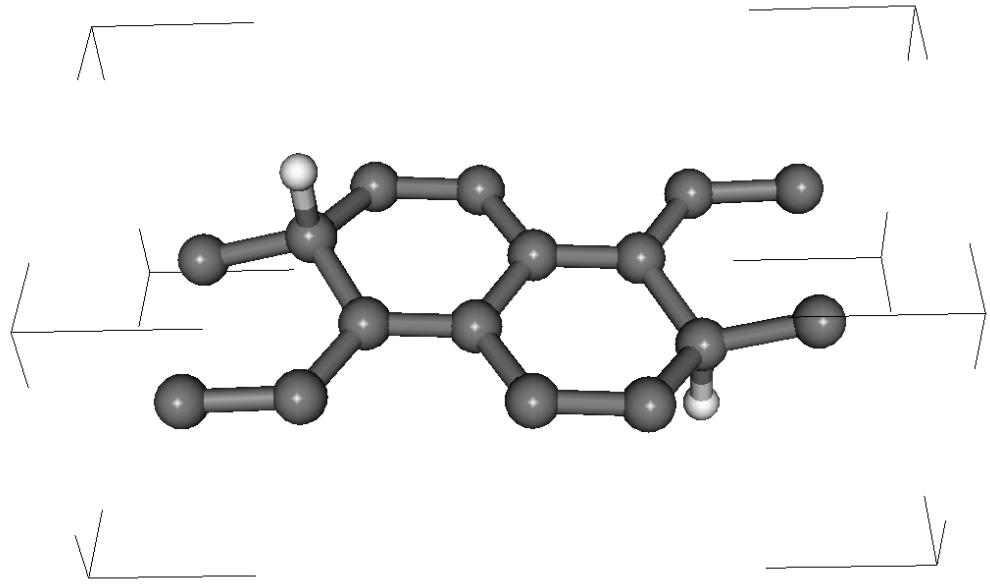

Figure 9.3: The $C_{16}H_2$ 2H Up Close Structure has both H atoms above the carbon plane. In this case, the 2 H atoms are bonded to carbon atoms that are not adjacent to each other, there is one carbon atom separating them. It should be noted that unlike in the "Row" case, the 2H atoms do not move to be beside each other.

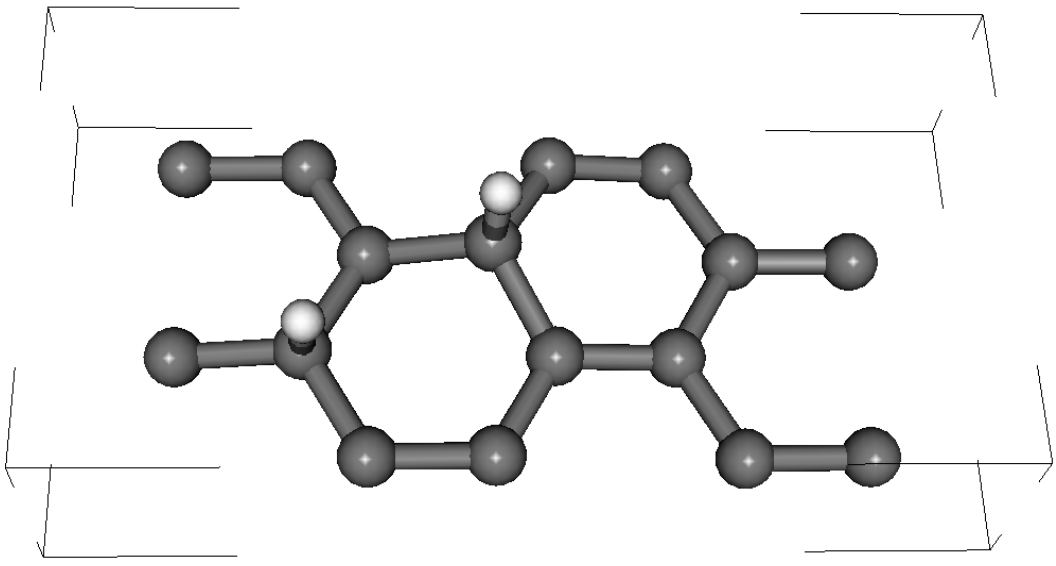

Figure 9.4: The $C_{16}H_2$ Row Far Structure has 1 H above the Carbon plane, and 1 H below the carbon plane. In this case, the 2 H atoms are separated by a multiple carbon atoms, which classifies it as the "Far" structure.

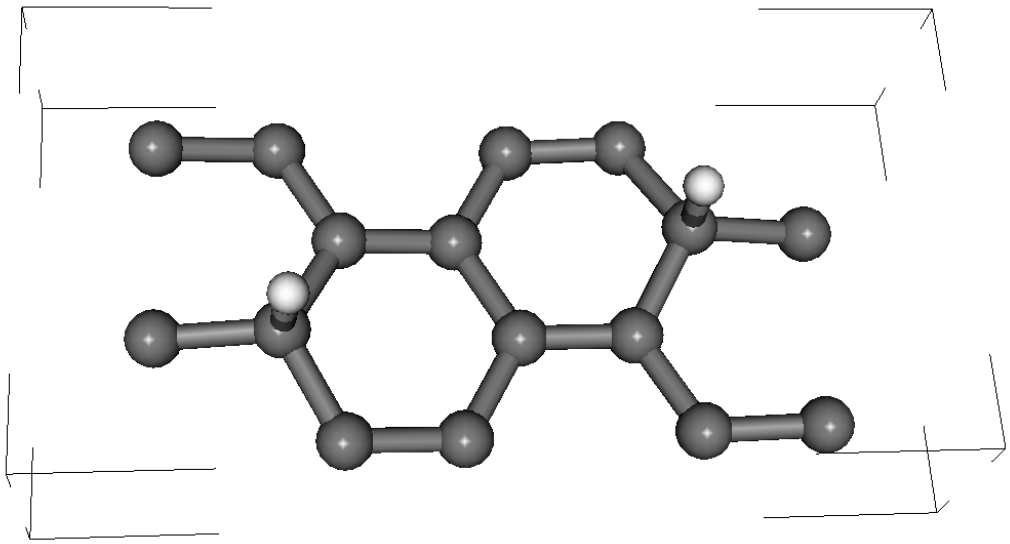

Table 4: Energies and Relevant Data for $C_{16}H_2$ Systems

%H	Structure Name	Average Buckling (A)	Band Gap (eV)	Energy (Ry)
12.5	$C_{16}H_2$ Row Close	0.124	1.751	-184.485
12.5	$C_{16}H_2$ Row Far	0.401	0.472	-184.415
12.5	$C_{16}H_2$ 2H Up Close	0.188	0.089	-184.325
12.5	$C_{16}H_2$ 2H Up Far	0.314	0.417	-184.405

When comparing these structures, it was seen that the structure of lowest energy and lowest buckling was the "Row Close" structure. It was also the structure with the highest band gap. The largest buckling was seen in the "Row Far" structure. The highest energy system was the "2H Up Close" system, which also had the lowest band gap. As mentioned earlier, for the "Row Close" structure, the input file had a carbon atom with no H bonded to it between the carbon atoms that are bonded to the hydrogen (there was a separation of one carbon atom). After the optimization, the H atoms shifted to be adjacent carbons. This did not occur in the 2H Up structure. As seen in the above tables, the band gaps for the C_{16} structures are much smaller than many of the band gaps calculated for the C_8 structures. As predicted, the lesser amount of hydrogen in the C_{16} cell did not distort the cell as much as with the C_8 cell, which lead to smaller band gaps. The factors that affect band gap will be discussed in more detail in later chapters,

but it is worth noting that buckling does play a secondary role in creating band gaps in these partially hydrogenated systems.

3.5: $C_{16}H_4$ Structures

To round out the C_{16} structures, there were 2 variants of $C_{16}H_4$ systems; “Row Far” and “4H Up Far”. The idea was to see if adding extra hydrogen to the C_{16} unit cell would lead to the high band gaps that were seen in the C_8 unit cells, or if the low band gaps seen in the C_{16} cells would remain. For a more fair comparison of energies between the C_8 and C_{16} unit cells, one should take the energy per 8 carbon atoms (i.e. divide the total energy of the C_{16} cells by 2). The descriptions and pictures are below:

Figure 10.1: The $C_{16}H_4$ Row Far has equal number of atoms above and below the carbon plane. In this case, the “Far” denotes that the H atoms are in 2 groups, with several carbon atoms in between the groups. This structure did experience strong buckling around the spots the H atoms were located.

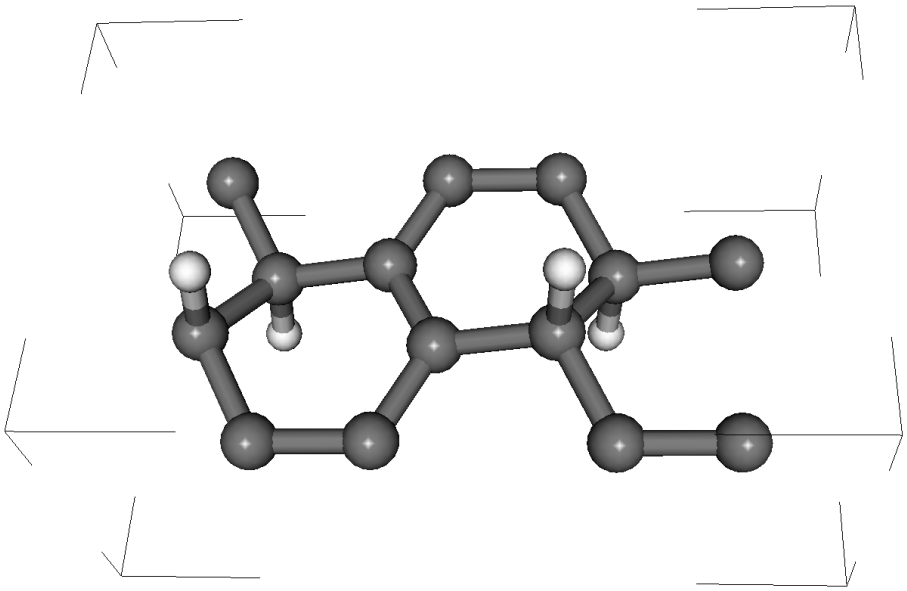

Figure 10.2: The $C_{16}H_4$ 4H UP Far has all 4 atoms above the carbon plane. In this case, the "Far" denotes that the H atoms are in 2 groups, with several carbon atoms in between the groups. This structure did not experience the same level of buckling around the spots the H atoms were located as the "Row" Structure did.

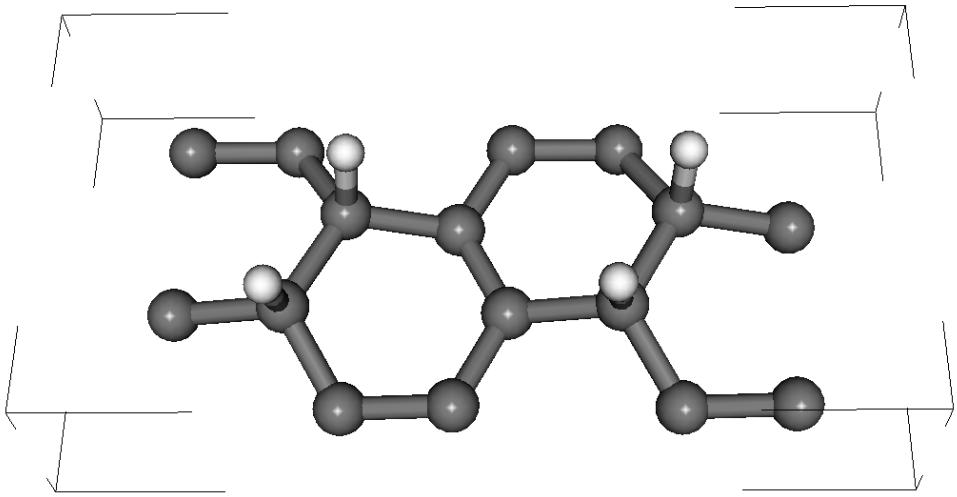

Table 5: Energies and Relevant Data for $C_{16}H_4$ Systems

%H	Structure Name	Average Buckling (A)	Band Gap (eV)	Energy (Ry)
25	$C_{16}H_4$ Row Far	0.314	0.343	-186.713
25	$C_{16}H_4$ 4H Up Far	0.355	0.701	-186.574

When comparing these systems, the "Row Far" system had the lowest energy, buckling and band gap. It was seen here that even though there was 25% hydrogenation (same as in the C_8H_2 structures), the band gaps here were much smaller. Therefore, it appears that the C_8 unit cells are too small and too much hydrogen to produce smaller band gaps, and that the C_{16} structures may be better suited.

3.6: Band Structures of Graphene and Graphane:

The band structure of graphene and graphane were well known at this point, so it made sense to compare the results given by the QE calculations to the actual band structure. This would determine how accurate the QE calculations were for graphene and graphene based systems. The band structure calculations for graphene and graphane (respectively) are given below.

Figure 11.1: QE Calculations of Band Structure for Graphene

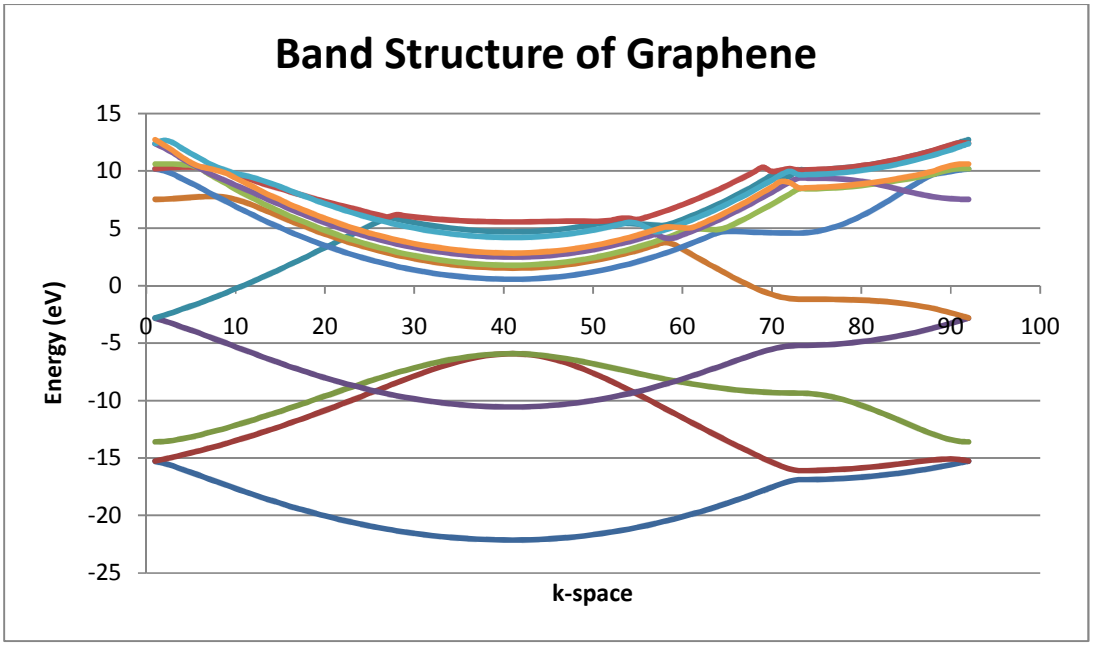

Figure 11.2: QE Calculations of Band Structure for Graphane

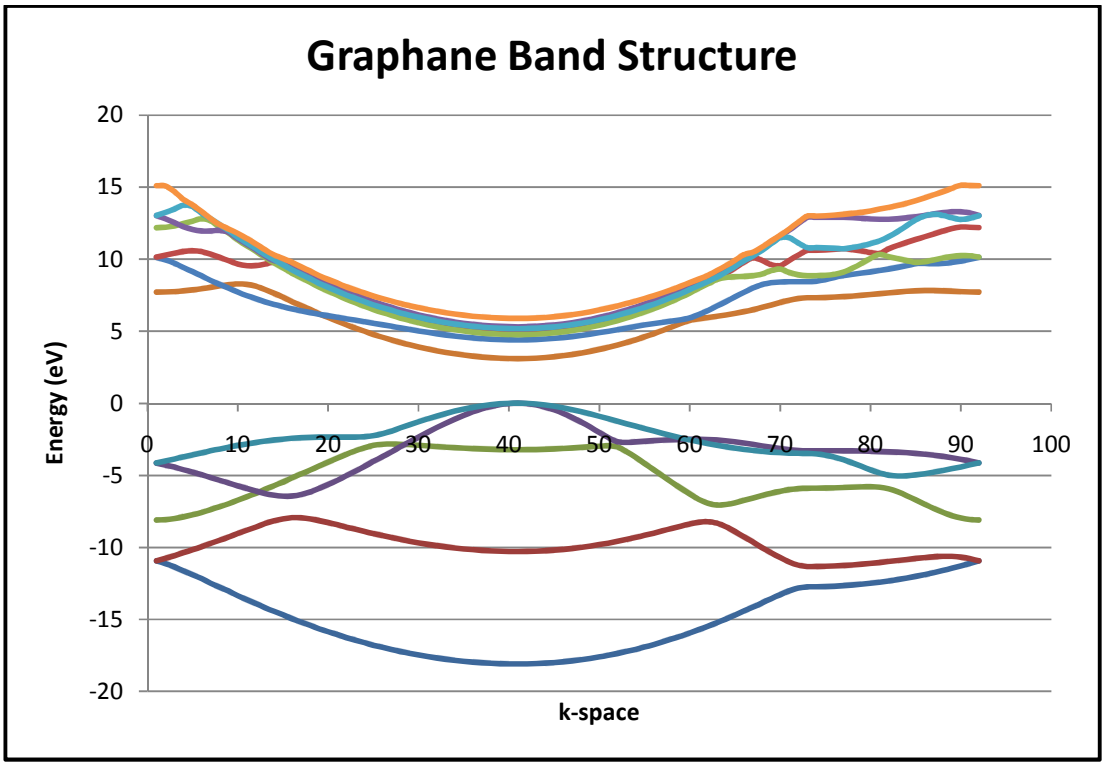

When looking at the actually band gap, the value for graphene was found to be 0 eV, and for graphane it was found to be 3.104 eV. The values (and shape of the band structures) were found to be in very good agreement with the actual values. Graphene has no band gap, and graphane has a band gap of about 3.1 eV when using DFT calculations. It is worth noting that DFT will underestimate the gap in these cases, and it should be around 5 eV.

The underestimation stems from DFT being primarily a ground state and one-electron method. In this method, one electron at a time is considered, and the other electrons are used as a self-consistent adjusted background that interacts with it as the electron is moved. This process is repeated for all the electrons. For band structure calculations, however, one excites electrons into the conduction band, so it is no longer purely a ground state situation. This excitation leaves a hole (empty space where an electron could have been, now seen as a positive charge), which must be accounted for. The DFT process should now count the electron + hole interactions against the electron background, however DFT negates the hole and still just counts the actual electron. This oversight leads to an underestimation of the band gap. There are computational methods to account for this underestimation, namely the GW corrections (or GW approximation), but that requires a huge amount of computational time and is not discussed here. The degree of underestimation is a known factor for graphane (about 2eV, or about 60%). Since these partially hydrogenated systems are similar to graphane, the factor of underestimation would be very close for all systems.

This underestimation means that the band gap results will be relative to each other, and not absolute. However, since the calculated values of the band gap were very close to what they should be for DFT calculations for both graphene and graphane when compared to the literature values, this method should be accurate enough to calculate the partially hydrogenated systems, which will be shown in the next sections.

3.7: Brillouin Zone Path

It is worth mentioning the path taken through the Brillouin zone that was taken in order to produce the band structures. More specifically, the path taken in the calculation borders what is known as the Irreducible Brillouin Zone, or IBZ. The IBZ is defined as the Brillouin zone reduced by all symmetries in the point group of the lattice. This further reduces calculation time as only the IBZ needs to be considered, and due to symmetry the IBZ can then be repeated to make up the full BZ. Graphene being a hexagonal lattice will result in the reciprocal lattice

also being a hexagonal lattice, making the BZ a hexagonal shape as well. An example of what the BZ and IBZ would look like is shown below: (**cite**)

Figure 11.3: BZ and IBZ for Band Structure Calculations:

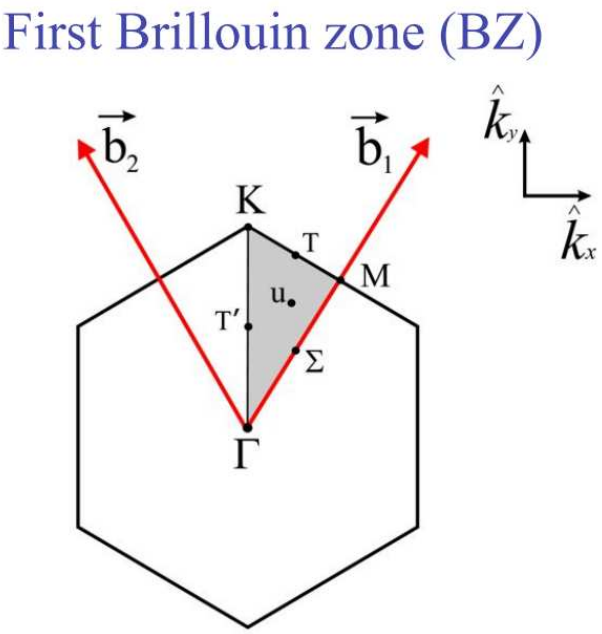

In the above picture, the white hexagon represents the BZ, the shaded region is the IBZ, and the red arrows denoted by $\vec{b}_1$ and $\vec{b}_2$ are the reciprocal lattice vectors. The letter K represents the middle of an edge joining 2 rectangular faces, M being the centre of a rectangular face, and Γ is known as the gamma point, denotes the centre of the BZ. The smaller letters T, T' and Σ are the midpoints of the edges of the IBZ, with u being the centre, but these points are not often used in band structure calculations and were not included in calculations for this thesis.

The path taken during the calculation starts at K, goes in a straight line to Γ, then from Γ in a straight line to M, then along the edge of the IBZ pack to K. The energy calculations are done on points along those lines (known simply as k-points), where the amount of k-points taken are included in the input file. A k-point grid is created using specified input values for the number of k-points taken in the X, Y and Z directions.

The Band Structure for graphene modified to include the points in the BZ is as follows:

11.4: Band Structure of Graphene Including BZ Labels:

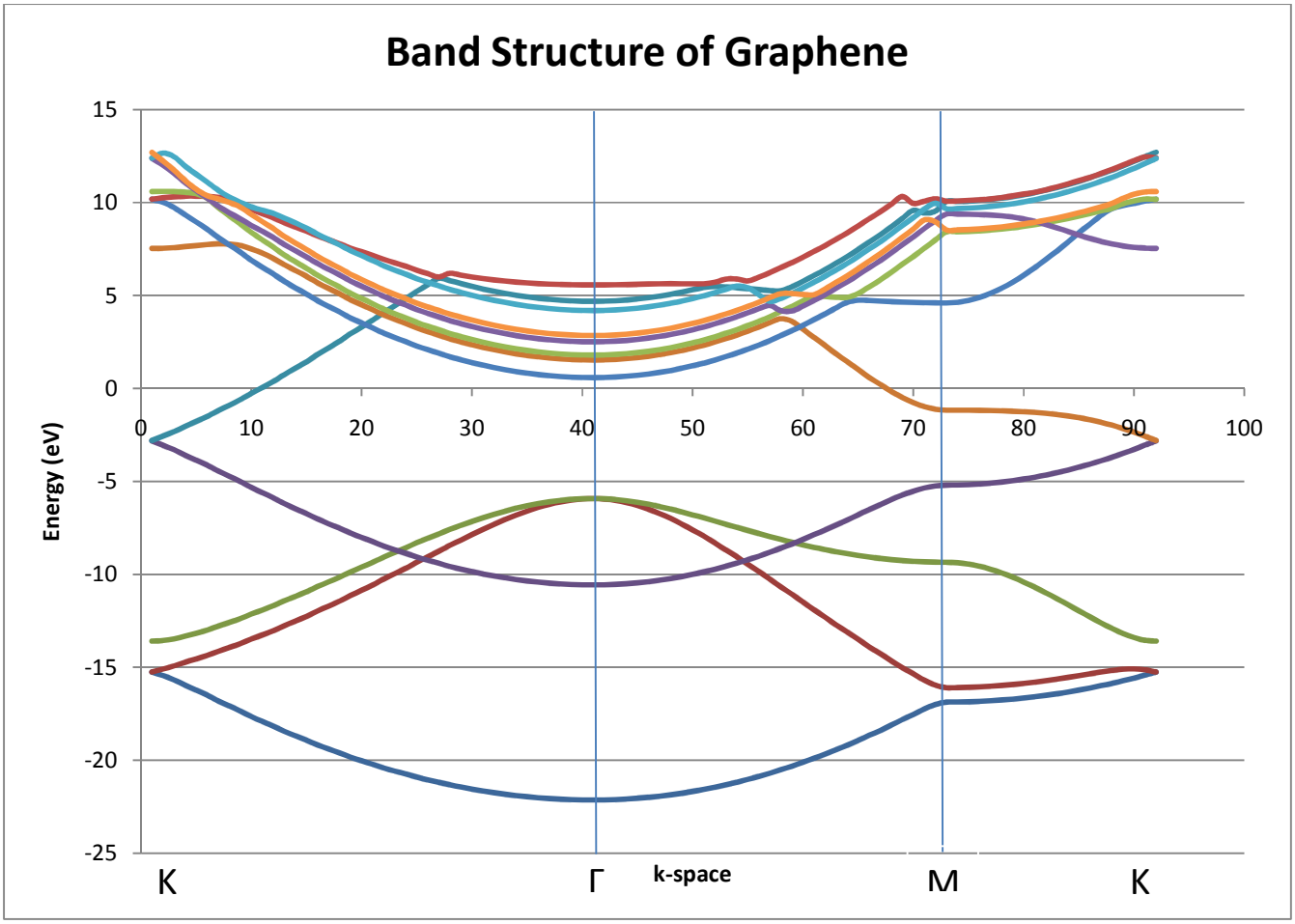

3.8: Comparison to Literature

Before proceeding with the research, it was pertinent to make sure that this methodology would be accurate. This was accomplished by comparing the QE calculations of the band structures of graphene and graphane, as well as the DoS of graphane to already known values published in the literature. Previously published band structures are shown below [53, 54]:

11.5: Literature Band Structures for Graphene and Graphane:

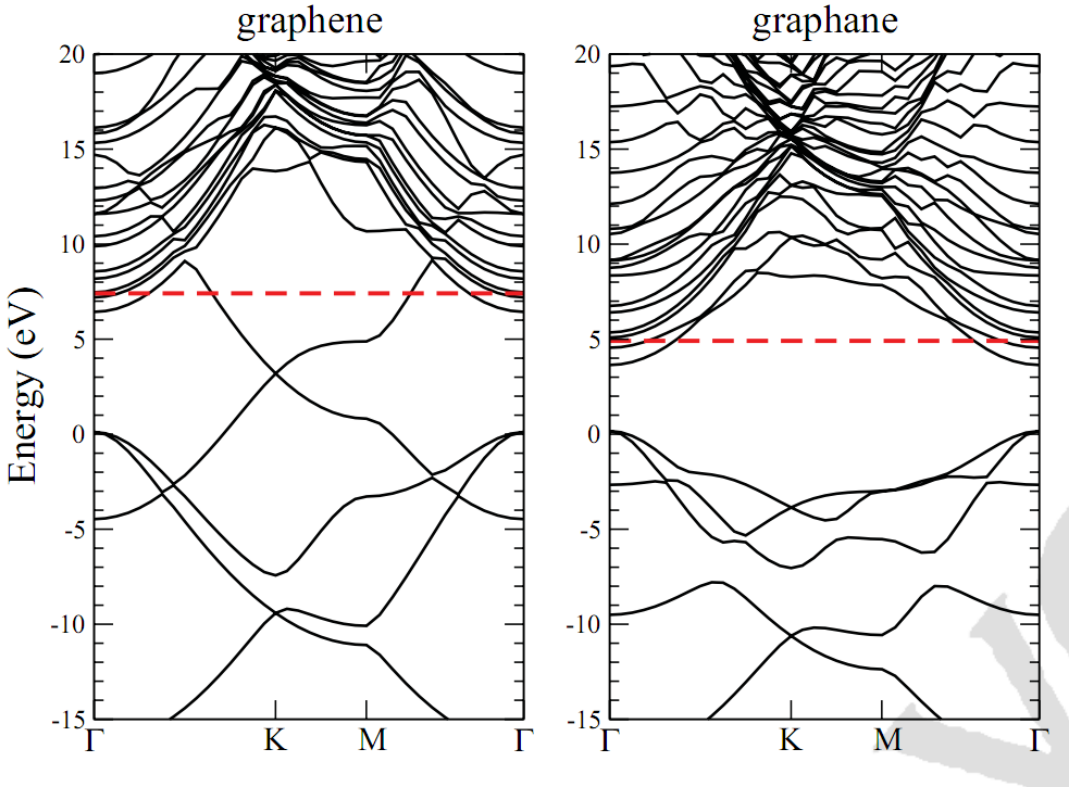

The above band structures are quite similar to the ones calculated by QE, although it should be noted that in the above structures the path through the BZ starts at the gamma point, instead of at K. The band gaps of graphene in the literature is seen to be 0 eV, while the gaps for graphane range between 3.1-3.5 eV, which compares well to the 0 eV and 3.1 eV, respectively found in this research. An easier to visualize band structure (with accompanying PDoS) is shown below:

11.6: Alternate Literature Band Structure and PDoS for Graphane:

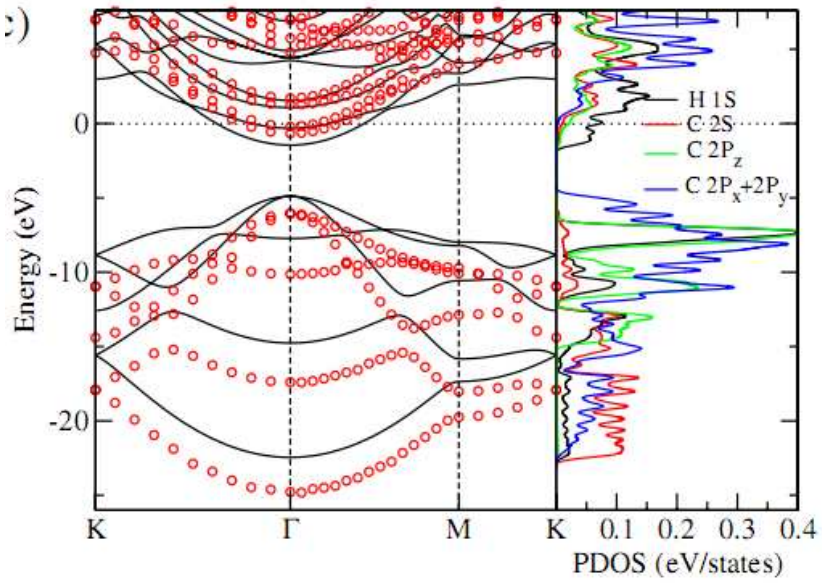

In the above band structure, the same path is taken through the BZ as in this research, and is again very similar, as is the DoS graph.

Due to the good matching between the literature band structures and band gaps of graphene and graphane with the calculated version of QE, there is good confidence the values for the partially hydrogenated systems will be accurate.

3.9: Possible Trends

After all the band structures were run, there was a strong belief that there would be obvious trends, such as the band gap being dependant on the hydrogen concentration, or the average buckling of the system. Since graphene has a band gap of 0, and graphane has a large band gap, it was reasonable to believe that going from 0 % hydrogenation (graphene), then 25%, 50% and 75% hydrogenation would produce a steady increase in band gap, and would peak at 100% hydrogenation (graphane). However, this did not emerge, as the following graph illustrates:

Figure 12: Graph of the relation between Hydrogenation of Graphene and Band Gap

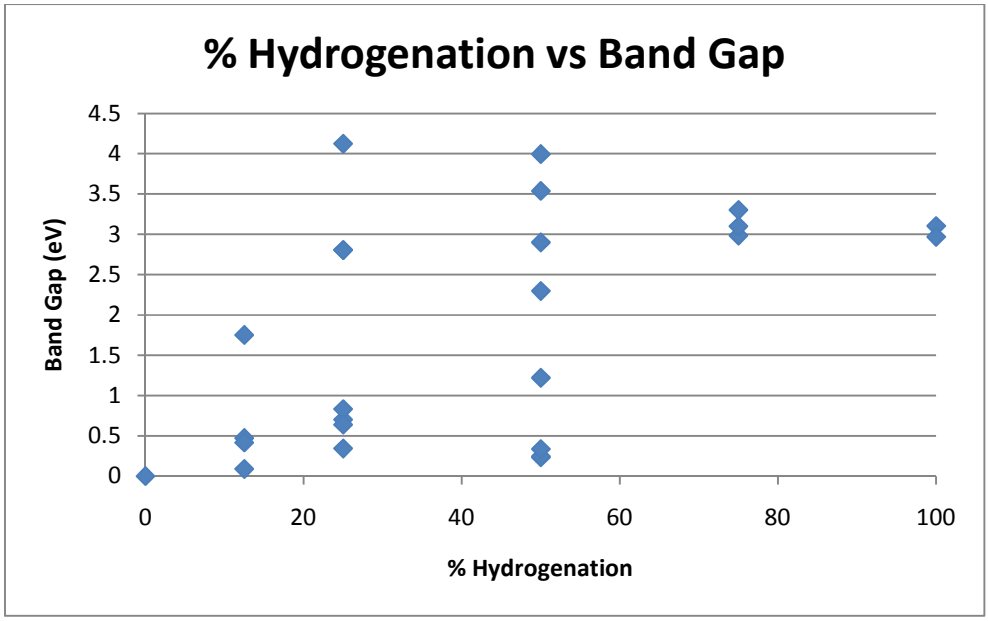

As seen in the above graph, no real pattern can be seen. The C_8H_6 structures have band gaps that are very close to graphane, so it appears that there is little difference from going between 75% and 100% hydrogenation. The 3 C_8H_6 systems all showed band gaps that were close to each other, and had the lowest difference out of all the different % hydrogenations, as the difference between the highest and lowest gaps was only 0.317 eV. The 50% hydrogenation had a huge variance in band gap, from 0.243 eV all the way up to 3.995 eV (a range of 3.752 eV). The 25% hydrogenation also showed a large variance, however the $C_{16}H_4$ systems had the lower two band gaps on the graph, and the C_8H_2 systems both had much higher gaps. The 12.5% hydrogenation systems ($C_{16}H_2$ structures) did in general have lower band gaps, with the highest being 1.751 eV, and the other 3 all having band gaps below 1 eV.

There is however one noticeable trend when going from the 50 % hydrogenation (C_8H_4) to graphane, where the band gap variance of the systems drastically drops. The variance in the C_8H_4 systems is very large, while the variance in the C_8H_6 is very small, and then drops off to none (or almost none). It seems that hydrogen content does play a role in determining the spread of the band gaps, if not the actual gap itself, as the 3 separate C_8H_6 all had different configurations, but very similar band gaps.

After finding that the hydrogen content was not the determining factor, it was theorised that the average buckling of the system could be determining factor of the band gap. When looking at a graph of average buckling vs. band gap:

Figure 13: Graph of the relation between Hydrogenation of Graphene and Band Gap

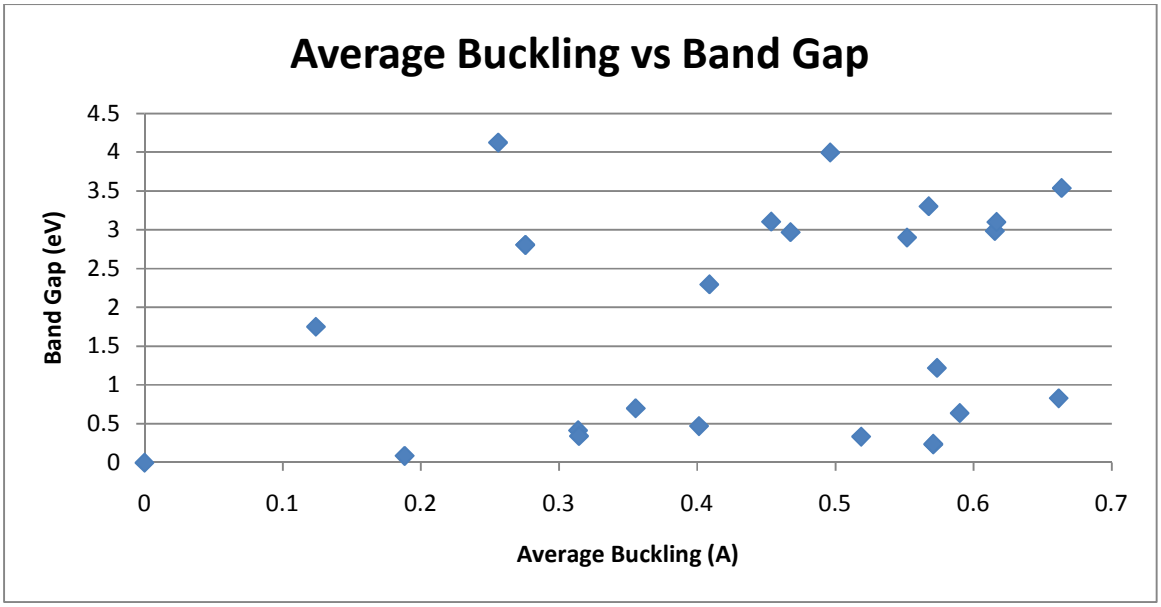

This graph appears even more scattered, and definitely no pattern emerges. While it is true that some of the highly buckled systems due have high band gaps, the system with the highest band gap does not have the highest buckling, and many systems with high buckling had small band gaps. It is clear that the average buckling does not play a large part in determining band gap.

When looking at the huge variance in band gap with the C_8H_4 (and to a lesser extent the 25% and 12.5% hydrogenated systems), the configuration of the system is more important than the hydrogen content, when looking at the C_8 systems. This would explain not only the huge differences in band gaps for systems with the same concentration of hydrogen, but also would show why some structures that were not fully hydrogenated had band gaps higher than that of graphane itself. It would also explain why the buckling of the system also did not have much importance. As mentioned before, it was believed that even 2 H was too much for most of the C_8 cells, but when discussing the large C_{16} unit cells, it seems that they can hold 2 or even 4 hydrogen, and still not have the gap open to near the extent of most of the C_8 systems.

It is worth taking a more thorough look at the C_8H_4 systems. As mentioned earlier, there is a huge variation in the band gaps of these systems, but it was unclear as to why this happens. It could be due to the way in which some of the hydrogen is bonded. In the structures with the highest band gaps, the "Row" and "Row Pair" systems, there is no case in where adjacent carbon atoms have hydrogen bonded to them, as well as those hydrogen atoms having the same configuration (both up or both down). In the remaining systems (excluding the 3H Up 1H

Down system as it likely has no gap), they all have at least one case per unit cell where this occurs, and it appears to lower (close the band gap).

This is not limited to the C_8H_4 systems either. In the C_8H_6 systems, the standard "Row" Shape is again the highest in band gap, however this time they are all closer together. This clumping of band gap is due to the configuration of the systems. In the C_8H_4 systems, the "Row" shapes produce the highest band gap, and the "2H Up" shapes have the lowest. When you reach the C_8H_6 systems, there is a high degree of hydrogenation. Even though the 14 atom unit cells shown earlier in the chapter do not show it, both the "Row Pair" and "4H Up 2H Down" structures have both 2H Up and Row (1 H up, 1 H Down) sections in the same structure when the structure is increased to a 32 carbon cell. The "Row" shape is the only one of the 3 that is a purely "Row" structure. Since there were only systems that included the Row configuration, all of the systems had a high band gap that were similar to each other. Although all the band structures were closes to each other, the Row shape was still the highest band gap, and again, the lowest energy.

There is undeniably a pattern that has developed. The 2H Up configurations produce lower band gaps than the alternating configuration in the Row structures. On top of this, the Row shape is of lower energy than the 2H Up shape, making the higher band gap configuration than most energetically desirable. An interesting pattern emerged when comparing the energy and the band gap in the C_8H_4 structures:

Figure 14: Energy vs. Band Gap for C_8H_4 Systems

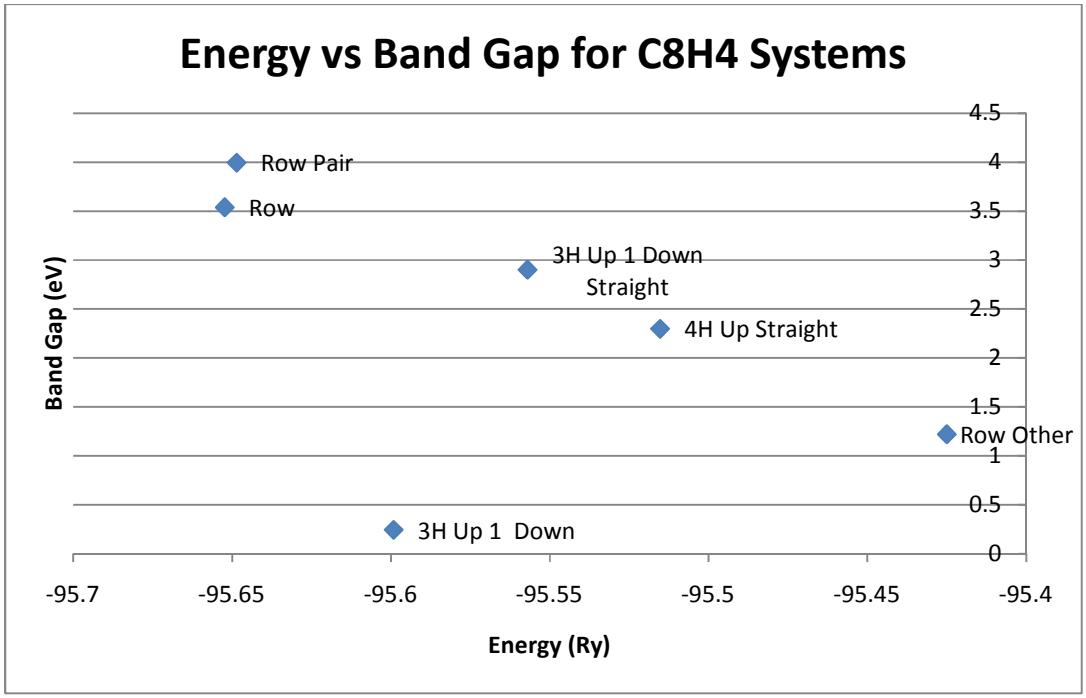

Looking at the above graph (if we exclude the 3H Up system, since the band gap is not really there), there is pretty linear increase for the energy and band gap for 4 of the systems, with the lowest energy system "Row" being slightly lower in band gap than the "Row Pair" system. Still, there is clearly a pattern that has emerged.

When looking at the reason that these patterns occur, it is likely that it has to do with the electron density of the systems. In standard graphene, there are dangling bonds (only three of 4 possible bonds are filled, leaving the other valence electrons free). In the case of graphane, there is no dangling bond, as the hydrogen atom makes the 4th bond (since there are no dangling bonds or Pi bonds, the graphane band gap is very large).

In the 2H Up cases the, C-H bonds are adjacent to on another (in at least part of the cell), since the bonds are beside each other, there is charge in that area. In the Row cases, there are no C-H bonds adjacent to each other and on the same side, so there charge density is reduced, as the C-H bonds are farther from each other. Since the electron density is lower in those regions in the Row shape, it is much more difficult for the charge to flow, and a lot of energy will be required to induce a current compared to the 2H up case.

As for the issue of why the energy is higher in the 2H Up cases, the C-H bonds will create a relative positive charge on the hydrogen atoms. Since the hydrogen atoms are close to each other, the positive hydrogen will repel each other (opposite to the hydrogen bonding effect). This repulsion will raise the energy of the system, while in the Row systems the hydrogen atoms are much farther away from each other and this repulsion will be much lower.

3.10: Discussion of Selected Systems

When examining all of the structures, it is clear that many of them fall outside the ideal 1-2 eV range. Most of the C_8 structures have an energy gap that is too large, and most of the C_{16} structures had a band gap that was too small. However, there are a number of systems that are in or at least close to the desired range. Below is the data for the 4 most promising systems:

Table 6: Table of Most Promising Systems Properties

% Hydrogen	Name	Band Gap (eV)	Average Buckling (A)	Energy (Ry)
12.5	C16H2_Row_Close	1.751	0.124	-184.485
25	C16H4_4Hup_Far	0.701	0.355	-186.574
50	C8H4_4Hup_Straight	2.297	0.409	-95.515
50	C8H4_Row_Other	1.22	0.574	-95.425

When looking at the above systems, it is clear that from the band structure calculations there are 2 systems that fit nicely into the range, the $C_{16}H_2$ Row Close system and the C_8H_4 Row Other. The other 3 systems are outside of the range, but as discussed previously are not out by a large amount, so they are still of interest. It is worth noting that none of the C_8H_6 systems tried appear in this list, as they have too high of a band gap (all around 3 eV, likely too much hydrogen on a small unit cell). Although the $C_{16}H_4$ 4H Up Far is below the threshold, since DFT is known to underestimate the band gap in these cases (such as with graphane), the real gap may well lie within the ideal range. Conversely, the structure with a band gap above 2 eV (C_8H_4 4H Up Straight) might actually have too large of a band gap, so employing the corrections to find the absolute band gap would be good work for the future.

There is another issue that exists, and that has to do with the energy of the systems. In the case of the $C_{16}H_2$ Row Close system, it is of a favourable band gap, and is also the lowest energy of the $C_{16}H_2$ structures (note that this only refers to the 4 structures that were run). Being the lowest energy would also make it the most energetically stable. In the other cases, they are not of lowest energy, and therefore would not be the most favourable configuration. However, since these structures have been shown to exist (computationally), as mentioned previously there could be an energy barrier that would need to overcome to cause the structure to shift, and these systems may still be stable.

3.11: Band Structure and DoS of Selected Systems

The following graphs are the results of the band structure calculations for the selected systems:

Figure 15.1: $C_{16}H_2$ Row Close Band Structure

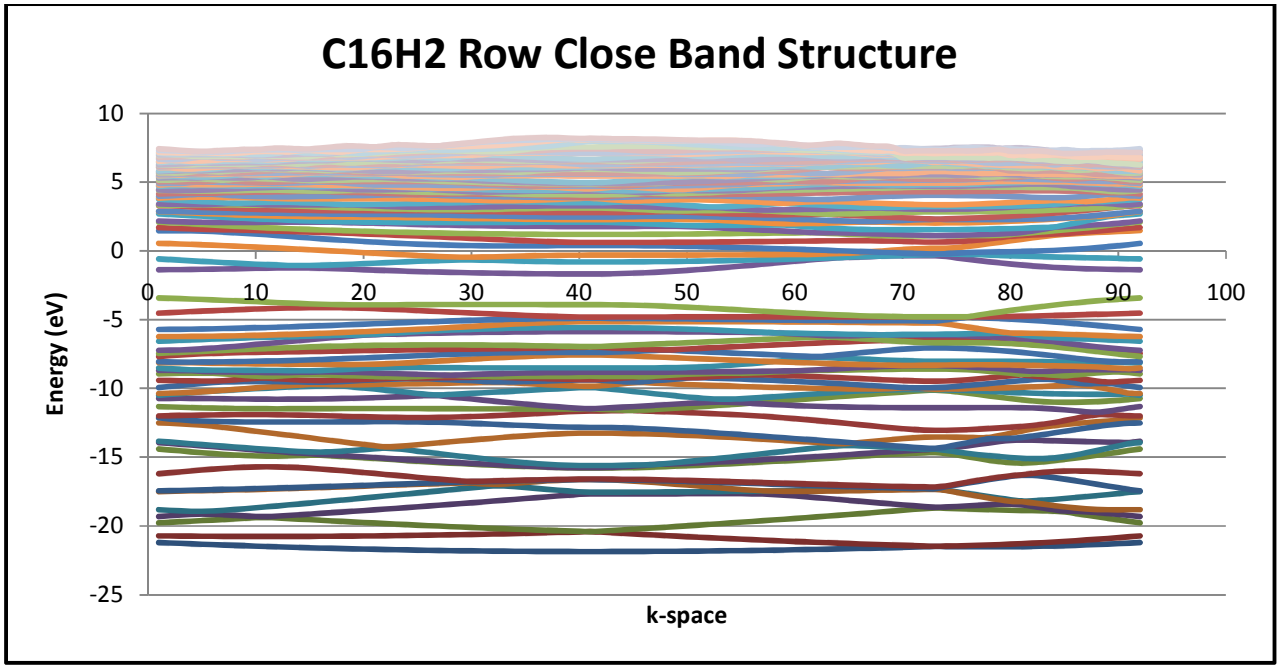

Figure 15.2: $C_{16}H_2$ Row Close Density of States

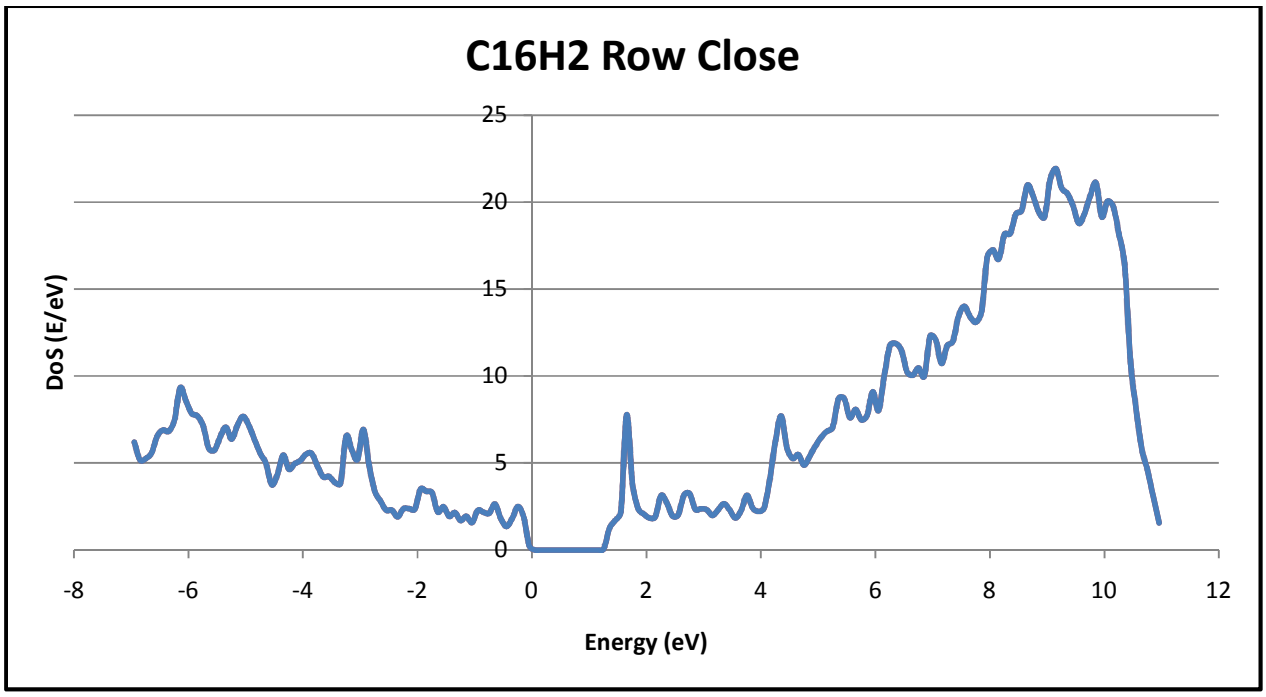

Figure 15.3: $C_{16}H_4$ 4H Up Far Band Structure

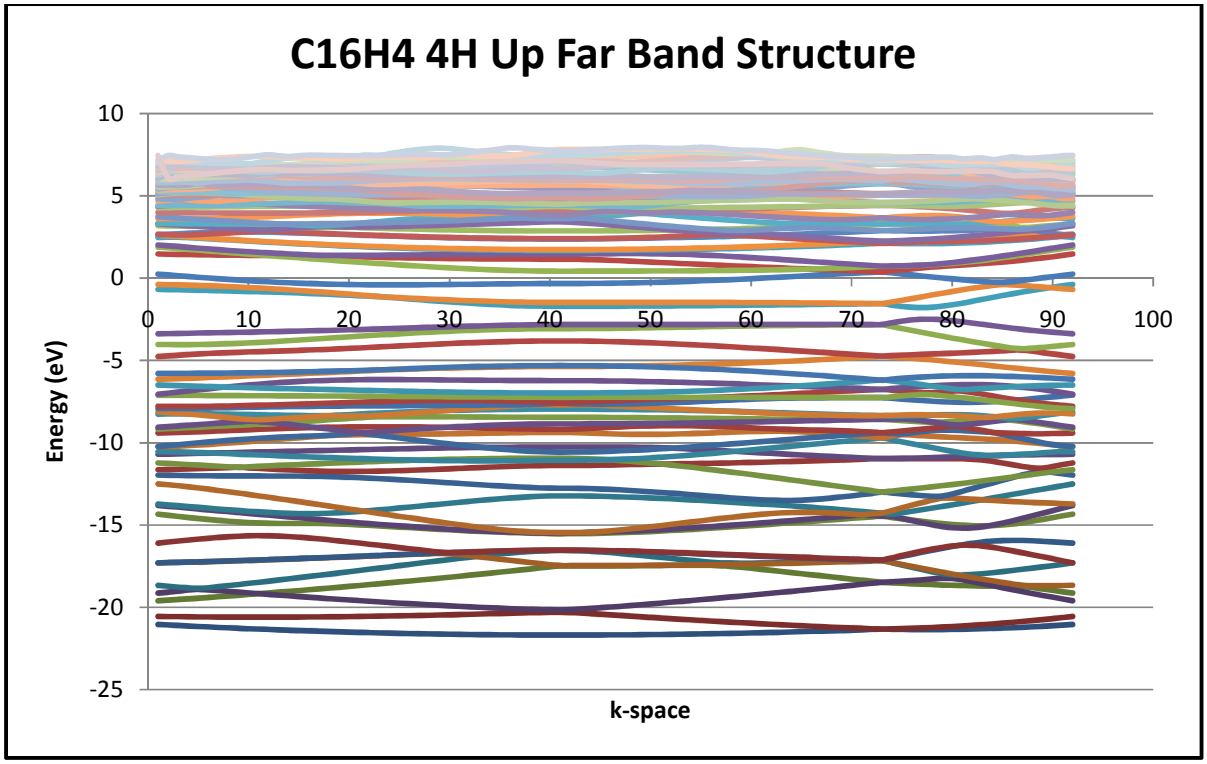

Figure 15.4: $C_{16}H_4$ 4H Up Far Density of States

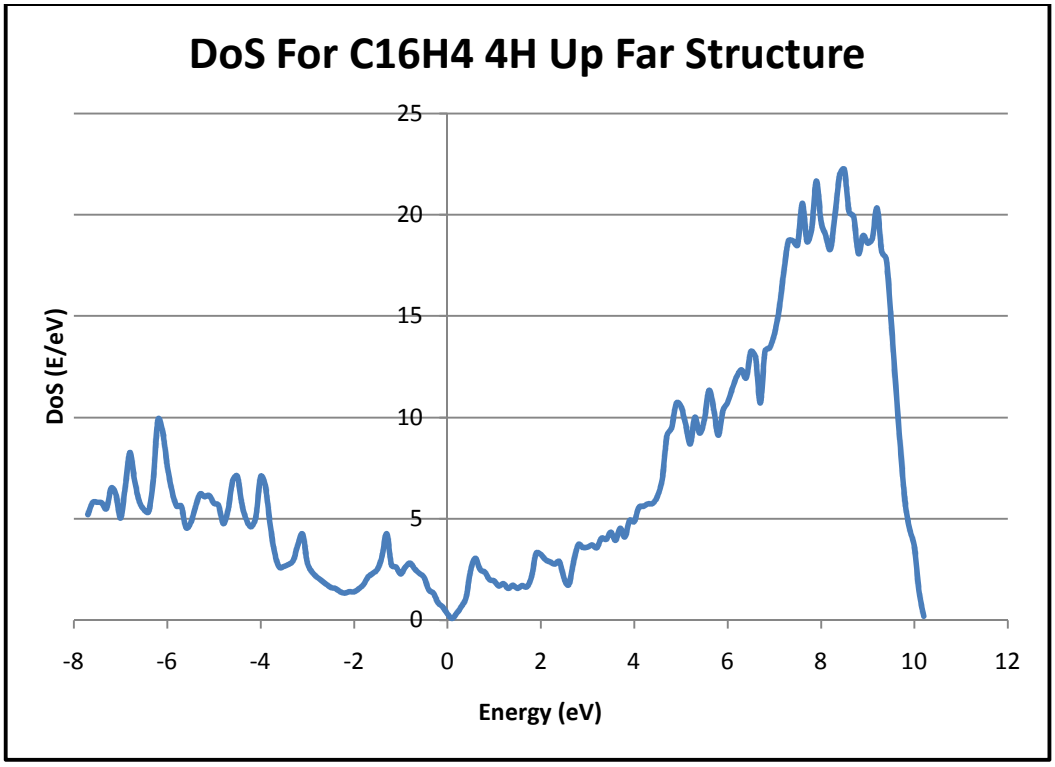

Figure 15.5: C_8H_4 4H Up Straight Band Structure

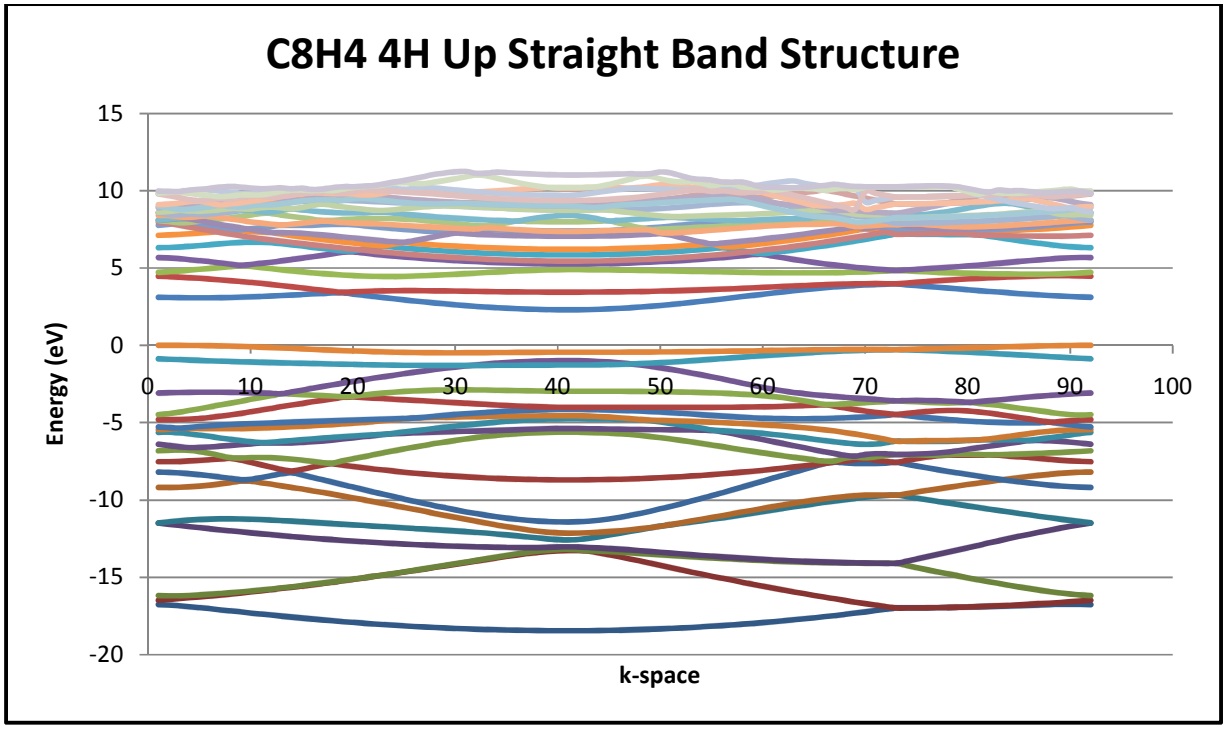

Figure 15.6: C_8H_4 4H Up Straight Density of States

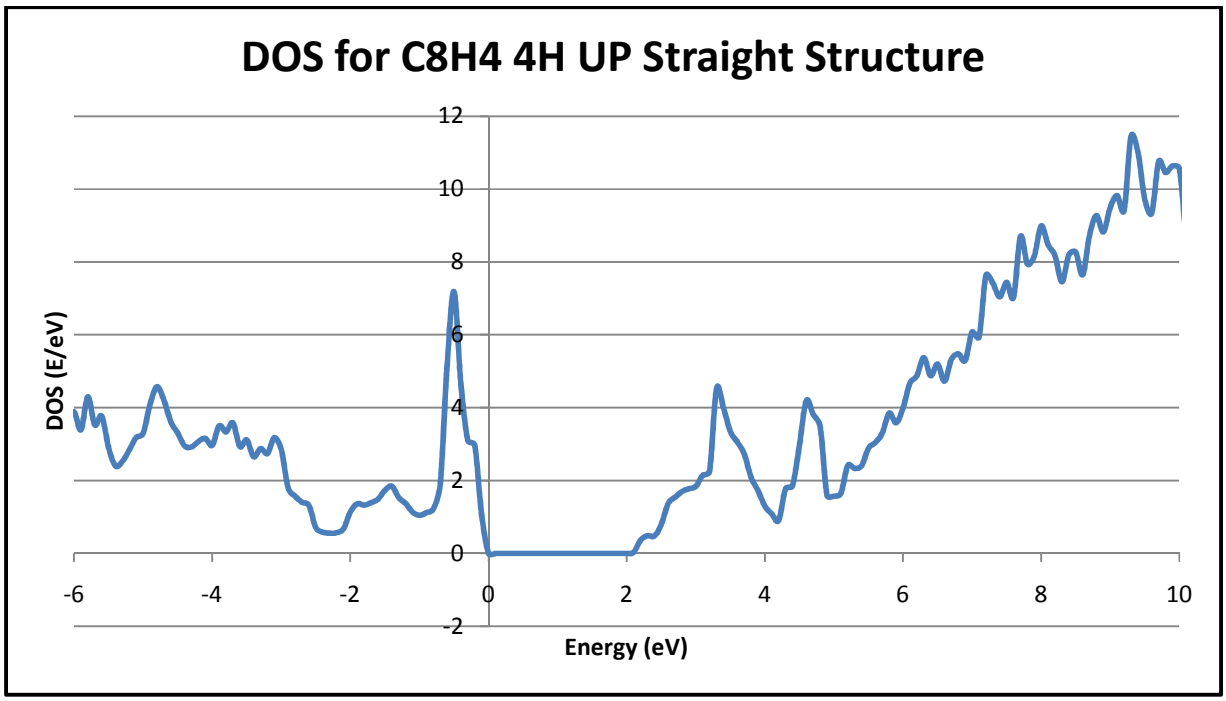

Figure 15.7: C_8H_4 Row Other Band Structure

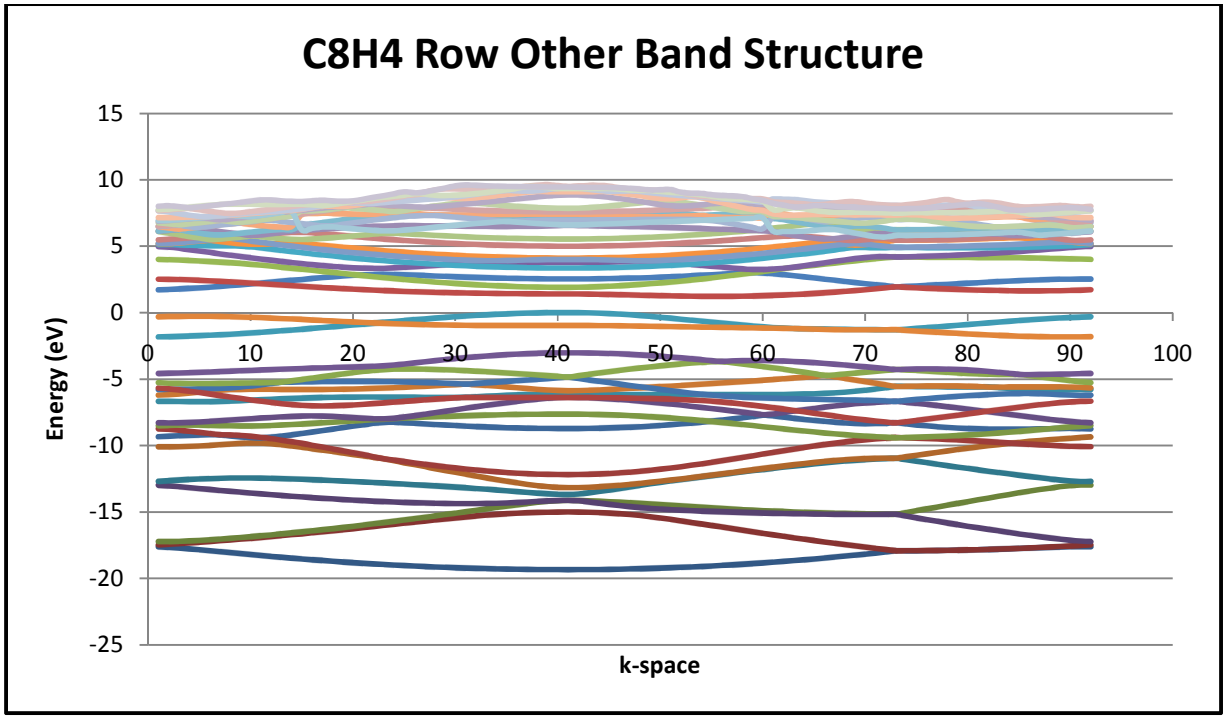

Figure 15.8: C_8H_4 Row Other Density of States

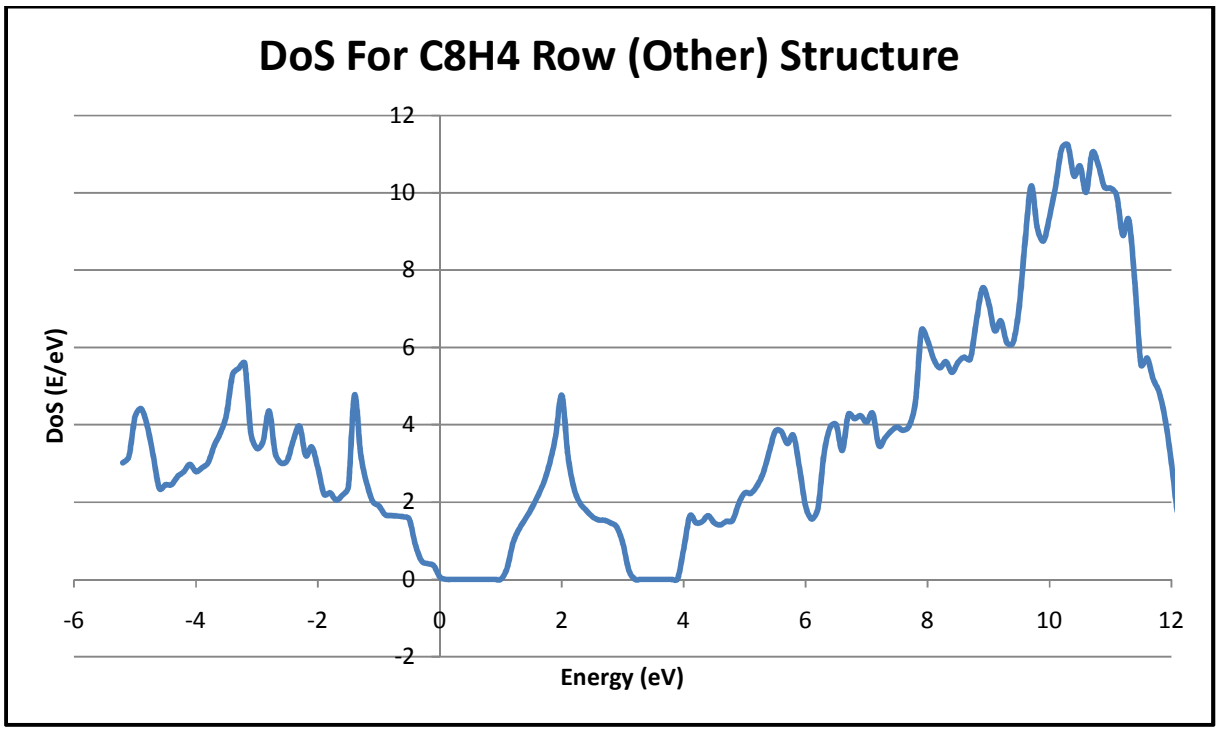

3.12: Analysis of DoS of Selected Systems

The DoS calculations are useful here as a way to quantize the systems, as it gives the distribution of states at an interval of energy for the energy levels that could be occupied in the systems. In the case of semi-conductors, it has a second use, and that is confirming if band gaps of a system are real (particularly if the band structure calculation gives a small gap). It is possible then when the band structure is performing that calculations at the certain k-points, that a point of lower (or lowest) energy is missed, resulting in a lower or even non-existent gap. In a DoS graph of a semiconductor (or insulator), there would be a part of the graph where the density would be 0 (this would be the band gap), as these states cannot be occupied. It did occur during the research for this thesis, as several of the structures (not shown here) had small band gaps that turned out to be non-existent when the DoS calculation was run.

In the case of the $C_{16}H_4$ 4H Up Far system, the band structure calculation gives a band gap of 0.701 eV. When the DoS was run, it came back giving no band gap, and this was also seen in the JDoS calculation (which is discussed in the next chapter). Although the band structure calculation for the $C_{16}H_4$ 4H Up Far system seemed promising, the DoS calculation showed that there is actually no band gap, so this system would not be useful for the sought after applications.

For other systems, it confirms the presence of the band gap, and of approximately equal size to the band gap found in the band structure calculations (there is some noise, and also a program used to smooth out the graphs can cause minor changes to band gap size). Running the DoS calculations helps give a deeper understanding of the electronic structures of these systems.

This concludes the work on structure optimization, band structure and DoS calculations. The next chapter will focus on the optical response properties of the systems.

Chapter 4: Optical Response

4.1: Introduction

At this point there are a few structures that are of interest, but they have all been constructed computationally. In order for any of these structures to be useful, they must be able to be created experimentally. In a computer, and unlike a real lab setting, one can easily place the amount of hydrogen that is desired, and at the right locations. This is obviously not the same case when the real system would be made. However, the optical response properties can be measured experimentally and be calculated computationally, meaning if some hydrogenated graphene structure was created, the optical response could be measured experimentally and compared to the computational result, to see what structure was created.

The optical characteristic that is computed here is the (imaginary part) of the dielectric tensor, ε(ω), (also referred to as the imaginary part of the dielectric constant of permittivity), as a function of frequency in eV. It is computed in all 3 directions (x, y, z). In terms of the coordinate axis, QE has a built-in grid, although it is not seen in QE itself, but can be seen in Molekel. In terms of visualizing the coordinate axis, the positive x axis is (generally) along the carbon plane, positive Z being downwards (pointing to the bottom of the page), with positive y being pointed out of the page, as shown below:

Figure 16.0: C8H4 Row Other Structure with Coordinate Axis:

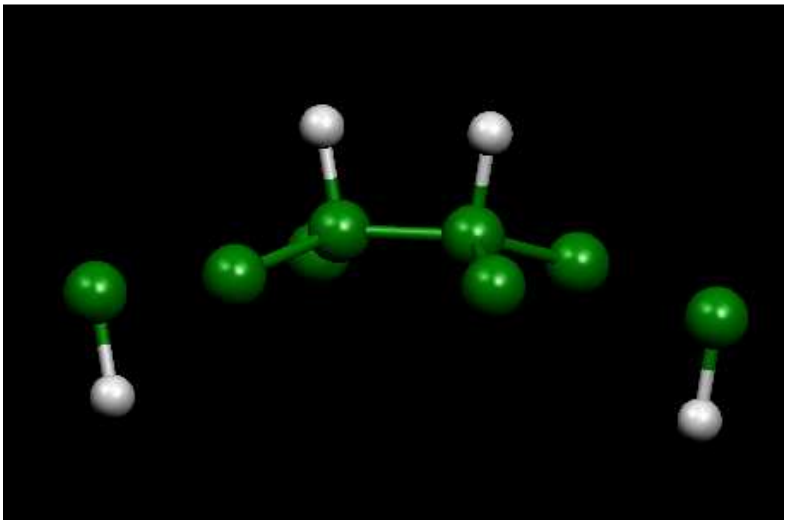

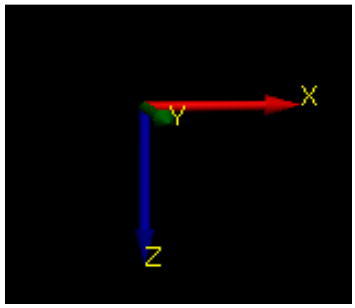

The optics program runs the calculations in the x direction, y direction and z direction to get the response in all 3 directions.

The Quantum Espresso program is capable of performing these calculations so it is used for this aspect as well. Another computation done was the Joint Density of States (JDOS). The JDOS is defined as “the number of electronic states in the conduction and valence bands that are separated by a given photon energy” [49]**.** One further calculation was the Radial Anisotropic Spectroscopy (RAS). It is simply the difference in the optical response in the x and y direction, to determine if the system is optically isotropic or not. This was a simple calculation, where the SHARCnet computers were not required (Excel would suffice for it).

4.2: Optical Response for Selected Systems (Epsilon and RAS)

The following graphs are the results of the epsilon (ε(ω)) calculations, and the corresponding RAS graphs for the four systems that were discussed earlier.

Figure 16.1: $C_{16}H_2$ Row Close Optical Response

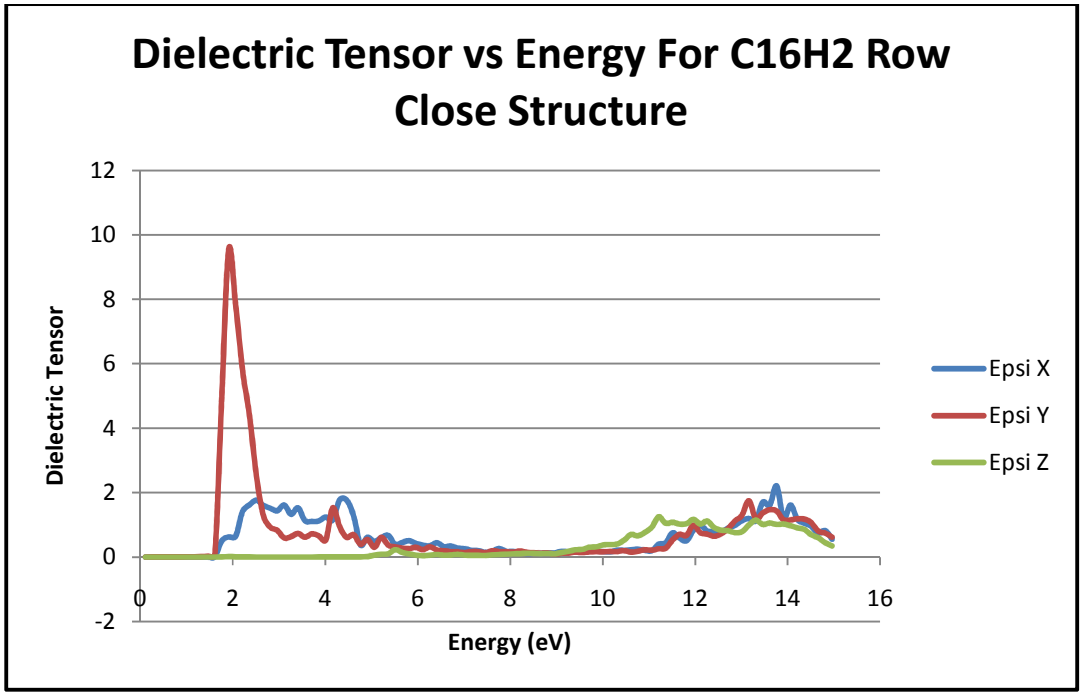

Figure 16.2: $C_{16}H_2$ Row Close RAS

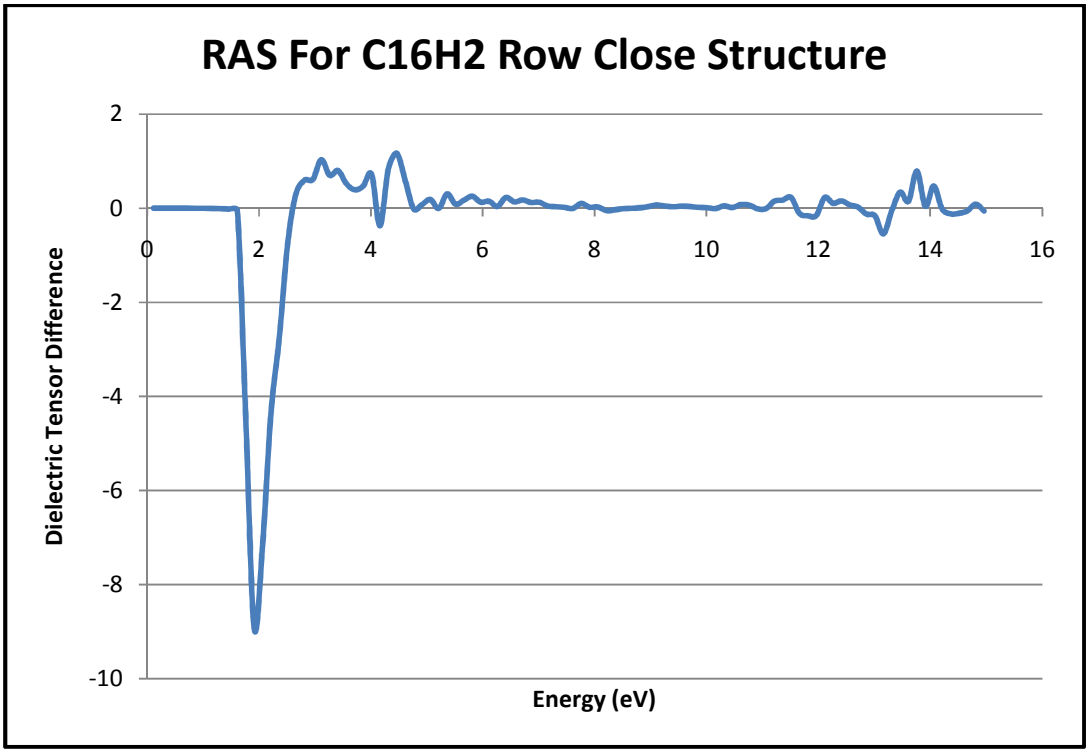

Figure 16.3: $C_{16}H_4$ 4H Up Far Optical Response

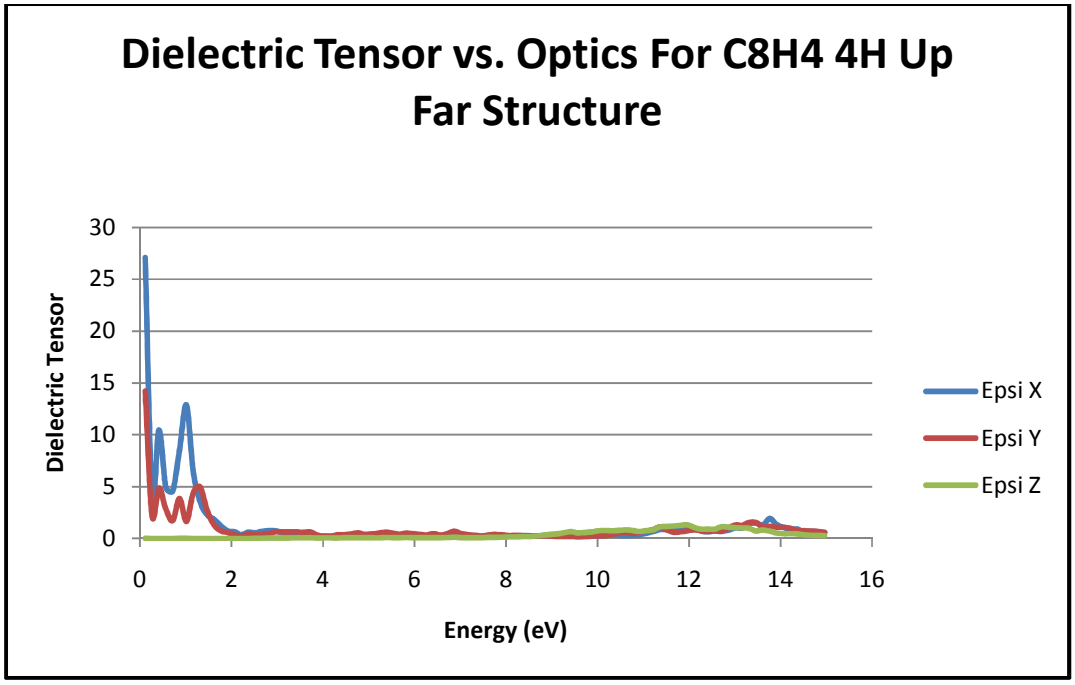

Figure 16.4: $C_{16}H_4$ 4H Up Far RAS

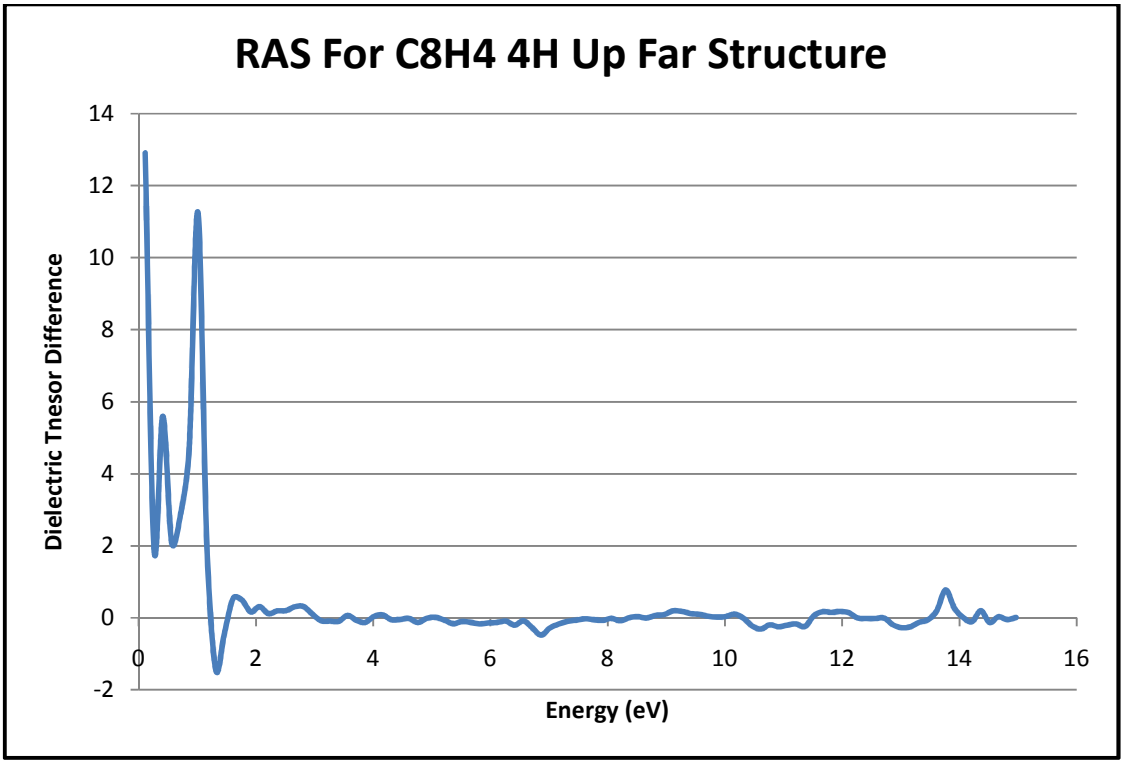

Figure 16.5: C_8H_4 4H Up Straight Optical Response

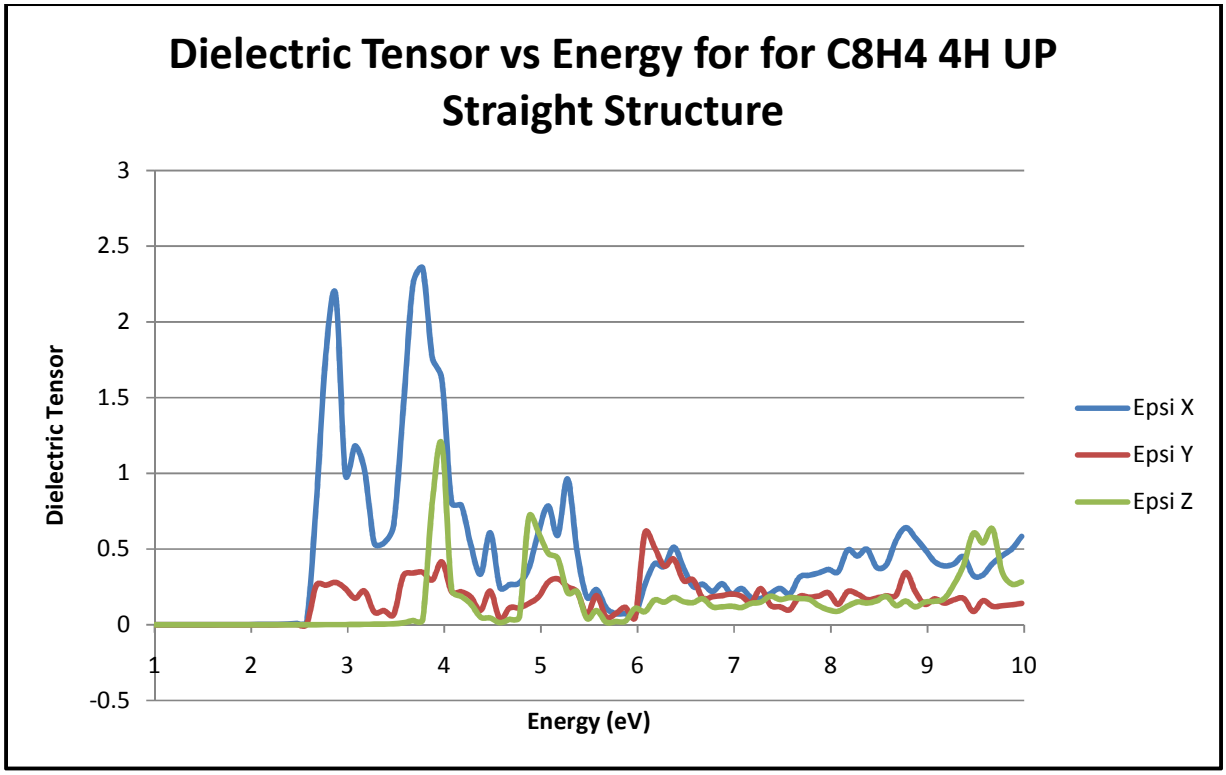

Figure 16.6: C_8H_4 4H Up Straight RAS

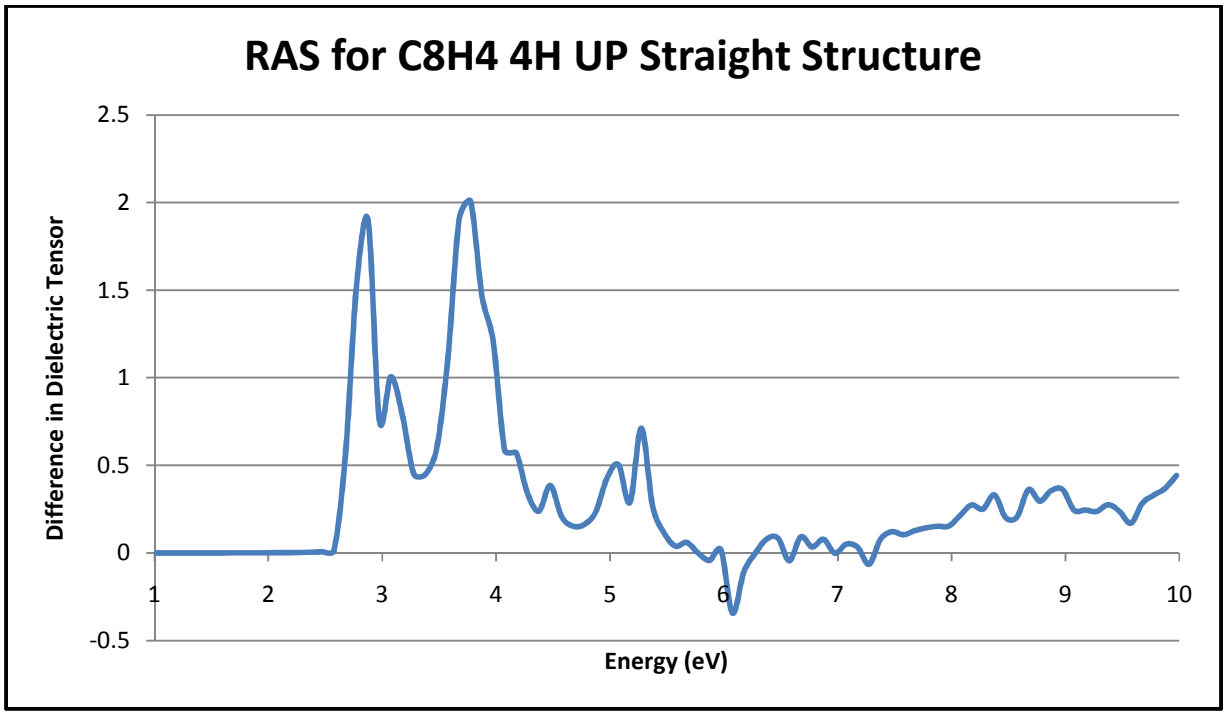

Figure 16.7: C_8H_4 Row Other Optical Response

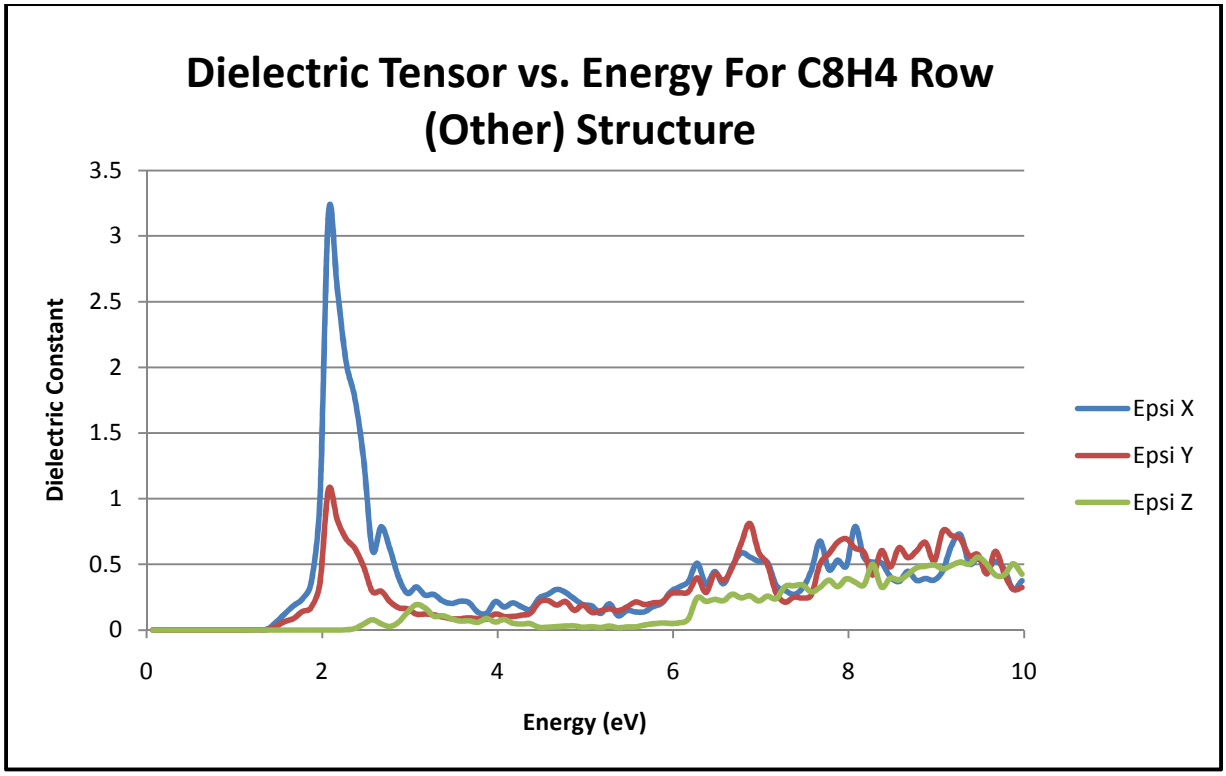

Figure 16.8: C_8H_4 Row Other RAS

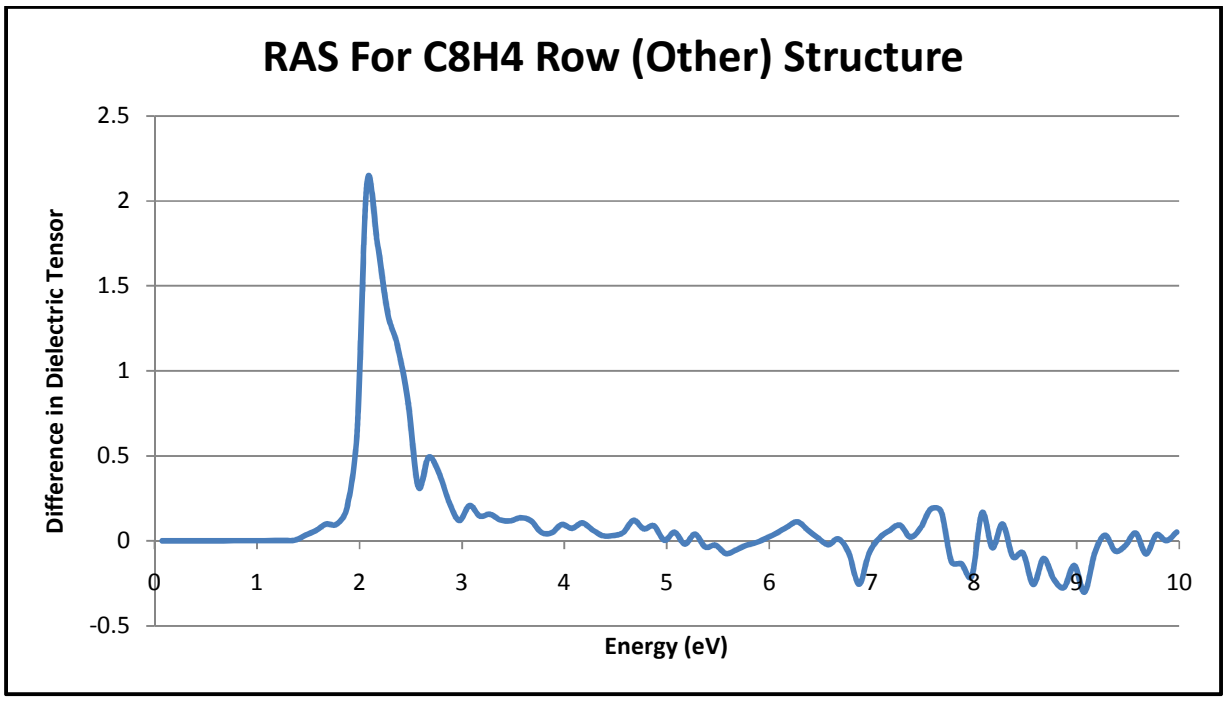

When looking at the optical response, it gives something to compare to if the systems were actually made (which is beyond the scope of this thesis). It is worth noting that no optical response occurs inside of the band gap, as there will be no transitions between the energy levels in the region (hence the gap). This also lends more confirmation to what the DoS calculation showed about the $C_{16}H_4$ 4H Up structure, as the optics start almost immediately, showing again that there is no band gap present. It is seen that all of these systems above (and other systems not shown), that there are all strongly anisotropic, which is clear when looking at the RAS graphs. In all cases there is a peak soon after the band gap (in $C_{16}H_4$ 4H Up structure there is a peak almost immediately after 0 eV), and in all except the $C_{16}H_2$ Row Close system, there is a larger response in the x direction, while $C_{16}H_2$ Row Close structure has a larger response in the y direction.

4.3: JDOS for Selected Systems

The following graphs are the results of the JDOS calculations for the selected systems:

Figure 17.1 $C_{16}H_2$ Row Close JDOS

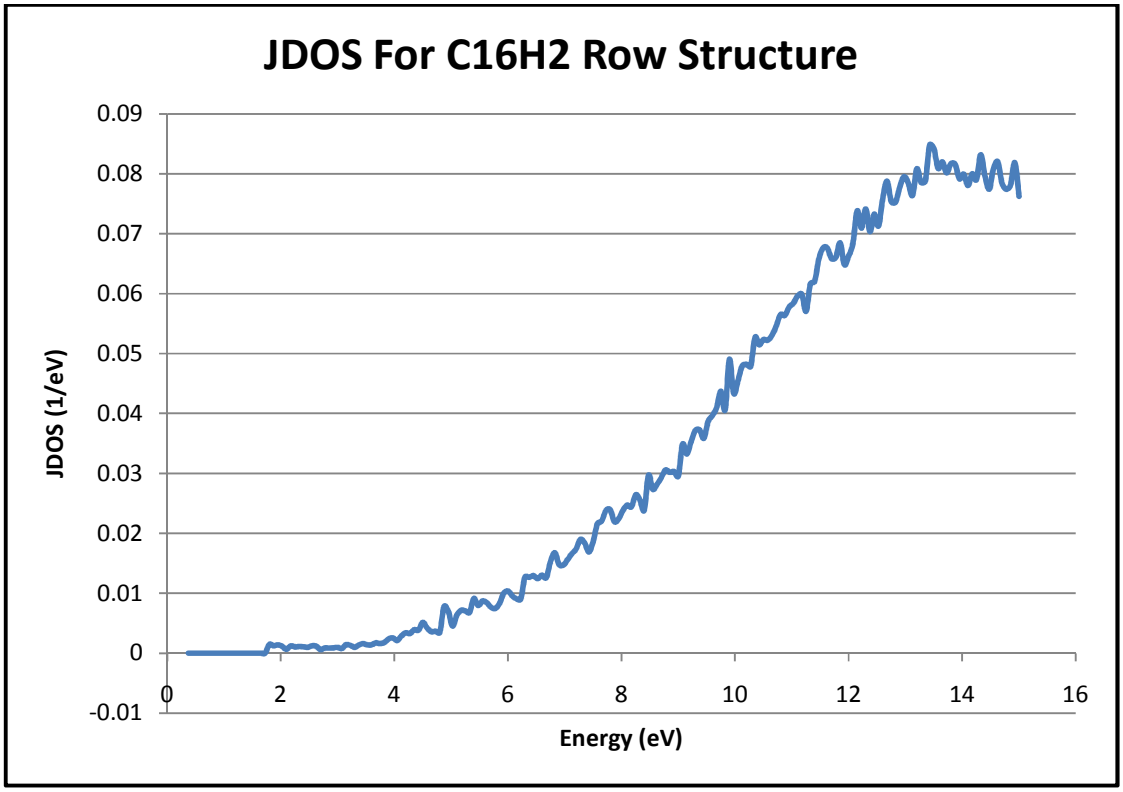

Figure 17.2: $C_{16}H_4$ 4H Up Far JDOS

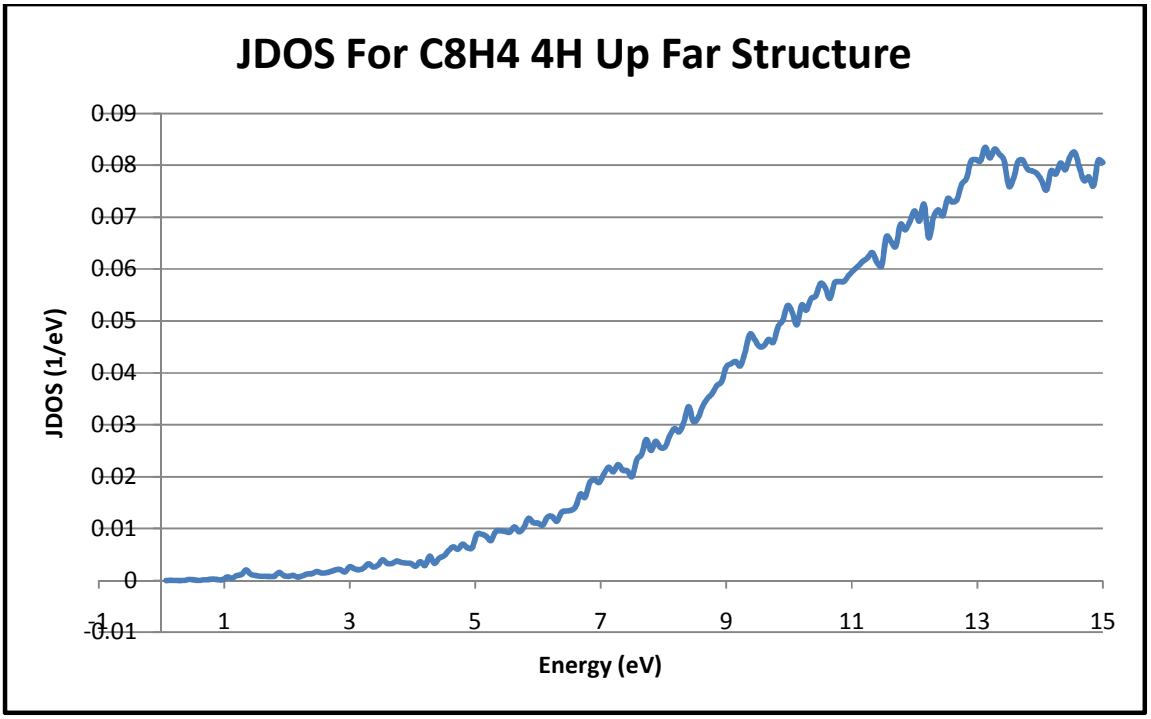

Figure 17.3: C_8H_4 4H Up Straight JDOS

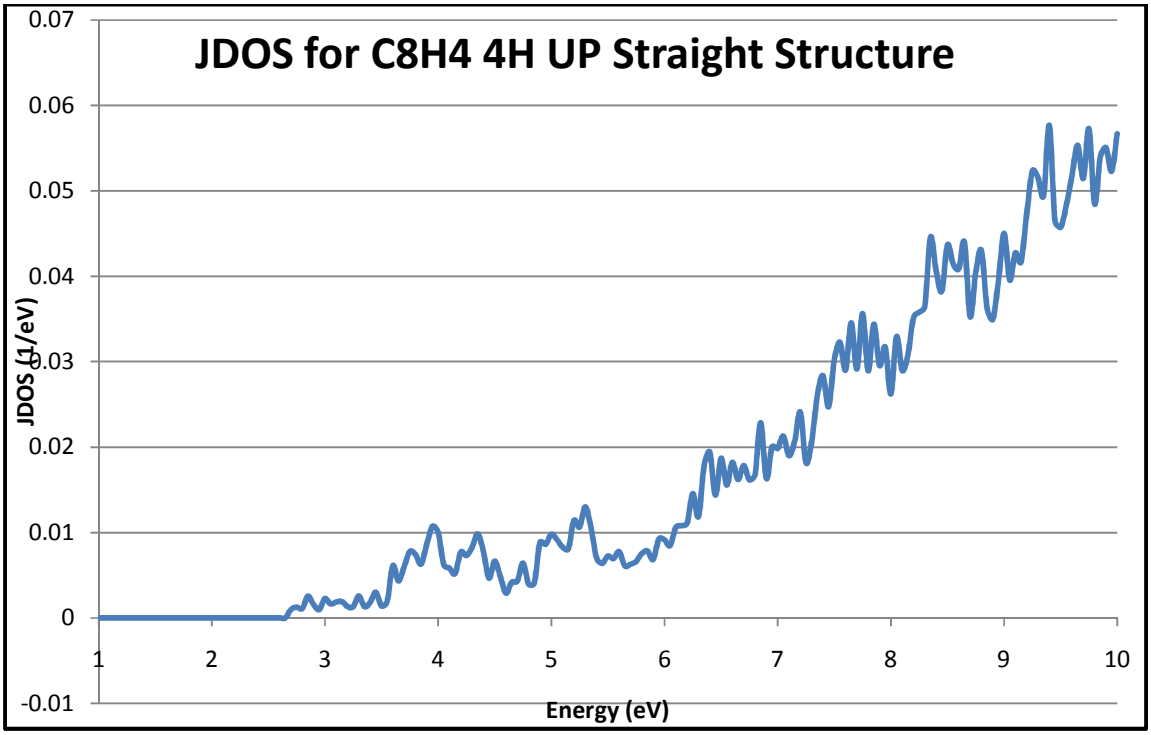

Figure 17.4: C_8H_4 Row Other JDOS

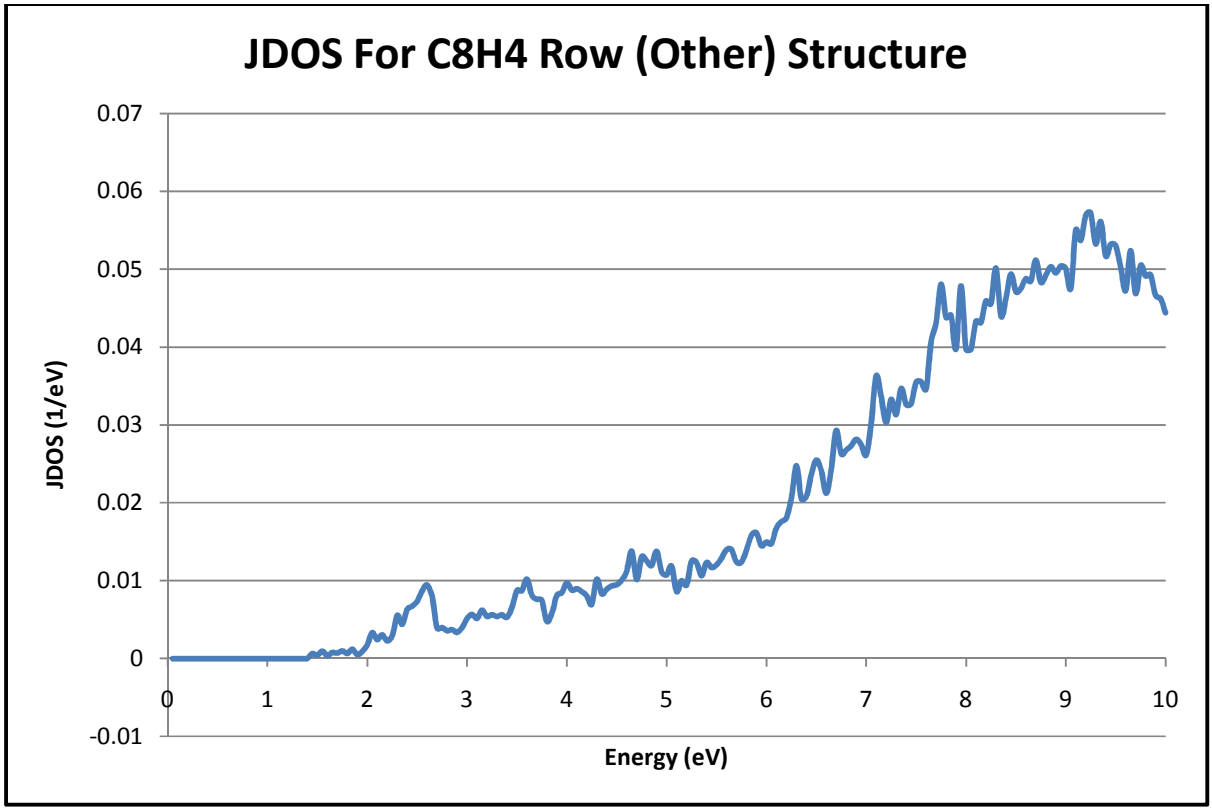

The JDOS graphs will again show the band gap (as with the standard DoS, there will be not any states that can be occupied. As expected, the JDOS for $C_{16}H_4$ 4H Up Far shows little gap (values are very small, so it appears that there is a gap when there should not be), while the JDOS graphs for the other 3 systems show an obvious gap.

The JDOS calculations are of use because it, like optics, can be measured experimentally and compared to these computationally obtained systems (however unlike the optical response the JDOS is directly related to the DoS and contains only real components). The JDOS, along with the standard DoS will give a better understanding of the underlying electronic structure of these systems. The functions used in the calculation of the JDOS are included in the QE optics manual (Appendix A).

4.4: Comparison with Graphane

When comparing the optics of partially hydrogenated graphene and graphane, there are two noticeable differences. The first difference is that in graphane, there is a delay between the end of the band gap and the start of the optical response. In terms of delay, it's not a time delay, but rather it means that the optical response does not start until a much higher energy than the energy level at the end of the band gap (conduction band). However, in the partially hydrogenated systems this is not the case, and the optics start right at the end of the band gap.

This is seen visually when comparing the DoS and optical response graphs of graphane and the partially hydrogenated systems:

Figure 18.1: DoS for Graphane (Chair Shape)

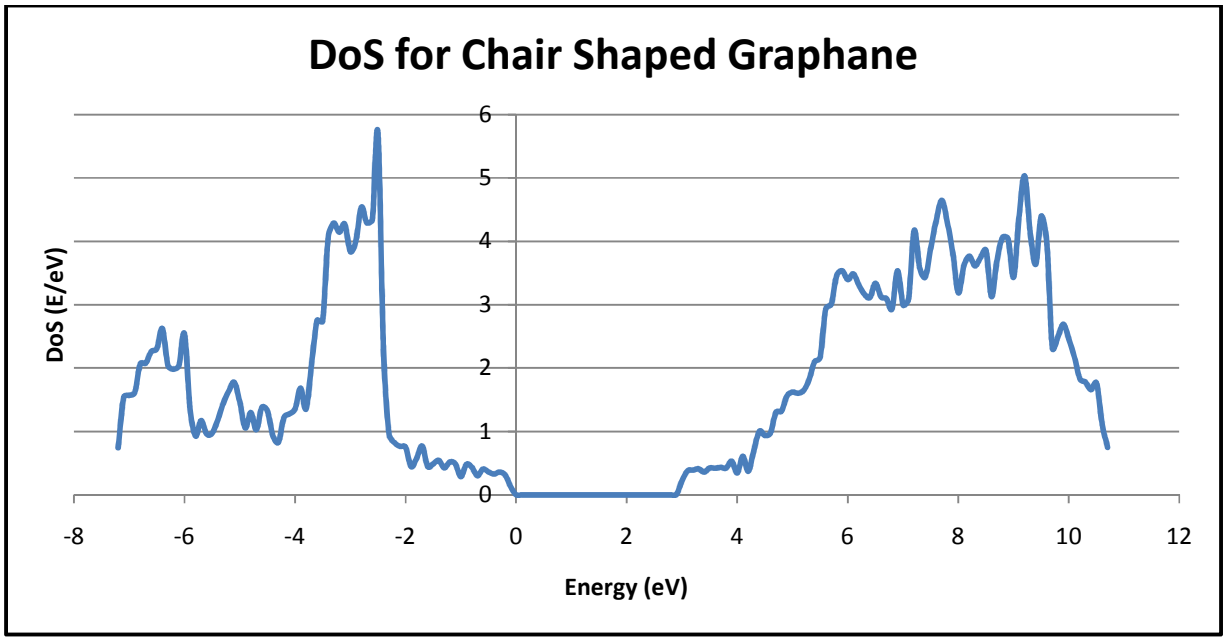

Figure 18.2: DoS for Graphane (Chair Shape)

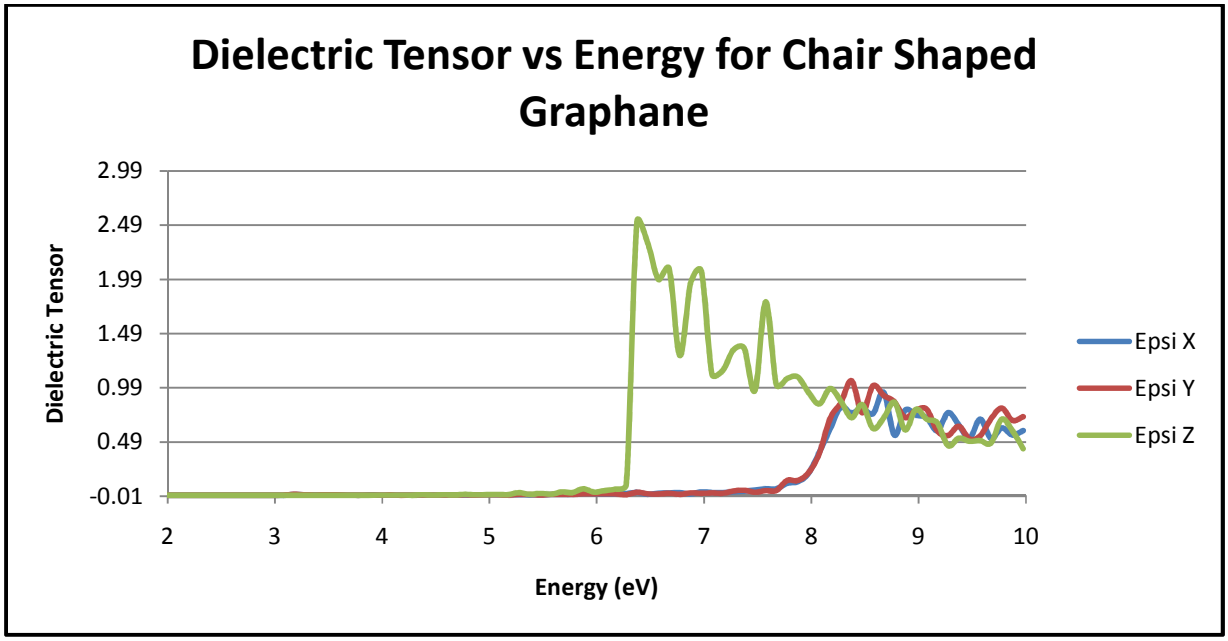

It is seen clearly in the above graphs, that graphane has a band gap calculated to be about 3.1 eV (seen in the DoS graph). In the optical response graph however, the optics do not start until about to 6 eV, approximately twice the energy of the band gap, meaning that there are a lot of states that are still not allowed optically.

It is very different when looking at any of the partially hydrogenated systems. In those structures there is no delay (energy wise) as the optical response will start right after the band gap. The delay in graphane is due to it being a fully sp^3 hybridized system and in the region from the end of the band gap (about 3.1 eV) to the start of the optics (about 6 eV), would correspond to P-state to P-state transitions. In quantum mechanics, same state transitions are not permitted, and will lead to little to know response, as seen in the optical response of graphane. In terms of the QE program, the (imaginary) dielectric tensor is calculated using the equations given in the QE optics manual (Appendix A). When looking at the matrix elements,

$$\hat{\mathbf{M}}_{\alpha,\beta} = \langle u_{\mathbf{k},n'} | \hat{\mathbf{p}}_\alpha | u_{\mathbf{k},n} \rangle \langle u_{\mathbf{k},n} | \hat{\mathbf{p}}_\beta^\dagger | u_{\mathbf{k},n'} \rangle$$

where n and n' represent the valence and conduction bands respectively, with **P** being an operator. In any case where n and n' are the same, meaning the state in the valence band is the

same as the conduction band, the matrix elements will end up as 0 when the operator is applied.

This is not seen in the partially hydrogenated system, as they are a mix of sp^2 and sp^3 states, giving a larger s state contribution and leading to S-state to P-state transitions immediately after the band gap.

The second difference is seen when looking at the RAS of the systems. The RAS of graphane (Chair shape) is shown below:

Figure 18.3: RAS for Graphane (Chair Shape)

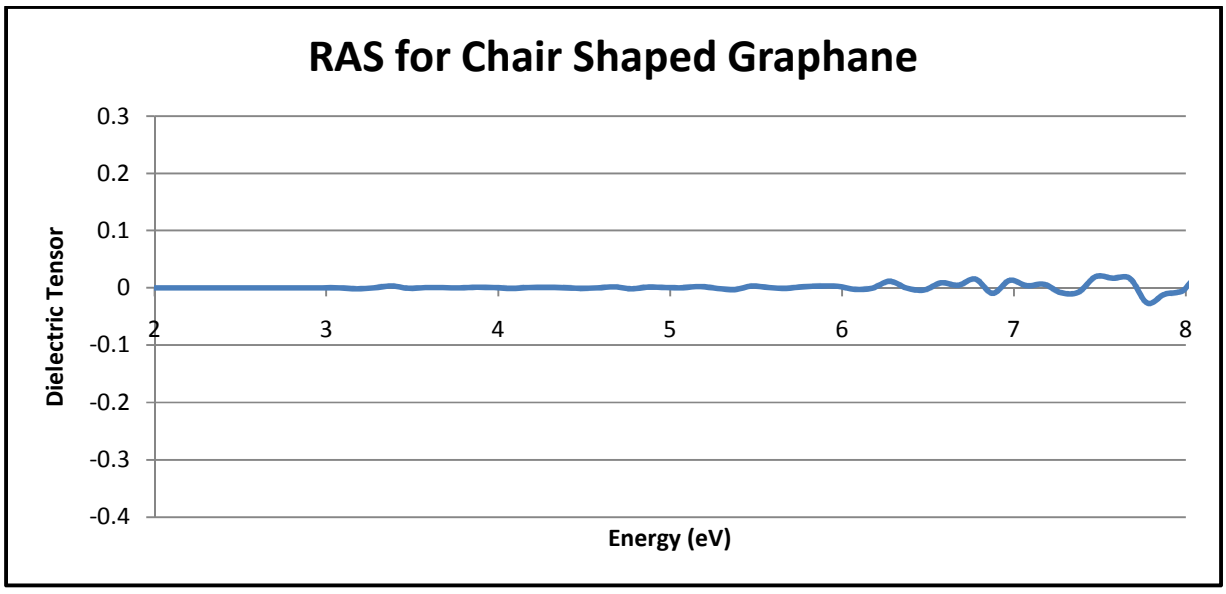

The anisotropy of graphane is much lower than that of the partially hydrogenated systems. In reality, graphane should be isotropic, but it is not seen as such here, due to the effect of noise. Still, it is close enough to isotropic to illustrate another difference between graphane and partially hydrogenated graphene. This is not especially surprising, since graphane is fully hydrogenated while the other systems were not. This would lead to no change when coming from the x or y direction in graphane, but in the partially hydrogenated systems there would be a different pattern in C-H bonds and dangling bonds, which would affect the optical response.

This concludes the chapter on the optical response properties of partially hydrogenated graphene. The next chapter will focus on the BOMD calculations and the vibrational frequencies that were attained from them.

Chapter 5: Molecular Dynamics and Vibrational Frequencies

5.1 Introduction

The next step in this research was to perform molecular dynamics calculations on some of the larger systems (for background information on BOMD, please refer to chapter 2). The larger systems were chosen due to them having more atoms, which would lead to more accuracy in the calculations since MD simulations are based around large numbers of atoms. This would entail the calculations for unit cells with 16 carbon atoms, as opposed to 8 or 32. It was hoped originally to use 32 carbon cells, but that would require too much computational and the vibrational frequency program worked best with the rectangular unit cells used in C_{16} systems. The output file from the molecular dynamics calculations is then used to calculate the vibrational frequencies, through a number of pre-existing AWK and Fortran programs (provided by Tim Teatro). Vibrational frequencies of systems can be measured experimentally; these graphs will provide another means of corroborating these systems with experimental systems. In experiments, this spectrum would usually be measured by infrared or Raman (visible) spectroscopy, since vibrational transitions usually need an energy that corresponds to somewhere in those ranges (infrared to visible light). The vibrational spectra for C_{16} (graphene), $C_{16}H_4$, $C_{16}H_8$, $C_{16}H_{24}$, and $C_{16}H_{16}$ (representing 0%, 25%, 50% and 100% hydrogenation, respectively) are all presented in this chapter.

5.2 Vibrational Frequencies of Graphene

The first step was again, the MD run for standard graphene, using the C_{16} unit cell, which was the largest we had at the time. The vibrational frequency graph is shown below:

Figure 19.1: Vibrational Frequencies for C_{16} (Graphene) after 2474 Iterations

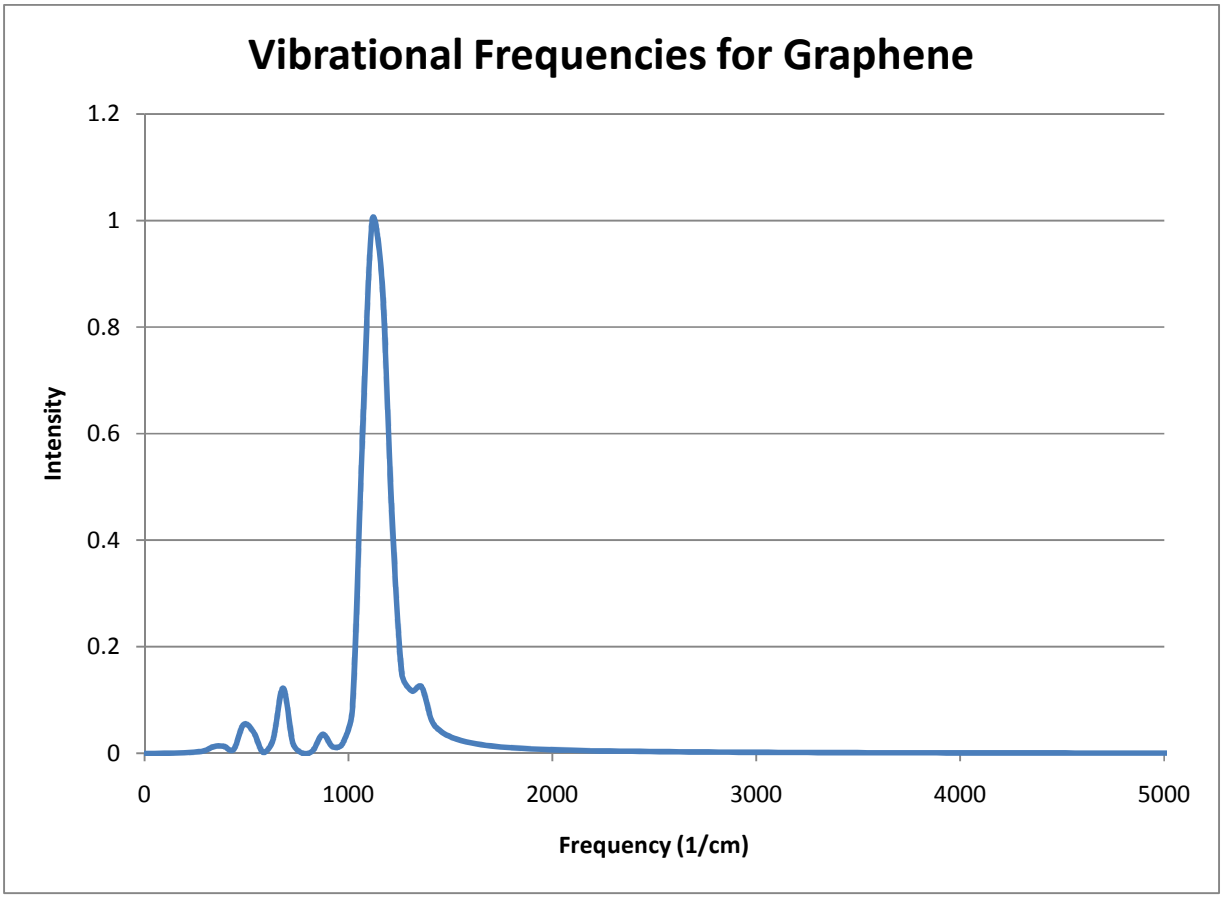

In a 2009 paper that also calculated the vibrational spectra of graphene using DFT, the authors found for a graphene monolayer of 32 atoms, the frequencies ranged from 42.24 cm^{-1} to approximately 1551.32 cm^{-1}. In another calculation they did involved a 30 carbon monolayer, and resulted in frequencies in the range of 23.12 cm^{-1} to 1546.26 cm^{-1} [40].

In this research, it was seen that the frequencies start at around 243 cm^{-1}, with a peak a large peak at about 1120 cm^{-1}, and then drops off towards 0 at 1310 cm^{-1}. Past about 1600 cm^{-1}, the intensity is very low. The values in this calculation are pretty close to the reference values given above for the end point, but are off by about 200 cm^{-1} at the starting point. This could be due to the lower number of carbon atoms used (16 vs. 30/32), as a larger cell would lead to more interactions and greater accuracy.

5.3 Correction Factor

As was discussed in the theoretical background back in chapter 2, all of these calculations are based on approximations, and although they are quite good, there is still some error in them. In the case of the vibrational frequencies, it simply requires a shift of the frequencies (shift on the x-axis), to make the peaks at the correct frequency.

To do this, one will run a similar system (such as CH_4, as it contains C-H bonds) using QE, and finding the vibrational spectra, and then comparing it to a reference value. Once this comparison is made, the spectra can be shifted to it matches the reference value, and then that correction can be applied to the other C-H systems that we use. In the reference case, the peaks of the CH_4 vibrational frequency occur at 3025.5 cm^{-1}, 1582.7cm^{-1}, 1367.4 cm^{-1} and 3156.8 cm^{-1}, although only the latter 2 modes will interact with IR light due to the symmetry of the system [41].

Table 7: Comparison of Theoretical and Calculated CH_4 Vibrational Spectra

Mode	Theoretical Peak (cm^{-1})	Calculated Peak (cm^{-1})	Ratio (Theory/Experiment)
v1	3025.5	2615	1.157
v2	1582.7	1415	1.119
v3	1367.4	1145	1.194
v4	3156.8	2817	1.121

This is an average of 1.145. Since the value is greater than 1, the shift should be to the right (calculated values were lower than the theoretical ones). Therefore, we multiply the calculated ones by 1.145 to match them up better with the theory. This will be done also for the partially hydrogenated carbon systems.

5.4 Vibrational Frequencies of Partially Hydrogenated Graphene

Now that the frequencies of graphene have been determined, it is time to look at the partially hydrogenated systems that were mentioned in section 5.1. The frequencies for those are shown below:

Figure 19.2: Vibrational Frequencies for $C_{16}H_4$ after 1811 Iterations

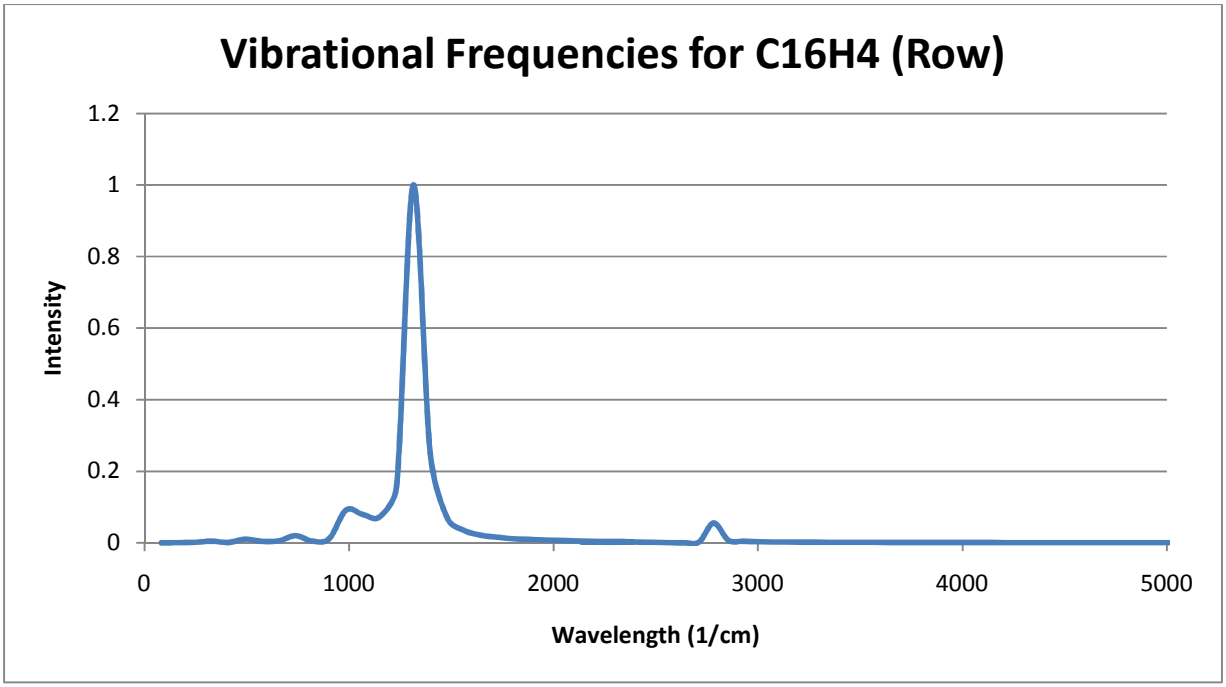

Figure 19.3: Vibrational Frequencies for $C_{16}H_8$ after 236 Iterations

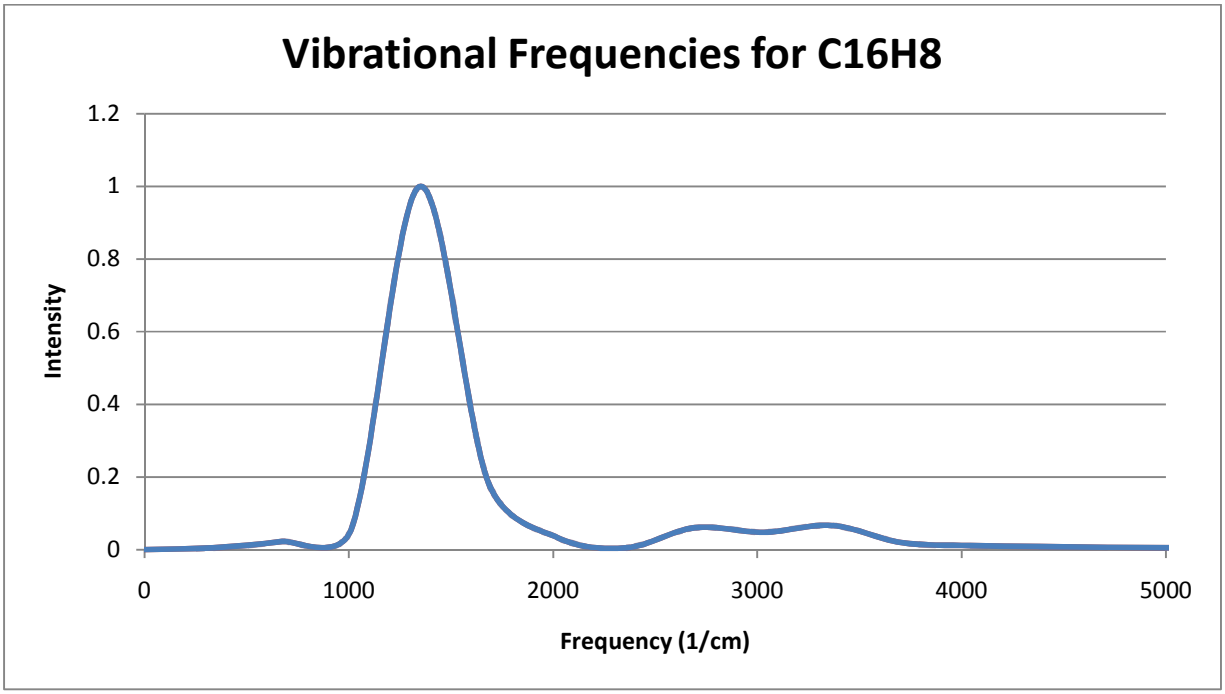

Figure 19.4: Vibrational Frequencies for $C_{16}H_{16}$ (graphane) after 1867 Iterations

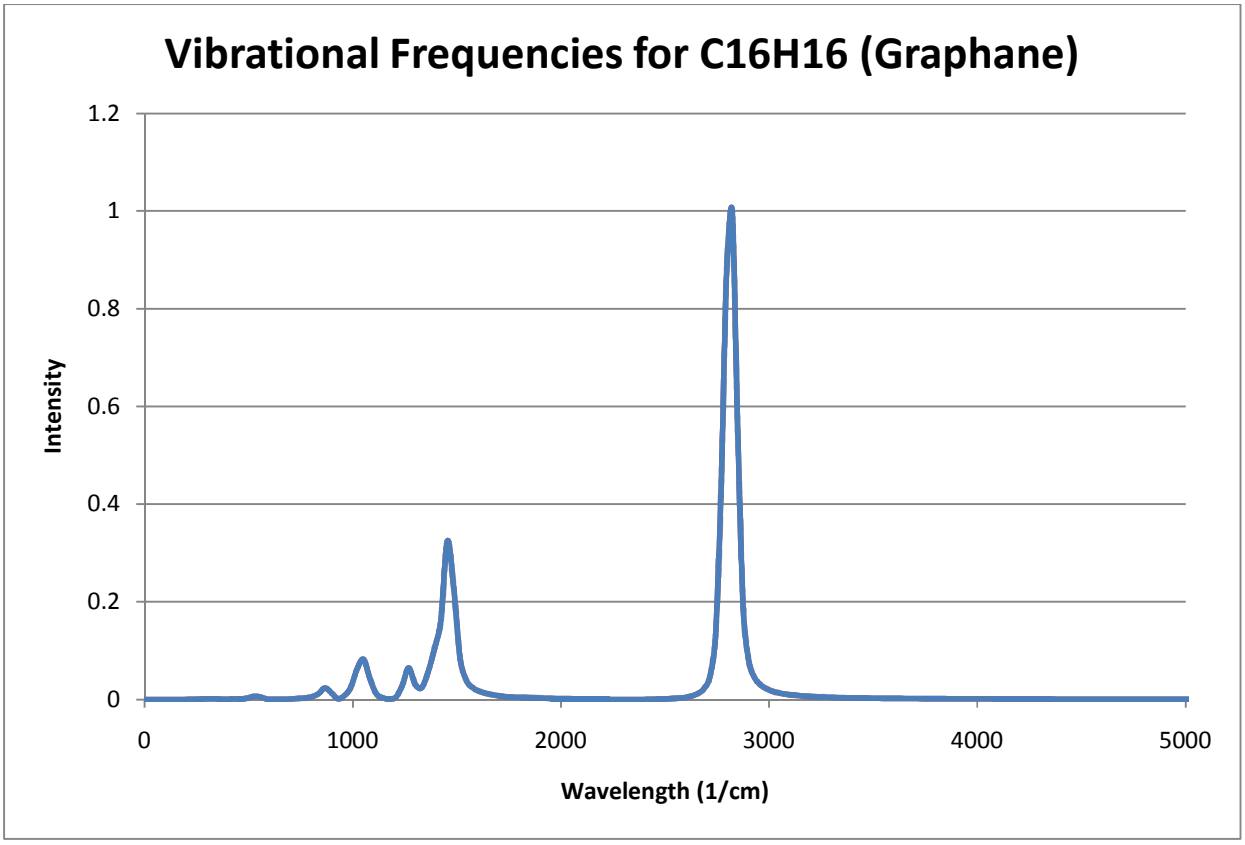

When looking at the hydrogenated systems (both partially and fully hydrogenated), the emergence of the vibrational frequencies of the C-H bonds are seen. Unsurprisingly, the more hydrogen in the system, the greater the intensity of the peak (the frequency this peak occurs at does not change). It is also seen that there is a small diminishing in the intensity of the smaller peaks in the C-C spectra that occur before the large peak.

As the hydrogen peak grows, so does the C-C peak shrink. There is a tiny decrease in maximum intensity of the large carbon peak going from the C_{16} to the $C_{16}H_4$ system, but a large decrease when it reaches graphane, as the carbon peak now appears less than 40% of what it was originally, and the hydrogen peak becomes the dominant one. It should be noted that these intensities are relative to each other and not absolute values. The carbon peak does not actually shrink, just that as the amount of hydrogen is increased, the intensity of the hydrogen peak will also increase, and in the case of graphane the C-H vibrations becomes much more intense than the C-C vibrations.

There is an issue with the $C_{16}H_8$ system, as you can see by the spectrum (Fig. 19.3); its hydrogen peak is very wide, and not as high as expected. This was due to time constraints, leading to a shorter run time, involving lower temperatures and many fewer iterations. In following work,

the temperature obtained was too high and it appears the system broke down, meaning it seems like the $C_{16}H_8$ system was more sensitive to temperature than graphene or graphane, and time constraints have prevented getting a proper spectra.

In a paper on the subject of hydrogen vibrational modes on graphene**,** the researchers there used DFT, and a "dynamical matrix" method to calculate the vibrational frequency of the C-H bond to peak at 2552 cm^{-1}. This was then adjusted to 2651 cm^{-1-}, which was extremely close to the experimental reference value that they used, of 2650 cm^{-1} [42]. Here, the calculated C-H peak occurred at about 2690 cm^{-1}, which is about a 1.51% error when compared to the experimental version, and a percent difference of about 1.47% when compared to the calculated value, for the corrected case. In the corrected case, the percent difference is 6.09% for the experimental and 8.71% for the calculated. As noted in the above paper (as well as seen here), the C-H frequencies of hydrogenated graphene systems are lower than in typical hydrocarbons (like methane). This causes the correction factor used here to overcompensate, and results in a larger frequency that in experiment, about 3087 cm^{-1}. All in all, it occurs close to where other calculated and experimental peaks occur. Had a larger cell been run (such as C_{32}) or more k-points taken, the accuracy would have been even better, but that would also greatly increase the time needed. It should be noted that methane was taken for its simplicity and the belief that the sp^3 hybridization would correlate well with the partially hydrogenated systems, although in reality it does not (see Conclusion). A more suitable molecule could have been cyclohexane (C_6H_{12}) or benzene (C_6H_6), as their configurations are closer to graphane than methane.

As mentioned before, these spectra can be determined experimentally, so the spectra that had been computed here could be matched up with experimental results to see what degree of hybridization occurred. Since there is an obvious pattern in the way the peak intensities vary with hydrogen content (hydrogen peak increases, carbon peak decreases), it would be easy to identify partially hydrogenated systems that have a hydrogenation content that falls between the above systems. Due to time constraints, the spectra for 75% hydrogenation ($C_{16}H_{12}$) was not calculated, but as was just mentioned, could be extrapolated from the patterns seen here.

5.5 Nitrogen Doped Partially Hydrogenated Graphene

5.5.1 Introduction

A topic of interest to an associate of Dr. Gaspari's, was the topic of small amounts of Nitrogen that replaced Carbon in the graphene layer, inside of a partially hydrogenated system. Nitrogen, being Carbon's neighbour on the periodic table and would make enough bonds to bond with

the three neighbouring carbon atoms. There could be a lot of research done into this topic, trying various amounts of N in different configurations in graphene cells, but here it will only be discussed briefly, as it was more of a side project [55]. It is included in the Molecular Dynamics section as the original reason for this side project was to determine computationally the vibrational spectra of this Nitrogen doped partially hydrogenated systems, to see if hydrogen was bonded to the N or C atoms.

5.5.2 Nitrogen Doped Systems

There were a small number of these systems that have been computed, two of which are shown below:

Figure 20.1: $C_6N_2H_2$ Row Structure

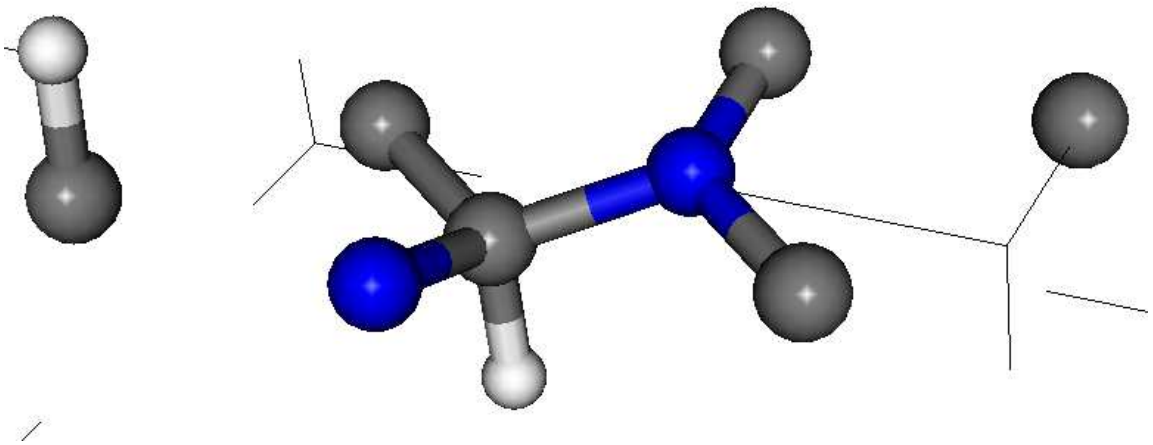

Figure 20.2: $C_{14}N_2H_2$ 2H Up Structure

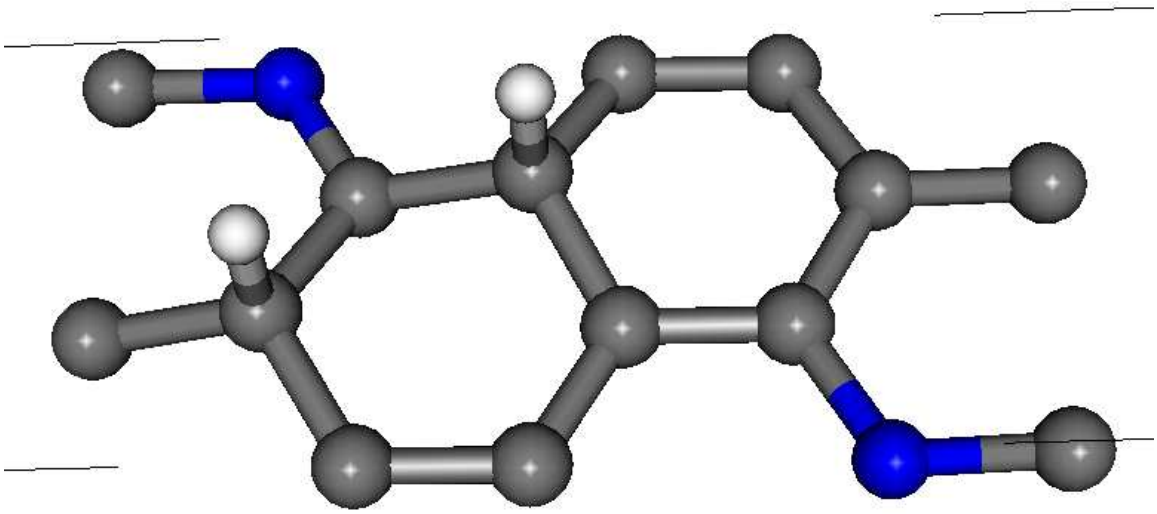

In the above systems, the blue denotes the nitrogen; black is carbon and white is hydrogen.

When comparing the band gaps of the nitrogen doped systems to the standard carbon structures, there is a noticeable difference, as shown in the following table:

Table 8.1: Comparison of Band Gaps between Nitrogen Doped and Non-Doped Systems

Structure Name	Band Gap (eV)
C_8H_2 Row	2.805
C_6N_2H Row	0.011
$C_{16}H_2$ 2H Up	0.089
$C_{14}N_2H_2$ 2H Up	0.465

There is clearly a big change to the band gap when Nitrogen is added to one of these systems. In the smaller unit cell, going from 8 carbon to 6 Carbon 2 Nitrogen caused the band gap to disappear. In the larger system, the band gap increased, and the DoS calculations showed that the gap is real. At the time, not enough research has been done into the Nitrogen doped systems so it is not possible as of yet to determine exactly what caused this change in band gap. It is known that Nitrogen has one more electron than Carbon, but typically only makes 3 bonds (3 valence electrons as opposed to 4 as in carbon), so the change in electron number and

valence likely is responsible for this change, but no real pattern or rule can be deduced at this time.

It seems very likely that in these nitrogen doped systems that the hydrogen would bond with the carbon as opposed to the nitrogen (as mentioned before, C makes 4 bonds opposed to N 3 bonds). However, it certain situations nitrogen is known to make a fourth bond, so it is worth looking into. The results are shown in the table below:

Table 8.2: Total Energies of $C_{14}N_2H_2$ Systems with Different Bonding Configurations

No. C-H Bonds	No. N-H Bonds	Total Energy (Ry)
2	0	-201.2963400870
1	1	-201.2818930721
0	2	-201.1676392496

All of these structures based on the $C_{14}N_2H_2$ 2H Up system, with the hydrogen atoms being moved around to bond with carbon or nitrogen. It is no surprise that the system where both H bond to C is the lowest energy system, followed by 1 H on C, 1 H on N, and the highest energy being when both H are bonded to Nitrogen. In fact there is a very large energy difference between 2H on C and 2H on N, about 0.7 eV per H atom. This is a very large value, and confirms the idea that the hydrogen atoms will bond with the carbon atoms and not the nitrogen atoms. The structures where the there are N-H bonds present are likely local minima, and likely not very stable.

5.5.3 Vibrational Spectra

At this point the research returns to the original point of the side project, the vibrational spectra. The spectrum below is that of the system shown in figure 20.2:

Figure 20.3: $C_{14}N_2H_2$ 2H Up Vibrational Frequencies

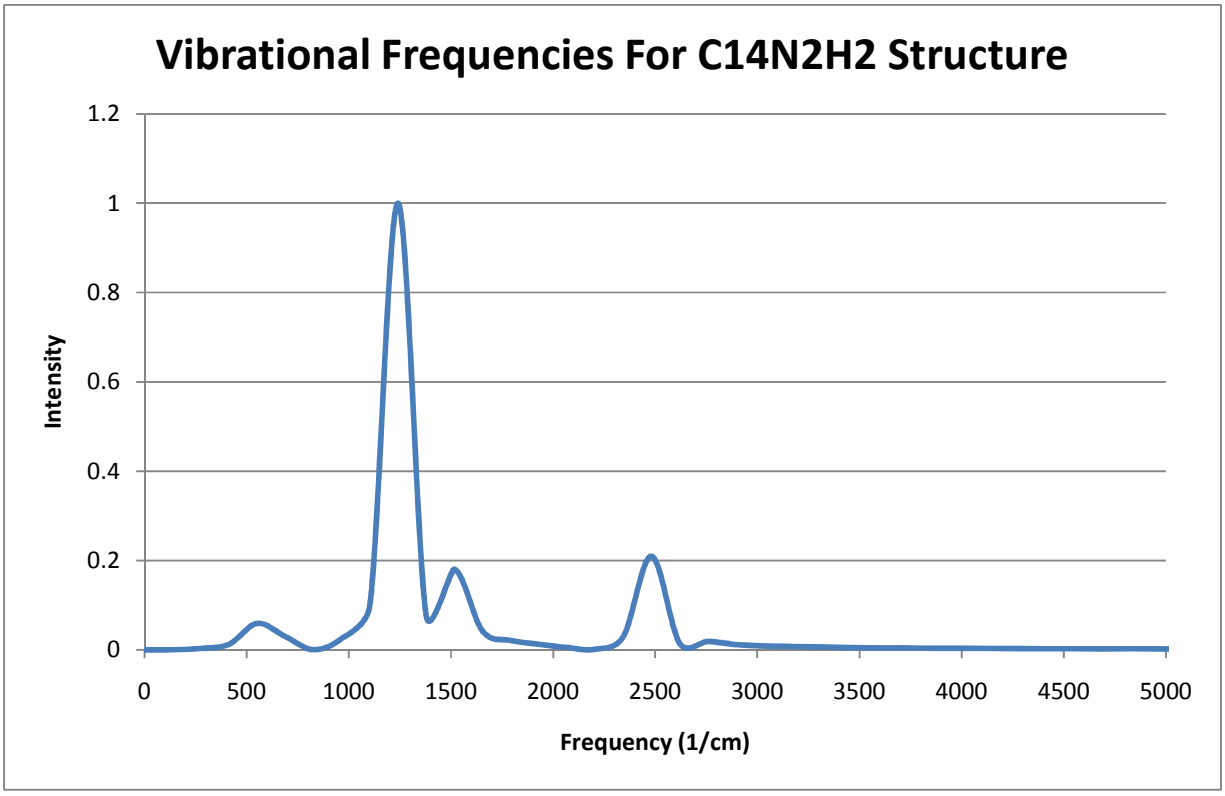

There is a large carbon peak at 1240 cm^{-1}, and a smaller one at about 560 cm^{-1}, with the C-N peak being at close to 1500 cm^{-1}, and the hydrogen peak being farther out, at about 2500 cm^{-1}. This is quite close to the spectra of other structures that have been shown earlier in the chapter, with the notable exception of nitrogen in the previous structures. The C-N frequency is typically smaller in hydrocarbons (around 1000-1250 cm^{-1}), but in this case it is not a hydrocarbon molecule (not just C-N, but really N bonded with 3 separate C), so the spectra will likely be different. If there were more nitrogen or hydrogen in the system, it is expected that their respected peaks would increase, and the carbon peaks would decrease.

Chapter 6: Conclusions

At the end of the research done for this thesis, there were a number of conclusions that can be drawn. First, it was discovered that it is possible to tune the band gap of graphene by adding hydrogen to it, as was hoped for and expected from the onset. The different compositions and configurations produced created a wide range of band gaps, some were Intermediate band gaps (between gaps of graphene and graphane), and some even higher than graphane. As mentioned before it was believed that the hydrogen content would be the largest factor in determining the band gap. When that was shown to be untrue, the next idea was that the average buckling of the system would be the deciding factor, but again that was shown to be untrue. In the C_8 systems at least, configuration was biggest factor and the C_8 cells are generally too small even with just 2 hydrogen, leading to (generally) too large of a band gap, and facilitated the move to larger unit cells.

There were some definite patterns that occurred, as the 2H up systems had lower band gaps, but higher energies than the Row systems. When looking at the reason that these patterns occurs, it has to do with the hybridization of the system. In standard graphene, there are dangling bonds (only three of 4 possible bonds are filled, leaving the other valence electrons free). In the case of graphane, there is no dangling bond, as the hydrogen atom makes the 4th bond (since there are no dangling bonds or Pi bonds, the graphane band gap is very large). It is a well known property that sp^2 hybridized structures (graphene) are strong conductors where sp^3 hybridized structures have very high band gaps, like diamond or graphane. As seen in the introduction, sp^3 hybrid structures should have bond angles of 109.5 degrees. A table comparing the Bond angles of the low gap system, C_8H_4 Row Other and a high gap system, C_8H_4 Row is shown below.

Table 9: Bond Angles of Selected Partially Hydrogenated Structures:

Bond	Angle (Row Other)	Angle (Row)
C-C	118.8	112.8
C-C	118.8	112.8
C-C	113.6	112.5
C-H	99.9	107.5

While none of the angles are exactly 109.5^o (small variance is expected in computational work), the angles in the Row structure are closer to the ideal angle, while the bond angles in the Row Other system show a large deviation from the ideal angle. Moreover, the variance between the individual angles in the Row structure is lower than the Row Other system. This means that while the Row structure is a true sp^3 hybridized system, the Row Other is not, and is a mix of sp^2

and sp^3 hybridization, which leads to a much lower band gap. Looking at the structures of Row Other (Figure 7.4) and Row (Figure 7.1), it is seen that the Row system has the true sp^3 shape, with the repeating up/down structure as seen in graphane. In the Row Other system, the 2 H Up atoms are both pulled in the same direction, not the opposite direction as in the standard sp^3 shape, making it not a true sp^3 hybridized structure.

The mixed hybridization is also what is responsible for the lower vibrational frequencies seen, since it is not a full sp^3 hybridized system, the hydrogen is not held as strongly as in standard hydrocarbons, which causes the lower vibrational frequencies. It has been seen in the course of this research that in order for a low band gap, one must try to minimize the Row configuration in the structures, especially in the C_8 systems, and aim for having 2H Up configurations present. In the larger systems, such as C_{16} or C_{32} systems, a small degree of the Row configuration could be used to create a potentially useful band gap (as seen in the $C_{16}H_2$ Row Close system).

As for the issue of why the energy is higher in the 2H Up cases, the C-H bonds will create a relative positive charge on the hydrogen atoms. Since the hydrogen atoms are close to each other, the positive hydrogen will repel each other (opposite to the hydrogen bonding effect). This repulsion will raise the energy of the system, while in the Row systems the hydrogen atoms are much farther away from each other and this repulsion will be much lower. This is seen when looking at the C_8H_4 Row Other structure (Figure 7.4), where the 2 H atoms on adjacent carbon atoms are angled away from each other. This does lead to an issue when trying to make these systems experimentally, as the most energetically stable systems also have band gaps far too large to be of use for the desired applications. However, it appears that the structures that do possess a good band gap exist at a local minimum, meaning that the structure may be meta-stable and still be able to exist under optimal conditions.

This also brings up the possibility of a tuneable electronic insulator, where the basis for this is that there would be a conductor or semiconductor that could be transformed into an insulator under certain conditions. It could be that in the C_8H_4 systems, that one could take a system with a good band gap (i.e. “Row Other”), apply energy to overcome the potential well of the local minimum, and transform to the more energetically stable, but much more insulating “Row” shape. At this point there is not much known about if these other configurations really are meta-stable, how deep the well is, or if you could easily return to the semiconducting configuration, but it is worth looking into in the future.

It should be noted that on top of creating many new structures and looking at the electronic structure computationally, this research also looked at several different ways in which to compare the computational systems to experiment. The optical response (epsilon), JDoS, and vibrational spectra can all be calculated experimentally, would give an experimentalist multiple ways to try and match the computed structure (or in the case of the vibrational spectra type of

structure) to the experimentally created systems, and see if any of the structures shown in this research were made.

On a final note, it is worth looking at how this research could be expanded on. While many different configurations using the C_8 cells were tried, there are still many more compositions and configurations for the larger C_{16} and C_{32} systems that could be tried. There is also more work to be done in nitrogen doped systems, as well as doping with Carbon's other neighbour on the periodic table, Boron. There are of course many other computations that could be run on the current systems to look deeper into their properties, such as CPA (Central Potential Approximation) to look into the disorder of the systems, looking into the charge densities, or other forms of spectra. The biggest next step however, would be actually trying to create these structures experimentally, to see if it is possible. While in theory there are a few promising structures, it is much more difficult to create them in a real lab setting. If it is possible to create these structures in the lab, then some of these systems may be able to actually be used in the microelectronic applications that were hoped for.

References

Endnotes

[1] K. S. Novoselov, A. K. Geim, S. V. Morozov, D. Jiang, Y. Zhang, S. V. Dubonos, I. V. Grigorieva, and A. A. Firsov, Science **306**, 666 (2004).

[2] A. K. Geim and K. S. Novoselov, Nat Mater **6**, 183 (2007).

[3] D. C. Elias, R. R. Nair, T. M. G. Mohiuddin*, et al*, Science **323**, 610 (2009).

[4] S. Bae, H. Kim, Y. Lee*, et al*, Nat Nano **5**, 574 (2010).

[5] H. Kageshima, H. Hibino, M. Nagase, and H. Yamaguchi, Applied Physics Express **2**, 065502 (2009).

[6] Pletikosi, M. Kralj, P. Pervan, R. Brako, J. Coraux, A. T. N'Diaye, C. Busse, and T. Michely, Phys. Rev. Lett. **102**, 056808 (2009).

[7] J. Coraux, A. T. N'Diaye, M. Engler, C. Busse, D. Wall, N. Buckanie, F. M. z. Heringdorf, R. v. Gastel, B. Poelsema, and T. Michely, New Journal of Physics **11**, 023006 (2009).

[8] C. Riedl, C. Coletti, T. Iwasaki, A. A. Zakharov, and U. Starke, Phys. Rev. Lett. **103**, 246804 (2009).

[9] A. Fasolino, J. H. Los, and M. I. Katsnelson, Nat Mater **6**, 858 (2007).

[10] B. Aufray, A. Kara, S. Vizzini, H. Oughaddou, C. Leandri, B. Ealet, and G. L. Lay, Appl. Phys. Lett. **96**, 183102 (2010).

[11] S. Cahangirov, M. Topsakal, E. Akturk, H. Fiahin, and S. Ciraci, Phys. Rev. Lett. **102**, 236804 (2009).

[12] J. O. Sofo, A. S. Chaudhari, and G. D. Barber, Phys.Rev.B **75**, 153401 (2007).

[13] A. Savchenko, Science **323**, 589 (2009).

[14] A. I. Shkrebtii, J. L. Cabellos, N. Arzate, B. S. Mendoza, and P. McNelles, *"Controlled hydrogenation of graphene, graphene-like silicon and germanium by optical injection current, linear and nonlinear optics"*, International School of Solid State Physics Epioptics-11, Erice, Sicily, 19-25 July 2010.

[15] A. I. Shkrebtii, J. L. Cabellos, N. Arzate, B. S. Mendoza, and P. McNelles, *"Nonlinear optical characterization of hydrogenated two-dimensional honeycomb carbon (graphene), silicon (silicene) and germanium layer"*, 7th International Symposium on Ultrafast Surface Dynamics (USD7) Croatia Brijuni Island, 22-26 Aug. 2010.

[16] J. C. Slater, Phys.Rev. 34, 1293 (1929).

[17] J. C. Slater, Phys.Rev. 32, 339 (1928).

[18] J. C. Slater, Phys.Rev. 81, 385 (1951).

[19] V. Fock, Zeitschrift, Physik A Hadrons and Nuclei **61**, 126 (1930).

[20] P. Hohenberg and W. Kohn, Phys.Rev. 136, -864 (1964).

[21] W. Kohn and L. J. Sham, Phys.Rev. 140, -1133 (1965).

[22] M. C. Payne, M. P. Teter, D. C. Allan, T. A. Arias, and J. D. Joannopoulos, Rev. Mod. Phys. **64**, 1045 (1992).

[23] B. H. Bransden and C. J. Joachain, *Physics of Atoms and Molecules* (Pearson Education Limited, Essex, England, 2003).

[24] J. Challice and D. Griffiths, *Introduction to Quantum Mechanics* (Prentice Hall, Upper Saddle River, NJ, 2005).

[25] F. L. Pilar, *Elementary Quantum Chemistry* (McGraw-Hill Pub., New York, 1990).

[26] M. Ernzerhof, J. Perdew, and K. Burke, *Density Functional Theory I: Functionals and Effective Potentials* (Springer, Berlin/Heidelberg, 1996), 180, p. 1.

[27] P. Giannozzi, *Lecture Notes per il Corso di Struttura della materia: Density Functional Theory for Electronic Structure Calculations*, 2005).

[28] J. P. Perdew and A. Zunger, Phys.Rev.B **23**, 5048 (1981).

[29] A. J. Cohen, P. Mori-Sanchez, and W. Yang, Physical Review B (Condensed Matter and Materials Physics) **77**, 115123 (2008).

[30] A. J. Cohen, P. Mori-Sanchez, and W. Yang, Science **321**, 792 (2008).

[31] A. J. Cohen, P. Mori-Sanchez, and W. Yang, *Fractional spins and static correlation error in density functional theory*, 2008).

[32] P. Mori-Sanchez, A. J. Cohen, and W. Yang, Physical Review Letters **102**, 066403 (2009).

[33] C. Kittel, *Introduction to Solid State Physics* (John Wiley and sons, New-York, 2005).

[34] N. W. Ashcroft and N. D. Mermin, *Solid State Physics* (Thomson Brook/Cole, 1976), p. 826.

[35] Quantum Espresso, *http://www.quantum-espresso.org*, 2007.

[36] D. Marx and J. Hutter, *Ab initio molecular dynamics: Theory and implementation; Modern Methods and Algorithms of Quantum Chemistry* (Forschungszentrum Jlich, 2000), 1.

[37] R. Oppenheimer, M. Born.. "Zur Quantentheorie der Moleküle." Annalen der Physik (1927): 457-484

[38] P. Giannozzi. H Pseudopotential : http://www.pwscf.org/pseudo/1.3/UPF/H.pz-vbc.UPF

[39] P. Giannozzi. C Pseudopotential: http://www.pwscf.org/pseudo/1.3/UPF/C.pz-vbc.UPF

[41] Molekel, http://molekel.cscs.ch/wiki/pmwiki.php, 2010.

[40] Rosli, Nazrul Ahmad, Hasan Abu Kassim and Keshav N. Shrivastava. "Graphene Infrared Spectroscopy: DFT Vibrational Frequencies." PROGRESS OF PHYSICS RESEARCH IN MALAYSIA (2010): 269-272.

[41] UCLA. Characteristic Vibrations of CH4 (Td symmetry). 10 February 2011 <http://www2.ess.ucla.edu/~schauble/MoleculeHTML/CH4_html/CH4_page.html>.

[42] S. Sakong and P. Kratzer, J. Chem. Phys. **133**, 054505 (2010).

[43] L.D. Landau. "Zur Theorie der phasenumwandlungen II." Phys. Z. Sowjetunion 11 (1937): 26-35.

[44] R.E. Peierls. "Quelques proprietes typiques des corpses solides." Ann. I. H. Poincare (1935): 177-222.

[45] Enrico Fermi. " Un Metodo Statistico per la Determinazione di alcune Prioprietà dell'Atomo." Rend. Accad. Naz. Lincei (1927): 602-607.

[46] L.H. Thomas. "The calculation of atomic fields." Proc. Cambridge Phil. Soc (1927): 542-548.

[47] Wikipedia Foundation. Kohn–Sham equations. 13 January 2011. 28 January 2011 <http://en.wikipedia.org/wiki/Kohn%E2%80%93Sham_equations>.

[48] Wikipedia Foundation. Local-density approximation. 1 December 2010. 29 January 2011 <http://en.wikipedia.org/wiki/Local-density_approximation>.

[49] Manuel Cardona, Peter Y. Yu. Fundamentals of Semiconductors - Physics and Materials Properties (3rd Edition). Dusseldorf: Springer Verlag, 2001.

[50] *Simulation of hydrogenated graphene field-effect transistors through a multiscale approach.* **Fiori, G. et al.** 2010, Physical Review B.

[51] *Tunable Band Gap in Hydrogenated Quasi-Free-standing Graphene.* **Haberer, D. et al.** 2010, Nano Letters, pp. 3360-3366.

[52] **Parr, Robert G. and Yang, Weitao.** *Density-Functional Theory of Atoms and Molecules.* Oxford : Oxford University Press, 1994.

[53] *Electronic and Optical Properties of Group IV two-dimensional Materials.* **Gori, P, et al.** 2009, Physica Status Solidi A.

[54] *Strong Charge-Transfer Excitonic Effects and the Bose-Einstein Exciton Condensate in Graphane.* **Cudazzo, P., et al.** 2010, Physical Review Letters, pp. 226804-1-4.

[55] *Pyridinic N doped graphene: synthesis, electronic structure, and electrocatalytic properties.* **Luo, Zhiqiang, et al.** s.l. : The Royal Society of Chemistry, 2011, Journal of Material Chemistry.

Works Cited

Ashcroft, N. W., and N. D. Mermin. *Solid State Physics*. Thomson Brook/Cole, 1976. Print.

Aufray, Bernard, et al. "Graphene-Like Silicon Nanoribbons on Ag(110): A Possible Formation of Silicene." *Applied Physics Letters* 96.18 (2010): 183102. Web.

Bae, Sukang, et al. "Roll-to-Roll Production of 30-Inch Graphene Films for Transparent Electrodes." *Nat Nano* 5.8 (2010): 574-8. Web.

Bransden, B. H., and C. J. Joachain. *Physics of Atoms and Molecules*. 2nd ed. Essex, England: Pearson Education Limited, 2003. Web.

Cahangirov, S., et al. "Two- and One-Dimensional Honeycomb Structures of Silicon and Germanium." *Phys.Rev.Lett.* 102.23 (2009): 236804. Web.

Cudazzo, P., et al. "Strong Charge-Transfer Excitonic Effects and the Bose-Einstein Exciton Condensate in Graphane." Physical Review Letters (2010): 226804-1-4.

Challice, John, and David Griffiths. *Introduction to Quantum Mechanics*. 2nd Edition ed. Upper Saddle River, NJ: Prentice Hall, 2005. Web.

Cohen, Aron J., Paula Mori-Sanchez, and Weitao Yang. "Fractional Charge Perspective on the Band Gap in Density-Functional Theory." *Physical Review B (Condensed Matter and Materials Physics)* 77.11 (2008): 115123. Web.

Cohen, Aron J., Paula Mori-Sanchez, and Weitao Yang. *Fractional Spins and Static Correlation Error in Density Functional Theory*., 2008. Web.

. "Insights into Current Limitations of Density Functional Theory." *Science* 321.5890 (2008): 792-4. Web.

Coraux, Johann, et al. "Growth of Graphene on Ir(111)." *New Journal of Physics* 11.2 (2009): 023006. Web.

Elias, D. C., et al. "Control of Graphene's Properties by Reversible Hydrogenation: Evidence for Graphane." *Science* 323.5914 (2009): 610-3. Web.

Ernzerhof, Matthias, John Perdew, and Kieron Burke. "Density Functional Theory I: Functionals and Effective Potentials." *Topics in Current Chemistry.* 180 Vol. Berlin/Heidelberg: Springer, 1996. 1-30. Web.

Fasolino, A., J. H. Los, and M. I. Katsnelson. "Intrinsic Ripples in Graphene." *Nat Mater* 6.11 (2007): 858-61. Web.

Fermi, Enrico. " Un Metodo Statistico per la Determinazione di alcune Prioprietà dell'Atomo." Rend. Accad. Naz. Lincei (1927): 602-607.

Fiori, G. et al. "Simulation of hydrogenated graphene field-effect transistors through a multiscale approach." Physical Review B (2010).

Fock, V. "Naherungsmethode Zur Losung Des Quantenmechanischen Mehrkorperproblems." *Zeitschrift fur Physik A Hadrons and Nuclei* 61.1 (1930): 126-48. Web.

Geim, A. K., and K. S. Novoselov. "The Rise of Graphene." *Nat Mater* 6.3 (2007): 183-91. Web.

Giannozzi, Paolo. *Lecture Notes Per Il Corso Di Struttura Della Materia: Density Functional Theory for Electronic Structure Calculations*., 2005. Web.

Gori, P, et al. "Electronic and Optical Properties of Group IV two-dimensional Materials." Physica Status Solidi A (2009).

Haberer, D. et al. "Tunable Band Gap in Hydrogenated Quasi-Free-standing Graphene." Nano Letters (2010): 3360-3366.

Hohenberg, P., and W. Kohn. "Inhomogeneous Electron Gas." *Phys.Rev.* 136.3B (1964): -864. Web.

Kageshima, Hiroyuki, et al. "Theoretical Study of Epitaxial Graphene Growth on SiC(0001) Surfaces." *Applied Physics Express* 2.6 (2009): 065502. Web.

Kittel, Charles. *Introduction to Solid State Physics*. 8th ed. New-York: John Wiley and sons, 2005. Web.

Kohn, W., and L. J. Sham. "Self-Consistent Equations Including Exchange and Correlation Effects." *Phys.Rev.* 140.4A (1965): -1133. Web.

Landau, L.D. "Zur Theorie der phasenumwandlungen II." Phys. Z. Sowjetunion 11 (1937): 26-35.

Luo, Zhiqiang, et al. "Pyridinic N doped graphene: synthesis, electronic structure, and electrocatalytic properties." Journal of Material Chemistry (2011).

Marx, D., and J. Hutter. "Ab Initio Molecular Dynamics: Theory and Implementation; Modern Methods and Algorithms of Quantum Chemistry." *NIC Series.* Ed. J. Grotendorst. 1 Vol. Forschungszentrum Julich, 2000. Web.

Mori-Sanchez, Paula, Aron J. Cohen, and Weitao Yang. "Discontinuous Nature of the Exchange-Correlation Functional in Strongly Correlated Systems." *Physical Review Letters* 102.6 (2009): 066403. Web.

Novoselov, K. S., et al. "Electric Field Effect in Atomically Thin Carbon Films." *Science* 306.5696 (2004): 666-9. Web.

Oppenheimer, R., Born, M. "Zur Quantentheorie der Moleküle." Annalen der Physik (1927): 457-484

Parr, Robert G. and Weitao Yang. Density-Functional Theory of Atoms and Molecules. Oxford: Oxford University Press, 1994.

Payne, M. C., et al. "Iterative Minimization Techniques for Ab Initio Total-Energy Calculations: Molecular Dynamics and Conjugate Gradients." *Rev. Mod. Phys.* 64 (1992): 1045-97. Print.

Peierls, R.E. "Quelques proprietes typiques des corpses solides." Ann. I. H. Poincare (1935): 177-222.

Perdew, J. P., and Alex Zunger. "Self-Interaction Correction to Density-Functional Approximations for Many-Electron Systems." *Phys.Rev.B* 23.10 (1981): 5048-79. Web.

Pilar, Frank L. *Elementary Quantum Chemistry*. 2nd ed. New York: McGraw-Hill Pub., 1990. Web.

Pletikosi I., et al. "Dirac Cones and Minigaps for Graphene on Ir(111)." *Phys.Rev.Lett.* 102.5 (2009): 056808. Web.

Quantum Espresso. "http://www.quantum-espresso.org."Web. <Quantum Espresso>.

Riedl, C., et al. "Quasi-Free-Standing Epitaxial Graphene on SiC obtained by Hydrogen Intercalation." *Phys.Rev.Lett.* 103.24 (2009): 246804. Web.

Rosli, Nazrul Ahmad, Hasan Abu Kassim and Keshav N. Shrivastava. "Graphene Infrared Spectroscopy: DFT Vibrational Frequencies." PROGRESS OF PHYSICS RESEARCH IN MALAYSIA (2010): 269-272.

Sakong, Sung, and Peter Kratzer. "Hydrogen Vibrational Modes on Graphene and Relaxation of the C--H Stretch Excitation from First-Principles Calculations." *The Journal of chemical physics* 133.5 (2010): 054505. Web.

Savchenko, Alex. "MATERIALS SCIENCE: Transforming Graphene." *Science* 323.5914 (2009): 589-90. Web.

Shkrebtii, A. I., et al. ""Controlled Hydrogenation of Graphene, Graphene-Like Silicon and Germanium by Optical Injection Current, Linear and Nonlinear Optics." (a) Print.

"Nonlinear Optical Characterization of Hydrogenated Two-Dimensional Honeycomb Carbon (Graphene), Silicon (Silicene) and Germanium Layer"." (b) Print.

Slater, J. C. "The Self Consistent Field and the Structure of Atoms." *Phys.Rev.* 32.3 (1928): 339-48. Web.

A Simplification of the Hartree-Fock Method." *Phys.Rev.* 81.3 (1951): 385-90. Web.

"The Theory of Complex Spectra." *Phys.Rev.* 34.10 (1929): 1293-322. Web.

Sofo, Jorge O., Ajay S. Chaudhari, and Greg D. Barber. "Graphane: A Two-Dimensional Hydrocarbon." *Phys.Rev.B* 75.15 (2007): 153401. Web.

Thomas, L.H. "The calculation of atomic fields." Proc. Cambridge Phil. Soc (1927): 542-548.

UCLA. Characteristic Vibrations of CH4 (Td symmetry). 10 February 2011 <http://www2.ess.ucla.edu/~schauble/MoleculeHTML/CH4_html/CH4_page.html>.

Wikipedia Foundation. Kohn–Sham equations. 13 January 2011. 28 January 2011 <http://en.wikipedia.org/wiki/Kohn%E2%80%93Sham_equations>.

Wikipedia Foundation. Local-density approximation. 1 December 2010. 29 January 2011 <http://en.wikipedia.org/wiki/Local-density_approximation>.

Yu, Peter Y., Cardona Manuel. Fundamentals of Semiconductors - Physics and Materials Properties (3rd Edition). Dusseldorf: Springer Verlag, 2001.

Appendix A:

Quantum Espresso Optics Manual